DETACHED LEVER CLOCK MECHANISM DYNAMICS

By

WILLIAM CLAIR MONDAY

Bachelor of Science
University of Kansas
Lawrence, Kansas
1952

Master of Science
University of Kansas
Lawrence, Kansas
1956

Submitted to the faculty of the Graduate School of the Oklahoma State University in partial fulfillment of the requirements for the degree of
DOCTOR OF PHILOSOPHY
May, 1965

DETACHED LEVER CLOCK MECHANISM

DYNAMICS

Thesis Approved:

Ladislaus J Fila
Thesis Adviser

R L Lowery

Dean of the Graduate School

ACKNOWLEDGEMENT

I wish to thank Sandia Corporation of Albuquerque, New Mexico, and especially Mr. John Ford, for sponsoring this research program at Oklahoma State University from 1962 to 1965 and for supplying equipment and test units. I appreciate the consultation and advice given by Mr. Jerry Shinkle and the help of Mr. Turk Levy and Mr. Ralph Stewart also of Sandia. My appreciation is given to the Faculty of the School of Mechanical Engineering, Oklahoma State University, for awarding me the graduate assistantship that made my doctoral study possible.

I offer my thanks to Professor L. J. Fila, research project leader and adviser, for his help and encouragement during the course of this research. I also appreciate the efforts of Dr. J. H. Boggs, Committee Chairman, and Dr. R. L. Lowery and Dr. R. G. McIntyre, committee members. The aid and cooperation of the staff of the Mechanical Engineering Laboratory, Professor F. C. McQuiston, J. A. McCandless, and G. Cooper in construction and operation of experimental equipment is recognized. I wish to thank undergraduate Donald Cott for designing and assembling the friction test equipment.

Appreciation is expressed to John Leonard, Leonard

Jewelry, for his help and craftsmanship in modifying and cleaning various timing escapements during the course of this study, and Mr. William F. Walker, for his assistance in programming the initial solution for the equation of motion.

For her aid in preparing and typing this manuscript and for her continued encouragement and hard work, I offer my appreciation to my wife, Norma.

I would also like to thank Mrs. Mildred Avery for her aid during the course of this research, and Mrs. E. Brann and Mrs. B. Stewart for their work on the interim reports and paper work for this program.

TABLE OF CONTENTS

LIST OF TABLES

LIST OF FIGURES

LIST OF FIGURES (CONTINUED)

LIST OF FIGURES (CONTINUED)

LIST OF PLATES

CHAPTER I

INTRODUCTION

Throughout the ages man has been interested in the measurement of time.[1,13] The first recorded time measuring devices were sundials in Babylonia in 2000 B.C. Then in 200 B.C. the Clepsydra (water clock) was introduced into Greece. Since the Clepsydra did not depend on the sun time which changed the weather conditions and seasonal variations, it reached a high state of development and was used in the homes of the more wealthy. The Clepsydra developed along two lines:

1. In dry countries the water was replaced by sand and the sand timer or hour glass was born.
2. In other countries it evolved into an elaborate and gilded mechanism.

This mechanization went to the extent that in 807 A.D. a water clock that had twelve doors representing the hours was presented to Charlemagne from Bagdad; each door opened at the hour it represented and out came the same number of little balls which dropped on a drum at intervals to signal the hour. When it was twelve o'clock, twelve horsemen in miniature issued forth at the same time and shut all the doors. This elaborate mechanism and train

of cogged wheels has made the water clock the ancestor in the direct line of modern clocks.

Between 960 and 1360 A.D. the true mechanical clock was invented, but the exact inventor is unknown. All clocks of this age were ponderous and the parts were made in blacksmith shops. All the mechanical clocks were weight driven. In 1500 the mainspring was invented by Peter Henlein of Nürnberg. This allowed portable timekeepers to be built, and by 1600 the spring-driven table clocks were at the height of their popularity and pocket watches were coming into extended use.

About 1685 the pendulum was applied to clocks and the curved hairspring and balance wheel to watches. From this time until well past 1800 the only clocks built, except special ones, were pendulum clocks and practically the only balance-controlled timekeepers were pocket watches. The reason for this abrupt change was the increased accuracy afforded by the pendulum and the hairspring balance wheel. In 1655 a clock did well to keep time to five minutes a day, but with the advent of the pendulum its error might drop to the order of five seconds a day; similarly, watches were brought from an almost unpredictable performance to within two or three minutes a day. While there are many claimants to the invention of both the pendulum and the hairspring, it is generally conceded that Christian Huygens was the first to apply them in practical form to timekeepers sold to the public in about 1674.[13]

From this time for the next 100 years, many types of escapements were patented. Among these were the cylinder, the anchor, the duplex, and in 1750 the detached lever escapement by Thomas Mudge.[13] This lever escapement practically replaced all the other types except the chronometer escapement which is used for extreme accuracy and which is too fragile for pocket watches and too expensive for the household clocks.[14]

The lever and chronometer escapements have one common feature by which they differ from other escapements. With most other escapements such as the verge, the cylinder, and the duplex, the balance is never free from interference by escapement friction. In both the lever and the chronometer, the balance is free and out of contact with the escapement during most of its oscillation and is acted upon only during the mid-part of its swing, where interference produces a minimum of disturbance to its timekeeping. This feature justifies the name "detached" lever escapement.

In this long chain of advances in the watch and clock technology there seems to be little evidence of a basic analytical approach to the escapement mechanism as a whole. True, certain elements of the escapement were studied individually. A. L. Rawlings and Laudius Saunier, for example, studied various portions of the escapement mechanism but, in general, did not consider the mechanism as an entity.[14,15] From all this the escapement evolved, to a large extent, by cut and try methods. If it worked,

it was used and all future parts were made just the same. This is permissible for clocks and watches where the load is essentially constant, but for varying loaded mechanisms, such as the timers used in ordnance and rockets, one could go on indefinitely with this method. Therefore, the purpose of this study is to define in general terms the basic escapement as an entity and to determine analytically the equations of motion. This will enable a prediction of the results of varying certain parameters in the equations and will give an idea of the operational characteristics with a minimum of the cut and try procedure. This method is compared with actual mechanisms to correlate actual performance with analytical results.

From this study an apparently improved method of torque sensitivity control evolved. This method is outlined in Chapter VIII.

CHAPTER II

PREVIOUS INVESTIGATIONS

One of the first mathematical treatments of a theoretical discussion on escapements was presented by G. B. Airy in about 1827. Although it forms a basis for almost all writings on the subject since that time, he confined his investigation explicitly to pendulums constructed to swing the bob over a cycloidal arc and therefore have the same time of oscillation for all amplitudes (isochronous pendulum). Many writers since that time overlooked this limitation. However, A. L. Rawlings attempted to re-establish Airy's more important results in a simplified manner.(14) Rawlings continued the Airy investigation on the pendulum and arrived at the same basic premise that (if zero is defined when the bob is hanging straight down) before zero a forward impulse shortens the period while a retarding impulse lengthens the period. After zero a forward impulse lengthens the period and a retarding impulse shortens it. But as long as the impulse is consistent, any losses can be taken out by regulating; thus it does not matter where the impulse occurs so long as it is predictable. Rawlings extended this approach to balance wheels and hairspring

escapements by shaping the hairspring into an overcoil to get isochronous results thus making Airy's analysis valid for balance wheels. His objective was directed to practical application rather than to derive an analytical tool.

K. Giebel, in his dissertation in 1905 on the influence of the escapement on the running of clocks, obtained an equation of motion of the form $\ddot{\theta} + x(\theta \pm f) = 0$ which he solved for a constant "x" and "f".(7) He indicated that a more rigorous treatment would be most difficult at that time (x is some function of the hairspring constant and f is a kinetic friction function with the sign change on the friction f to accommodate velocity change). He discussed the effect of the forcing torque but handled it separately and apparently did not include it in his basic equation of motion. His equation, as far as it goes, is similar to the one derived in this study; however, this study does include more effects than previously considered and it combines the experimental and theoretical approaches. Several authors attempted to define the function of the escapement, but they most generally tried to do it from a practical rather than an analytical viewpoint. They tended to treat a theoretical approach similar to the quote by Mr. Saunier:

> Analytical solutions possess a degree of accuracy far beyond that which it is possible to obtain in practice; and besides this we are ignorant of the exact values of several of the principal elements involved in the calculations, friction for example, and this would render any purely theoretical results

> open to question; we shall therefore, as in the former case, only resort to elementary mechanical principles. Supported by experimental evidence; the solutions they afford will abundantly suffice to satisfy all the requirements of practical Horology.(15)

The tendency to rely on experimental data and previous successes has been prevalent throughout the history of clock and watch development without an attempt to arrive at an over-all analytical solution or the logical approach of coupling the analytical solution with experimental data. Those who did attempt analytical solutions, did so with an interest in only one portion of the mechanism rather than the unit as a whole.

CHAPTER III

THEORETICAL CONSIDERATION

The balance wheel hairspring assembly is the main factor controlling the time rate of the escapement; therefore, it is logical to begin the theoretical considerations here and progress through the other stages. The forces acting on the balance wheel are the hairspring torque, driving torque, frictional torque, and inertia torque. These make up all the external forces acting on the balance wheel during its operation. Each of these forces requires a closer examination.

The hairspring torque acts with the balance wheel to give an oscillatory torsional spring mass system. If there were no other forces acting on the wheel and the external conditions were unchanged, the system would oscillate at a given amplitude indefinitely and the time of oscillation would be identical for each oscillation. This is the optimum condition toward which one should strive. This gives an equation of the form:

$$\ddot{\theta} + \omega_o^2 \theta = 0$$

where θ is displacement and ω_o^2 is spring constant K_o divided by the moment of inertia I, with the solution,

$$\theta = \theta_o \cos \omega_o t,$$

provided the boundary conditions are

$$\theta = \theta_o;\ \dot{\theta} = 0 \text{ at } t = 0.$$

Friction is inevitable in any mechanical device. There is a possibility of three friction forces acting on the balance and hairspring assembly: (a) viscous friction; (b) kinetic or sliding friction; and (c) aerodynamic friction or damping. It is reasonably apparent that if there are any lubricants there is bound to be viscous friction of considerable magnitude. Since there are bearings, there is also bound to be sliding friction. Aerodynamic friction exists but to a lesser degree; according to calculations it is about 10-100 to 1 smaller. Aerodynamic friction is not included as a separate term in this analysis because it is small and will occur as a part of one of the other damping terms. This does not invalidate the analysis as the correlation is good.

By adding the damping terms for viscous and sliding friction, the equation of the balance wheel now becomes

$$\ddot{\theta} + \omega_o^2\theta + C\dot{\theta} + R\frac{\dot{\theta}}{|\dot{\theta}|} = 0,$$

where $C = \dfrac{\text{viscous damping coefficient}}{\text{moment of inertia of balance}}$

and $R = \dfrac{\text{sliding friction coefficient}}{\text{moment of inertia of balance}}$.

One more term, the forcing function, must be considered before attempting to solve the equation. A look at the forcing function reveals that this is the method by

which power is supplied to offset the decrease in amplitude caused by the friction terms. A further look reveals that this is supplied to the balance over a relatively short period of time; and, as was pointed out in Chapter I, this is the big advantage of the detached lever. During this short period of attachment to the balance wheel, all of the energy needed to maintain oscillation is supplied to the balance along with any reflected motions generated between the power source and the balance wheel. Basically, by determining the shape, amplitude, and duration of the pulse, the sum total of the train and escapement characteristics can be applied to the balance wheel. This pulse will then include such items as train inertia, gear friction, tooth irregularity, etc. Since this is the only time the train connects with the balance, this must be true. Therefore, by putting in this pulse, which includes the oddities of the escapement train and power supply, the escapement as a whole has been taken into consideration and not part by part. The equation of motion for the escapement is then as follows:

$$\ddot{\theta} + \omega_o^2\theta + C\dot{\theta} + R\frac{\dot{\theta}}{|\dot{\theta}|} + X_\theta = 0,$$

where X_θ is the above-described forcing function divided by the moment of inertia of the balance wheel assembly.

As can be seen, this equation as it stands is nonlinear since both the R and X terms can be nonlinear functions. The R and X terms warrant further consideration.

If $\theta \neq 0$ when the balance wheel is at rest, there is a forcing function of the general form shown in Figure 1.

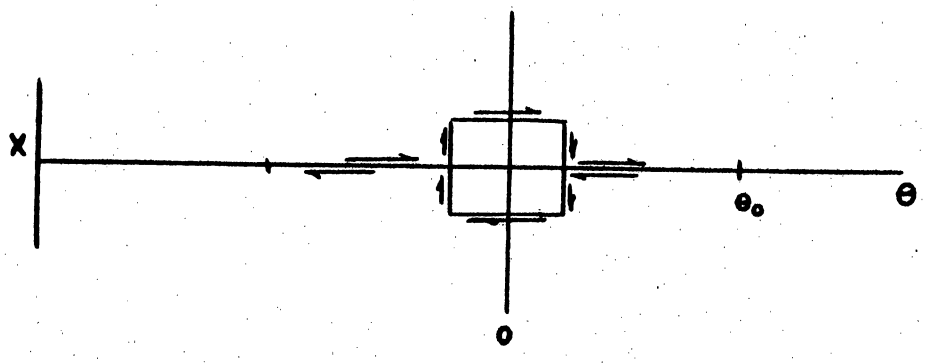

Figure 1. Simplified Force Function

This forcing function is not normal in the sense that it is not time dependent but actually θ dependent. The force is applied at a certain angle regardless of the time. The balance wheel determines when the system reaches that angle. This forcing function acts more as a negative damping term than a forcing function. This can, however, be converted to a time function by considering θ_0 to be at time $t = 0$. The above plot then becomes Figure 2.

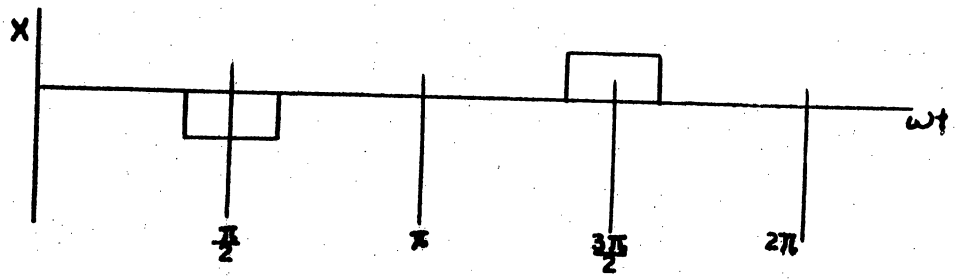

Figure 2. Force Function vs. ωt

Because of the unlocking of the escapement before the power stroke, a more exact plot of X_θ vs ωt is shown in Figure 3. R_θ is, in general, constant over the complete cycle; however, since $\dot{\theta}$ changes sign at π, the plot of R_θ vs ωt is approximately as shown in Figure 3.

A comparison of the two functions reveals that between each set of vertical lines both functions are constant over the interval. This allows the original equation to be separated into fourteen equations with matching end conditions between each segment. This can be programmed for the IBM 1410 computer. This program is defined in Appendix B. The fourteen equations are of the form

$$\ddot{\theta}_1 + \omega_{o1}^2\theta_1 + C\dot{\theta}_1 + R_1 + X_1 = 0,$$

,

,

,

$$\ddot{\theta}_{14} + \omega_{o1}^2\theta_{14} + C\dot{\theta}_{14} + R_{14} + X_{14} = 0.$$

X and R are now constants. The solutions are then of the form

$$\theta_1 = e^{-Ct/2}(A_1\cos\omega_1 t + B_1\sin\omega_1 t) + \frac{R_1}{\omega_{o1}^2} + \frac{X_1}{\omega_{o1}^2},$$

,

,

,

$$\theta_{14} = e^{-Ct/2}(A_{14}\cos\omega_1 t + B_{14}\sin\omega_1 t) + \frac{R_{14}}{\omega_{o1}^2} + \frac{X_{14}}{\omega_{o1}^2}.$$

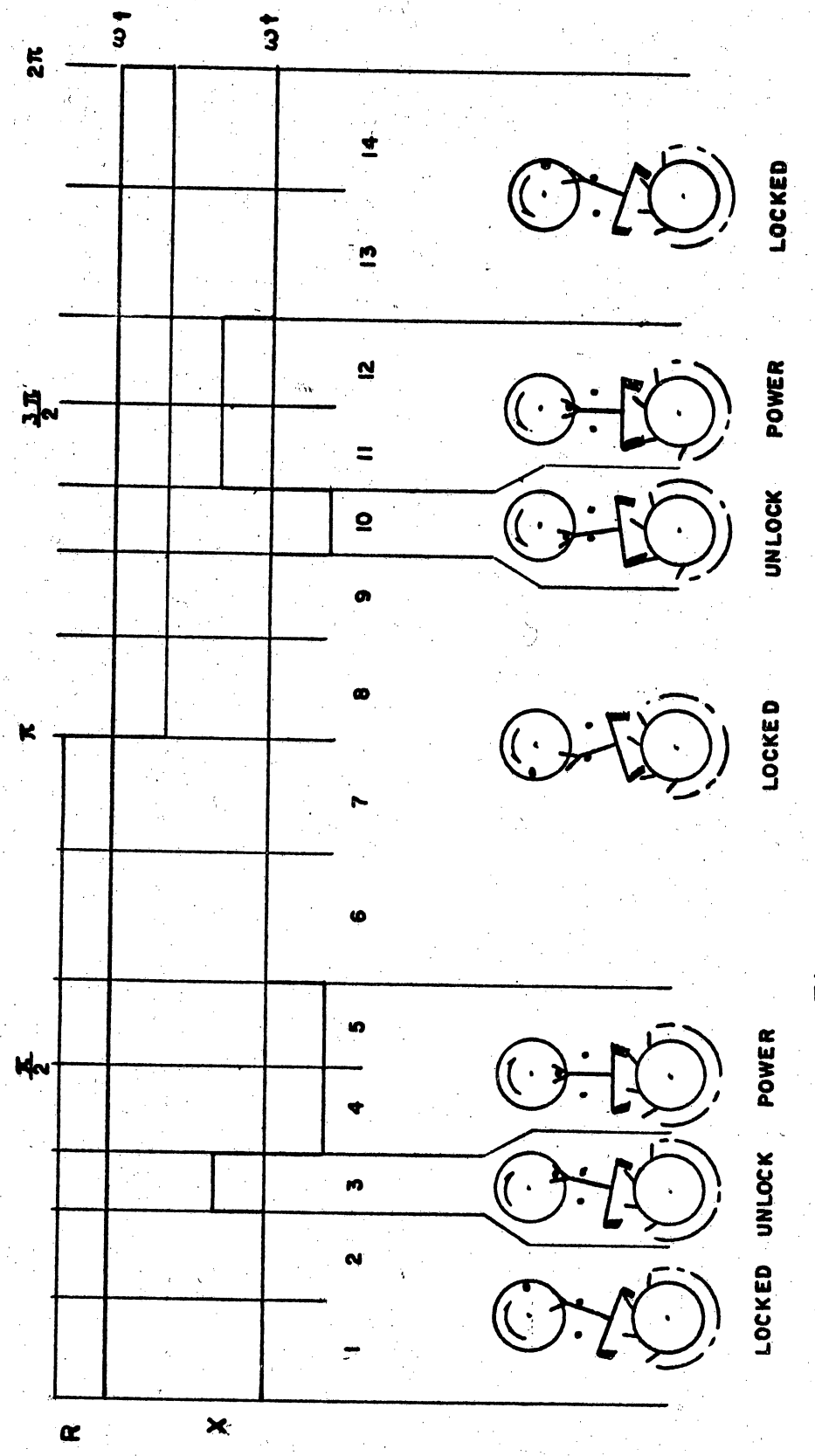

Figure 3. True X-R Diagram

One may observe in Figure 4 that some of the segments do not end at a change in X or R such as between 1 and 2, 6 and 7, 8 and 9, and 13 and 14. This is simply an additional segmentation to allow for compensating a nonlinear hairspring constant if this happened to be the case. It might also be observed that this basic equation can be used not only of the detached lever escapement but also for any of the other escapements provided suitable R and X functions can be described.

Now that the mathematical model has been determined, the equations can be solved.

The previous graphs of the functions over one cycle, or 2π, form the basis for the solution. For computational purposes, the sign as shown in the graphs must be observed. For instance, X_3, X_{11}, X_{12} carry a plus sign while X_4, X_5, X_{10} carry a minus sign. R_1 through R_7 carry a plus sign and R_8 through R_{14} carry a minus sign. The sign convention represents the dissipative system influences, the direction of rotation of the balance wheel, and the change in the sign of the velocity at π.

In the X_θ vs ωt plot, X_3 and X_{10} are dissipated energies caused by unlocking the escapement, while X_4, X_5, X_{11}, and X_{12} are augmentative terms arising from the escape wheel acting on the pallet.

In the R vs ωt graph (Figure 4) all the energies are dissipative kinetic friction terms. Normally, with true kinetic friction, all R's should be equal. Should there

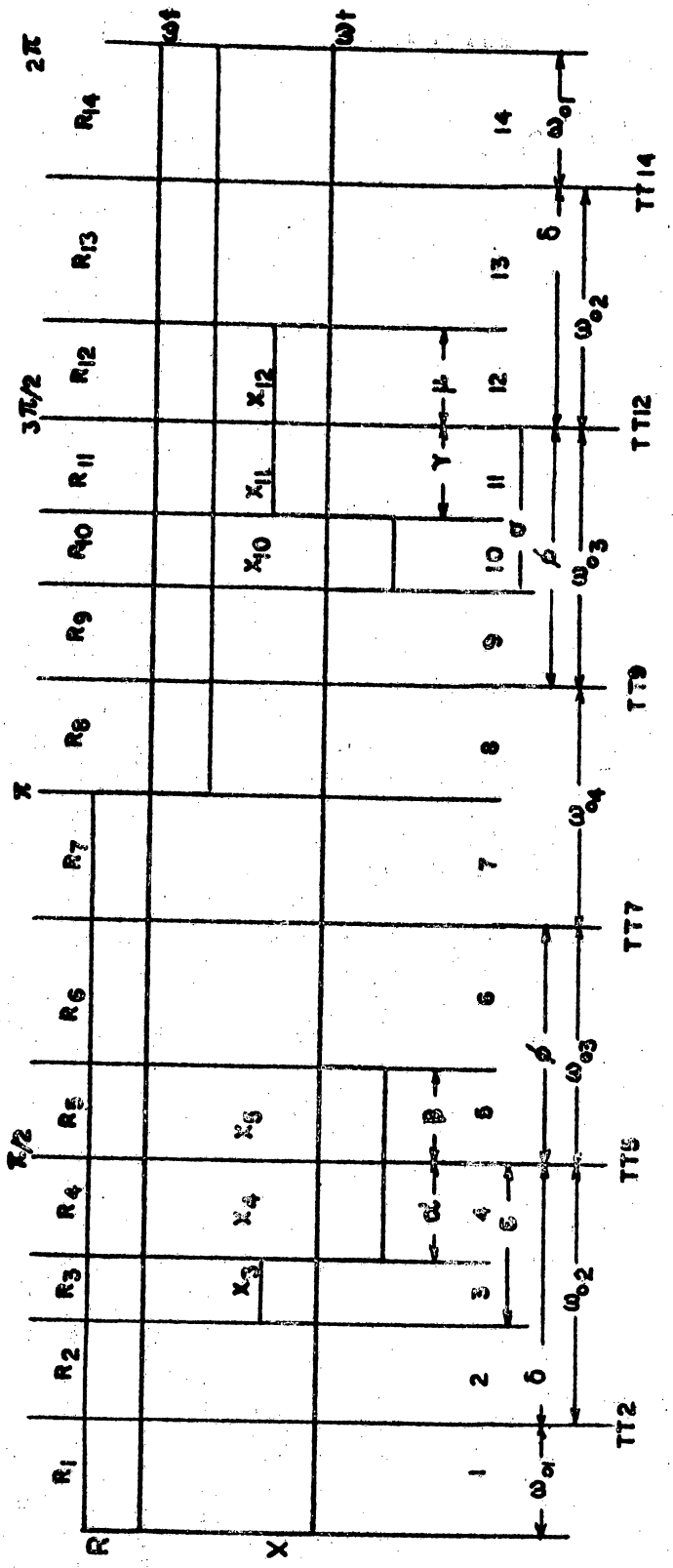

Figure 4. Division of X and R

be a deviation arising from some nonlinearity in friction that is known, it can be remedied by changing some of the $R_{(n)}$ terms. The ω_o terms allow for four shifts in the hairspring constant if it is found to be nonlinear. These shifts are at θ_1, θ_5, θ_7, θ_9, θ_{12}, and θ_{14}. If the hairspring is linear, ω_o is left constant and the equations are considerably simplified.

The fourteen segment "end times" are

$$TT_2 = \frac{\frac{\pi}{2} - \delta}{\omega_1}, \qquad TT_3 = \frac{\frac{\pi}{2} - \delta}{\omega_1} + \frac{\delta - \varepsilon}{\omega_2},$$

$$TT_4 = \frac{\frac{\pi}{2} - \delta}{\omega_1} + \frac{\delta - \alpha}{\omega_2}, \qquad TT_5 = \frac{\frac{\pi}{2} - \delta}{\omega_1} + \frac{\delta}{\omega_2},$$

$$TT_6 = TT_5 + \frac{\beta}{\omega_3}, \qquad TT_7 = TT_5 + \frac{\phi}{\omega_3},$$

$$TT_8 = TT_7 + \frac{\frac{\pi}{2} - \phi}{\omega_4}, \qquad TT_9 = TT_7 + \frac{2(\frac{\pi}{2} - \phi)}{\omega_4},$$

$$TT_{10} = TT_9 + \frac{\phi - \sigma}{\omega_3}, \qquad TT_{11} = TT_9 + \frac{\phi - \gamma}{\omega_3},$$

$$TT_{12} = TT_9 + \frac{\phi}{\omega_3}, \qquad TT_{13} = TT_{12} + \frac{\mu}{\omega_2},$$

$$TT_{14} = TT_{12} + \frac{\delta}{\omega_2}, \qquad TT_{15} = TT_{14} + \frac{\frac{\pi}{2} - \alpha}{\omega_1}.$$

The equation to be solved is

$$\ddot{\theta} + \omega_o^2\theta + C\dot{\theta} + R_\theta\frac{\dot{\theta}}{|\dot{\theta}|} + X_\theta = 0;$$

the boundary conditions are

$$\theta = \theta_o;\ \dot{\theta} = 0;\ t = 0.$$

The solution is

$$\theta = e^{-Ct/2}(A\cos \omega t + B\sin \omega t) + \frac{R_\theta}{\omega_o^2}\frac{\dot{\theta}}{|\dot{\theta}|} + \frac{X_\theta}{\omega_o^2}.$$

The solution to the equation, when separated into fourteen linear equations, is of the form

$$\theta_n = e^{-Ct/2}(A_n\cos \omega_i t + B_n\sin \omega_i t) + \frac{R_n}{\omega_{oi}^2} + \frac{X_n}{\omega_{oi}^2}.$$

These solutions are tabulated below. (See Appendix A for a more complete derivation).

These solutions are based on the sign convention previously discussed.

θ_1 valid from $t = 0$ to $t = TT_2$:

$$\theta_1 = e^{-Ct/2}(A_1\cos \omega_1 t + B_1\sin \omega_1 t) + \frac{R_1}{\omega_{o1}^2},$$

$$\omega_1 = \frac{\sqrt{4\omega_{o1}^2 - C^2}}{2},$$

$$BL_1 = \frac{2}{2\omega_1},$$

$$A_1 = \theta_o - \frac{R_1}{\omega_{o1}^2},$$

$$B_1 = (\theta_o - \frac{R_1}{\omega_{o1}^2})BL_1.$$

θ_2 valid from t= TT_2 to t = TT_3:

$$\theta_2 = e^{-Ct/2}(A_2\cos \omega_2 t + B_2 \sin \omega_2 t) + \frac{R_1}{\omega_{o1}^2},$$

$$\omega_2 = \frac{\sqrt{4\omega_{o2}^2 - C^2}}{2},$$

$$BL_2 = \frac{C}{2\omega_2},$$

$$E = \omega_1(TT_2),$$

$$A_2 = -\frac{B_1}{\omega_2}(\omega_2 \sin E(BL_2 \sin E - \cos E)$$

$$-\omega_1 \sin E(BL_1 \sin E - \cos E))$$

$$+ \frac{A_1}{\omega_2}(\omega_2 \cos E(\cos E - BL_2 \sin E)$$

$$+ \omega_1 \sin E(\sin E + BL_1 \cos E))$$

$$- \left(\frac{R_1}{\omega_{o1}^2} - \frac{R_2}{\omega_{o2}^2}\right)\left(\frac{BL_2 \sin E - \cos E)}{e^{-CTT_2/2}}\right),$$

$$B_2 = \frac{\omega_1}{\omega_2}\left(\frac{A_1(\sin E + BL_1 \cos E) + B_1(BL_1 \sin E - \cos E)}{(BL_2 \sin E - \cos E)}\right)$$

$$- A_2\left(\frac{\sin E + BL_2 \cos E}{BL_2 \sin E - \cos E}\right).$$

θ_3 valid from t = TT_3 to t = TT_4:

$$\theta_3 = e^{-Ct/2}(A_3\cos \omega_2 t + B_3 \sin \omega_2 t) + \frac{R_3}{\omega_{o2}^2} + \frac{X_3}{\omega_{o2}^2},$$

$$\omega_2 = \frac{\sqrt{4\omega_{o2}^2 - C^2}}{2},$$

$$F = \omega_2(TT_3),$$

$$A_3 = A_2 - \frac{(R_2 - R_3 - X_3)}{\omega_{o2}^2 e^{-CTT_3/2}}(BL_2 \sin F - \cos F),$$

$$B_3 = B_2 + \frac{(R_2 - R_3 - X_3)}{\omega_{o2}^2 e^{-CTT_3/2}}(\sin F + BL_2 \cos F).$$

Θ_4 valid from $t = TT_4$ to $t = TT_5$:

$$\Theta_4 = e^{-Ct/2}(A_4 \cos \omega_2 t + B_4 \sin \omega_2 t) + \frac{R_4}{\omega_{o2}^2} + \frac{X_4}{\omega_{o2}^2},$$

$$G = \omega_2(TT_4),$$

$$A_4 = A_3 - \frac{(R_3 - R_4 + X_3 - X_4)}{\omega_{o2}^2 e^{-CTT_4/2}}(BL_2 \sin G - \cos G),$$

$$B_4 = B_3 + \frac{(R_3 - R_4 + X_3 - X_4)}{\omega_{o2}^2 e^{-CTT_4/2}}(\sin G + BL_2 \cos G).$$

Θ_5 valid from $t = TT_5$ to $t = TT_6$:

$$\Theta_5 = e^{-Ct/2}(A_5 \cos \omega_3 t + B_5 \sin \omega_3 t) + \frac{R_5}{\omega_{o3}^2} + \frac{X_5}{\omega_{o3}^2},$$

$$\omega_3 = \frac{\sqrt{4\omega_{o3}^2 - C^2}}{2},$$

$$BL_3 = \frac{C}{2\omega_3},$$

$$H = \omega_2(TT_5),$$

$$A_5 = -\frac{B_4}{\omega_3}(\omega_3 \sin H(BL_3 \sin H - \cos H)$$

$$- \omega_2 \sin H(BL_2 \sin H - \cos H))$$

$$+ \frac{A_4}{\omega_3}(\omega_3 \cos H(\cos H - BL_3 \sin H)$$

$$+ \omega_2 \sin H(\sin H + BL_2 \cos H))$$

$$- \left(\frac{R_4 + X_4}{\omega_{o2}^2} - \frac{R_5 + X_5}{\omega_{o3}^2}\right)\left(\frac{BL_3 \sin H - \cos H}{e^{-CTT_5/2}}\right),$$

$$B_5 = \frac{\omega_2}{\omega_3}\left(\frac{A_4(\sin H + BL_2 \cos H) + B_4(BL_2 \sin H - \cos H)}{(BL_3 \sin H - \cos H)}\right)$$

$$- A_5\left(\frac{\sin H + BL_3 \cos H}{BL_3 \sin H - \cos H}\right).$$

θ_6 is valid from $t = TT_6$ to $t = TT_7$:

$$\theta_6 = e^{-Ct/2}(A_6 \cos \omega_3 t + B_6 \sin \omega_3 t) + \frac{R_6}{\omega_{o3}^2},$$

$$L = \omega_3(TT_6),$$

$$\omega_3 = \frac{\sqrt{4\omega_{o3}^2 - C^2}}{2},$$

$$A_6 = A_5 - \frac{(R_5 - R_6 + X_5)}{\omega_{o3}^2 e^{-CTT_6/2}}(BL_3 \sin L - \cos L),$$

$$B_6 = B_5 + \frac{(R_5 - R_6 + X_5)}{\omega_{o3}^2 e^{-CTT_6/2}}(\sin L + BL_2 \cos L).$$

θ_7 is valid from $t = TT_7$ to $t = TT_8$:

$$\theta_7 = e^{-Ct/2}(A_7 \cos \omega_4 t + B_7 \sin \omega_4 t) + \frac{R_7}{\omega_{o4}^2},$$

$$\omega_4 = \frac{\sqrt{4\omega_{o4}^2 - C^2}}{2},$$

$$BL_4 = \frac{C}{2\omega_4},$$

$$M = \omega_3(TT_7),$$

$$A_7 = -\frac{B_6}{\omega_4}(\omega_4 \sin M(BL_4 \sin M - \cos M) - \omega_3 \sin M(BL_3 \sin M - \cos M))$$

$$+ \frac{A_6}{\omega_4}(\omega_4 \cos M(\cos M - BL_4 \sin M) + \omega_3 \sin M(\sin M + BL_3 \cos M))$$

$$- \left(\frac{R_6}{\omega_{o3}^2} - \frac{R_7}{\omega_{o4}^2}\right)\left(\frac{BL_4 \sin M - \cos M}{e^{-CTT_7/2}}\right),$$

$$B_7 = \frac{\omega_3}{\omega_4}\left(\frac{A_6(\sin M + BL_3 \cos M) + B_6(BL_3 \sin M - \cos M)}{(BL_4 \sin M - \cos M)}\right)$$

$$- A_7\left(\frac{\sin M + BL_4 \cos M}{BL_4 \sin M - \cos M}\right).$$

θ_8 is valid from $t = TT_8$ to $t = TT_9$

$$\theta_8 = e^{-Ct/2}(A_8 \cos \omega_4 t + B_8 \sin \omega_4 t) + \frac{R_8}{\omega_{o4}^2},$$

$$N = \omega_4(TT_8),$$

$$A_8 = A_7 - \left(\frac{R_7 - R_8}{\omega_{o4}^2 e^{-CTT_8/2}}\right)(BL_4 \sin N - \cos N),$$

$$B_8 = B_7 + \left(\frac{R_7 - R_8}{\omega_{o4}^2 e^{-CTT_8/2}}\right)(\sin N + BL_4 \cos N).$$

θ_9 is valid from $t = TT_9$ to $t = TT_{10}$:

$$\theta_9 = e^{-Ct/2}(A_9 \cos \omega_3 t + B_9 \sin \omega_3 t) + \frac{R_9}{\omega_{o3}^2},$$

$$\omega_3 = \frac{\sqrt{4\omega_{o3}^2 - C^2}}{2},$$

$$P = \omega_4(TT_9),$$

$$A_9 = -\frac{B_8}{\omega_3}(\omega_3 \sin P(BL_3 \sin P - \cos P) - \omega_4 \sin P(BL_4 \sin P - \cos P))$$

$$+ \frac{A_8}{\omega_3}(\omega_3 \cos P(\cos P - BL_3 \sin P) + \omega_4 \sin P(\sin P + BL_4 \cos P))$$

$$- \left(\frac{R_8}{\omega_{o4}^2} - \frac{R_9}{\omega_{o3}^2}\right)\left(\frac{BL_3 \sin P - \cos P}{e^{-CTT_9/2}}\right),$$

$$B_9 = \frac{\omega_4}{\omega_3}\left(\frac{A_8(\sin P + BL_4 \cos P) + B_8(BL_4 \sin P - \cos P)}{(BL_3 \sin P - \cos P)}\right)$$

$$- A_9\left(\frac{\sin P + BL_3 \cos P}{BL_3 \sin P - \cos P}\right).$$

θ_{10} is valid from $t = TT_{10}$ to $t = TT_{11}$:

$$\theta_{10} = e^{-Ct/2}(A_{10}\cos \omega_3 t + B_{10}\sin \omega_3 t) + \frac{R_{10}}{\omega_{o3}^2} + \frac{X_{10}}{\omega_{o3}^2},$$

$$Q = \omega_3(TT_{10}),$$

$$A_{10} = A_9 - \frac{(R_9 - R_{10} - X_{10})}{\omega_{o3}^2 e^{-CTT_{10}/2}}(BL_3\sin Q - \cos Q),$$

$$B_{10} = B_9 + \frac{(R_9 - R_{10} - X_{10})}{\omega_{o3}^2 e^{-CTT_{10}/2}}(\sin Q + BL_3\cos Q).$$

θ_{11} is valid from $t = TT_{11}$ to $t = TT_{12}$:

$$\theta_{11} = e^{-Ct/2}(A_{11}\cos \omega_3 t + B_{11}\sin \omega_3 t) + \frac{R_{11}}{\omega_{o3}^2} + \frac{X_{11}}{\omega_{o3}^2},$$

$$R = \omega_3(TT_{11}),$$

$$A_{11} = A_{10} - \frac{(R_{10} - R_{11} + X_{10} - X_{11})}{\omega_{o3}^2 e^{-CTT_{11}/2}}(BL_3\sin R - \cos R),$$

$$B_{11} = B_{10} + \frac{(R_{10} - R_{11} + X_{10} - X_{11})}{\omega_{o3}^2 e^{-CTT_{11}/2}}(\sin R + BL_3\cos R).$$

θ_{12} is valid from $t = TT_{12}$ to $t = TT_{13}$:

$$\omega_2 = \frac{\sqrt{4\omega_{o2}^2 - C^2}}{2},$$

$$BL_2 = \frac{C}{2\omega_2},$$

$$S = \omega_3(TT_{12}),$$

$$A_{12} = -\frac{B_{11}}{\omega_2}(\omega_2 \sin S(BL_2 \sin S - \cos S) - \omega_3 \sin S(BL_3 \sin S - \cos S)) + \frac{A_{11}}{\omega_2}(\omega_2 \cos S(\cos S - BL_2 \sin S) + \omega_3 \sin S(\sin S + BL_3 \cos S)) - \left(\frac{R_{11} + X_{11}}{\omega_{o3}^2} - \frac{R_{12} + X_{12}}{\omega_{o2}^2}\right)\left(\frac{BL_2 \sin S - \cos S}{e^{-CTT_{12}/2}}\right),$$

$$B_{12} = \frac{\omega_3}{\omega_2}\left(\frac{A_{11}(\sin S + BL_3 \cos S) + B_{11}(BL_3 \sin S - \cos S)}{(BL_2 \sin S - \cos S)}\right) - A_{12}\left(\frac{\sin S + BL_2 \cos S}{BL_2 \sin S - \cos S}\right).$$

Θ_{13} is valid from $t = TT_{13}$ to $t = TT_{14}$:

$$\Theta_{13} = e^{-Ct/2}(A_{13} \cos \omega_2 t + B_{13} \sin \omega_2 t) + \frac{R_{13}}{\omega_{o2}^2},$$

$$T = \omega_2(TT_{13}),$$

$$A_{13} = A_{12} - \frac{(R_{12} - R_{13} + X_{12})}{\omega_{o2}^2 e^{-CTT_{13}/2}}(BL_2 \sin T - \cos T),$$

$$B_{13} = B_{12} + \frac{(R_{12} - R_{13} + X_{12})}{\omega_{o2}^2 e^{-CTT_{13}/2}}(\sin T + BL_2 \cos T).$$

Θ_{14} is valid from $t = TT_{14}$ to $t = TT_{15}$:

$$\Theta_{14} = e^{-Ct/2}(A_{14} \cos \omega_1 t + B_{14} \sin \omega_1 t) + \frac{R_{14}}{\omega_{o1}^2},$$

$$\omega_1 = \frac{\sqrt{4\omega_{o1}^2 - C^2}}{2},$$

$$BL_1 = \frac{C}{2\omega_1},$$

$$U = \omega_1(TT_{14}),$$

$$A_{14} = -\frac{B_{13}}{\omega_1}(\omega_1 \sin U(BL_1 \sin U - \cos U) - \omega_2 \sin U(BL_2 \sin U - \cos U))$$

$$+ \frac{A_{13}}{\omega_1}(\omega_1 \cos U(\cos U - BL_1 \sin U) + \omega_2 \sin U(\sin U + BL_2 \cos U))$$

$$- \left(\frac{R_{13}}{\omega_{o2}^2} - \frac{R_{14}}{\omega_{o1}^2}\right)\left(\frac{BL_1 \sin U - \cos U}{e^{-CTT_{14}/2}}\right),$$

$$B_{14} = \frac{\omega_2}{\omega_1}\left(\frac{A_{13}(\sin U + BL_2 \cos U) + B_{13}(BL_2 \sin U - \cos U)}{(BL_1 \sin U - \cos U)}\right)$$

$$- A_{14}\left(\frac{\sin U + BL_1 \cos U}{BL_1 \sin U - \cos U}\right)$$

For the second cycle the first term is:

$$\Theta_1 = e^{-Ct/2}(A_1 \cos \omega_1 t + B_1 \sin \omega_1 t) + \frac{R_1}{\omega_{o1}^2},$$

with $V = \omega_1(TT_{15})$.

The new A_1 and B_1 are:

$$A_1 = A_{14} - \frac{(R_{14} - R_1)}{\omega_{o1}^2 e^{-CTT_{15}/2}}(BL_1 \sin V - \cos V),$$

$$B_1 = \frac{(R_{14} - R_1)}{\omega_{o1}^2 e^{-CTT_{15}/2}}(\sin V - BL_1 \cos V).$$

All future terms are the same provided TT_{15} is added to all the times. That is, TT_3 would now be equal to the old $TT_3 + TT_{15}$; TT_4 = old $TT_4 + TT_{15}$, etc.

If ω_{o1} is linear, many of the coefficients simplify considerably:

$$\omega_{o1} = \omega_{o2} = \omega_{o3} = \omega_{o4} = \omega_o,$$

$$BL_1 = BL_2 = BL_3 = BL_4 = b_1,$$

$$\omega_1 = \omega_2 = \omega_3 = \omega_4,$$

A_1 remains equal to $(\theta_o - \frac{R_1}{\omega_o^2})b_1$,

$$A_2 = A_1 - (R_1 - R_2)(b_1 \sin E - \cos E)/\omega_o^2 e^{-CTT_2/2},$$

$$B_2 = B_1 + (R_1 - R_2)(\sin E + b_1 \cos E)/\omega_o^2 e^{-CTT_2/2},$$

$$A_3 = A_2 - (R_2 - R_3 - X_3)(b_1 \sin F - \cos F)/\omega_o^2 e^{-CTT_3/2},$$

$$B_3 = B_2 + (R_2 - R_3 - X_3)(\sin F + b_1 \cos F)/\omega_o^2 e^{-CTT_3/2},$$

$$A_4 = A_3 - (R_3 - R_4 + X_3 - X_4)(b_1 \sin G - \cos G)/\omega_o^2 e^{-CTT_4/2},$$

$$B_4 = B_3 + (R_3 - R_4 + X_3 - X_4)(\sin G + b_1 \cos G)/\omega_o^2 e^{-CTT_4/2},$$

$$A_5 = A_4 - (R_4 - R_5 + X_4 - X_5)(b_1 \sin H - \cos H)/\omega_o^2 e^{-CTT_5/2},$$

$$B_5 = B_4 + (R_4 - R_5 + X_4 - X_5)(\sin H + b_1 \cos H)/\omega_o^2 e^{-CTT_5/2},$$

$$A_6 = A_5-(R_5-R_6+X_5)(b_1\sin L - \cos L)/\omega_o^2 e^{-CTT_6/2},$$

$$B_6 = B_5+(R_5-R_6+X_5)(\sin L + b_1\cos L)/\omega_o^2 e^{-CTT_6/2},$$

$$A_7 = A_6-(R_6-R_7)(b_1\sin M - \cos M)/\omega_o^2 e^{-CTT_7/2},$$

$$B_7 = B_6+(R_6-R_7)(\sin M + b_1\cos M)/\omega_o^2 e^{-CTT_7/2},$$

$$A_8 = A_7-(R_7-R_8)(b_1\sin N - \cos N)/\omega_o^2 e^{-CTT_8/2},$$

$$B_8 = B_7+(R_7-R_8)(\sin N + b_1\cos N)/\omega_o^2 e^{-CTT_8/2},$$

$$A_9 = A_8-(R_8-R_9)(b_1\sin P - \cos P)/\omega_o^2 e^{-CTT_9/2},$$

$$B_9 = B_8+(R_8-R_9)(\sin P + b_1\cos P)/\omega_o^2 e^{-CTT_9/2},$$

$$A_{10} = A_9-(R_9-R_{10}-X_{10})(b_1\sin Q - \cos Q)/\omega_o^2 e^{-CTT_{10}/2},$$

$$B_{10} = B_9+(R_9-R_{10}-X_{10})(\sin Q + b_1\cos Q)/\omega_o^2 e^{-CTT_{10}/2},$$

$$A_{11} = A_{10}-(R_{10}-R_{11}+X_{10}-X_{11})(b_1\sin R - \cos R)/\omega_o^2 e^{-CTT_{11}/2},$$

$$B_{11} = B_{10}+(R_{10}-R_{11}+X_{10}-X_{11})(\sin R + b_1\cos R)/\omega_o^2 e^{-CTT_{11}/2},$$

$$A_{12} = A_{11}-(R_{11}-R_{12}+X_{11}-X_{12})(b_1\sin S - \cos S)/\omega_o^2 e^{-CTT_{12}/2},$$

$$B_{12} = B_{11}+(R_{11}-R_{12}+X_{11}-X_{12})(\sin S + b_1\cos S)/\omega_o^2 e^{-CTT_{12}/2},$$

$$A_{13} = A_{12}-(R_{12}-R_{13}+X_{12})(b_1\sin T - \cos T)/\omega_o^2 e^{-CTT_{13}/2},$$

$$B_{13} = B_{12}+(R_{12}-R_{13}+X_{12})(\sin T + b_1 \cos T)/\omega_o^2 e^{-CTT_{13}/2},$$

$$A_{14} = A_{13}-(R_{13}-R_{14})(b_1 \sin U - \cos U)/\omega_o^2 e^{-CTT_{14}/2},$$

$$B_{14} = B_{13}+(R_{13}-R_{14})(\sin U + b_1 \cos U)/\omega_o^2 e^{-CTT_{14}/2}.$$

CHAPTER IV

APPLICATIONS

This chapter will discuss the uses of this work in evaluating unit data and what can be expected as a general result. It will be divided into four topics to simplify discussion:

1. Unit curves,
2. Computed unit curves,
3. Estimation of unit parameters, and
4. Operational curve estimation.

Graphic plots are generalized to a great degree in order to obtain the most information on a minimum number of plots. There are four different types of graphs presented here. The most numerous type is the "computed unit curves." This is a graph computed from the solution of the equation of motion with certain values of viscous friction (C), forcing function (X), and kinetic friction (R). Since it is possible to convert readily between R and X, they are combined into a function (K) that will be discussed later. Each graph is for a constant C/ω_o with each curve on the graph at a different K. The ordinate of the graph is balance wheel amplitude and the abscissa

is number of cycles from release or zero time. The second type of curve, "unit curves," is identical to the "computed unit curves" except it is a measured curve plotted with data taken from an actual operating unit. This plot will be compared with the "computed unit curves" later in order to obtain the parameters C, X, and R. The other two curves allow any Xn/ω_o^2 to be converted to an equivalent Rx/ω_o^2. Both have as ordinate Rx/ω_o^2; one has an abscissa of X_2/ω_o^2 and the other X_3/ω_o^2 with $\beta = 0$ and $\alpha = 0$, respectively, with individual curves for variations in the duration of X_2 and X_3 where α and β are the angular measure of the duration of the forcing function.

Unit Curves

The "unit curve" is nothing more than a plot of the peak amplitude for each cycle of the balance wheel in radians vs. the number of cycles or time for a specific input torque. The recording begins when the unit is at zero cycles with a maximum amplitude of "overbank" (6.28 radians for the units tested) and allowed to continue until a steady amplitude is reached. The recording is then plotted as an amplitude decay curve to a suitable scale.

The reason for obtaining unit curves is twofold. First, considerable information can be gained about the operating unit with the unit curve alone; and, second, the evaluation of the unit curves in conjunction with

the "computed unit curves" will allow a quick estimate of the relative values of C, X, and R. For instance, if one obtains three unit curves from the unit of interest for input torques of A, 2A, and 3A, they might resemble Figure 5.

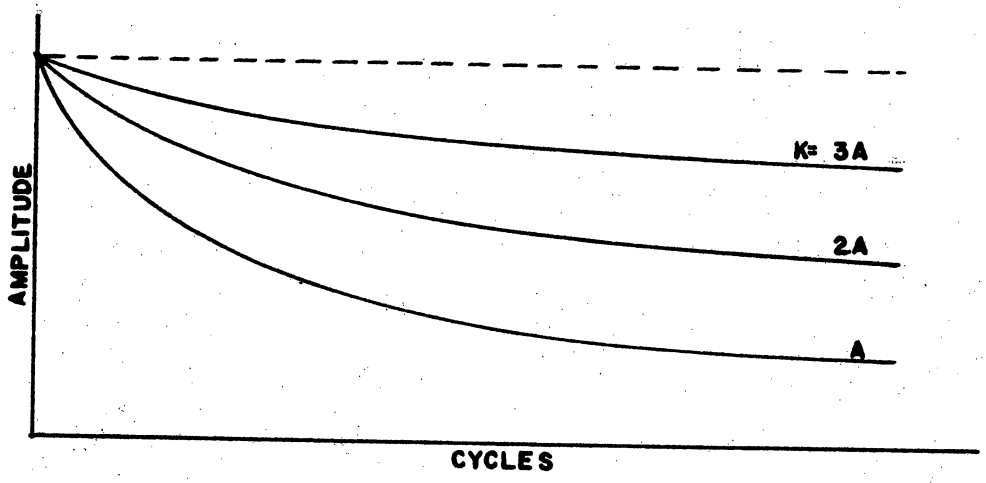

Figure 5. Unit Plot

First, one notices that the change in amplitude between A and 2A is the same as between 2A and 3A (within the tolerance of measurement). Thus, for any torque condition, except those approaching zero amplitude, one can estimate closely the amplitude of oscillation. In this instance, overbank would occur at about 4A. The unit must maintain some minimum amplitude to operate, and near this minimum the unit does not exhibit this linear property necessarily.

The method of measurement of the maximum amplitude

per cycle was by means of a light beam photo-cell arrangement. This was supplied by Sandia Corporation. The light beam to the photo-cell was broken each time a notch in the balance wheel passed between the bulb and the photo-cell. The output was applied to a Hewlett Packard 450A Amplifier and then a CEC 5-124 oscillograph. The results were recorded on light-sensitive paper. There were sixty notches in the balance wheel giving a resolution of plus or minus one notch or plus or minus six degrees in amplitude. The testing procedure was to apply a known torque to the escapement through a test fixture and to displace manually the balance wheel to the overbank condition. The recorder was then started and the balance wheel released. The recording was allowed to continue until a steady oscillation had been reached (for these tests about six seconds). This procedure was repeated for three different torques, and then the number of notches were counted and plotted on graph paper corresponding to the amplitude that number represented. In order to obtain the same representative portion of the cycle, every second set of oscillations was used. To obtain a more accurate amplitude count, the notch under the light source with the balance at zero amplitude was shortened. This short tooth gave less signal and was easy to distinguish as depicted in Figure 6.

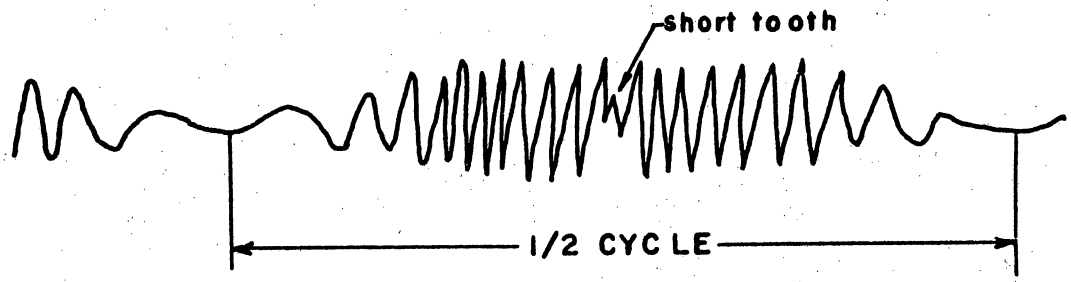

Figure 6. Recorder Chart

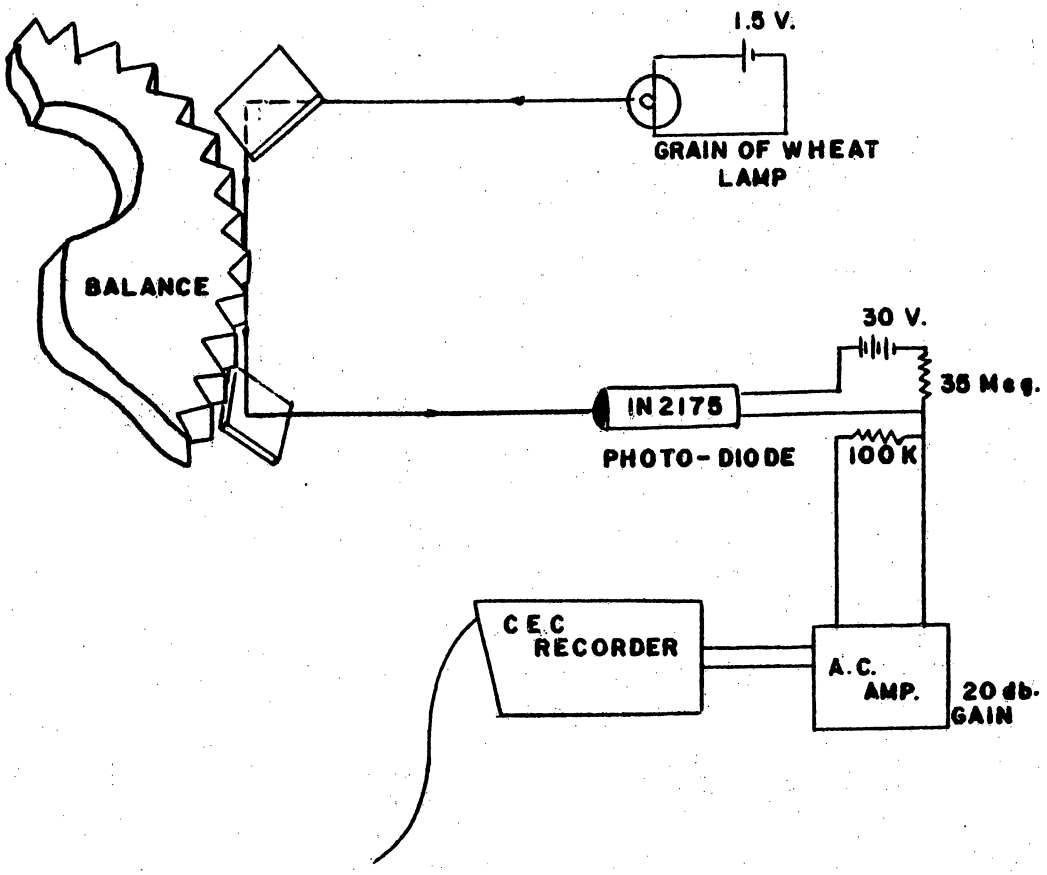

Figure 7. Schematic of Amplitude Measuring Equipment

PLATE I AMPLITUDE TEST EQUIPMENT

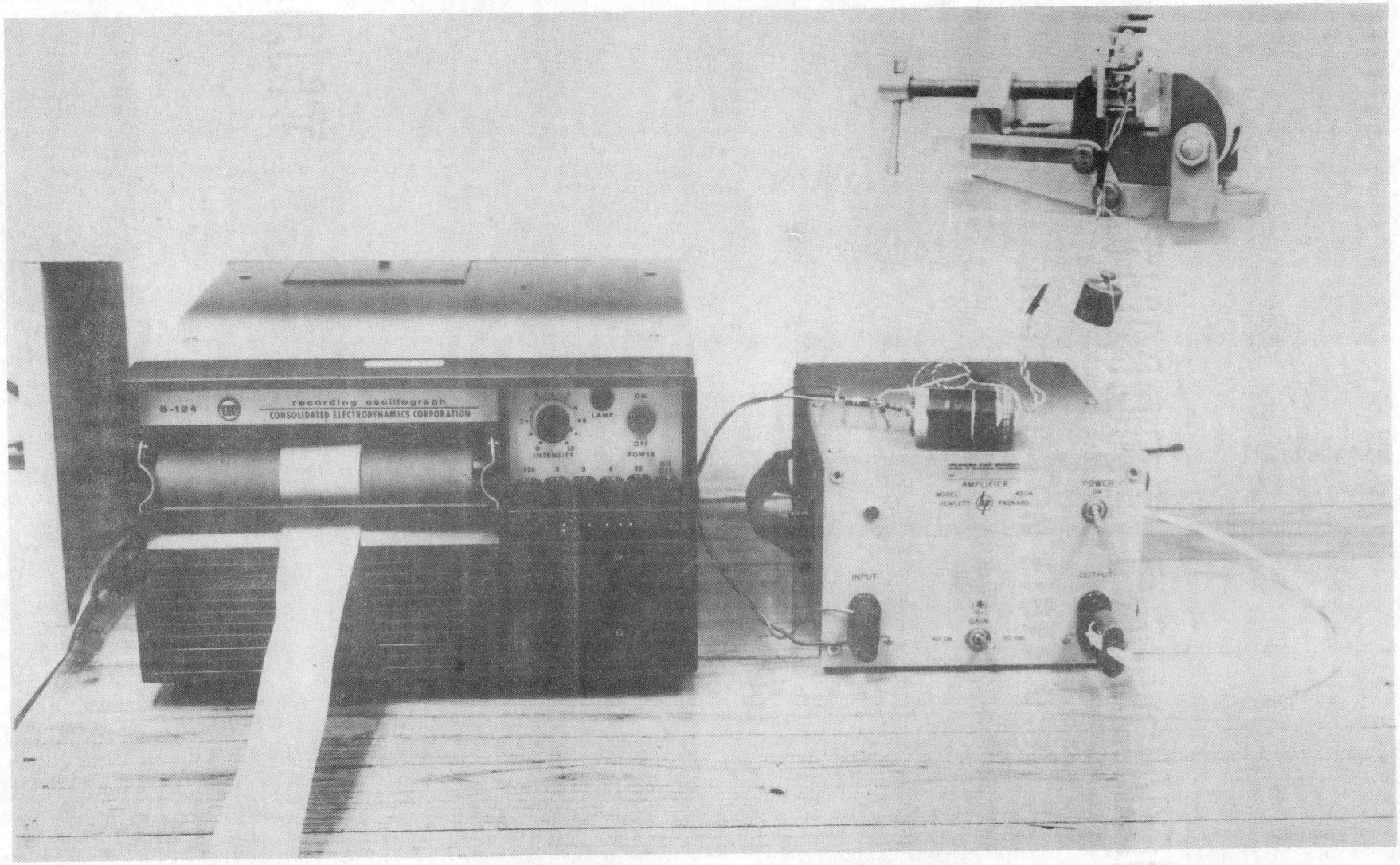

PIATE II TEST FIXTURE AND UNIT

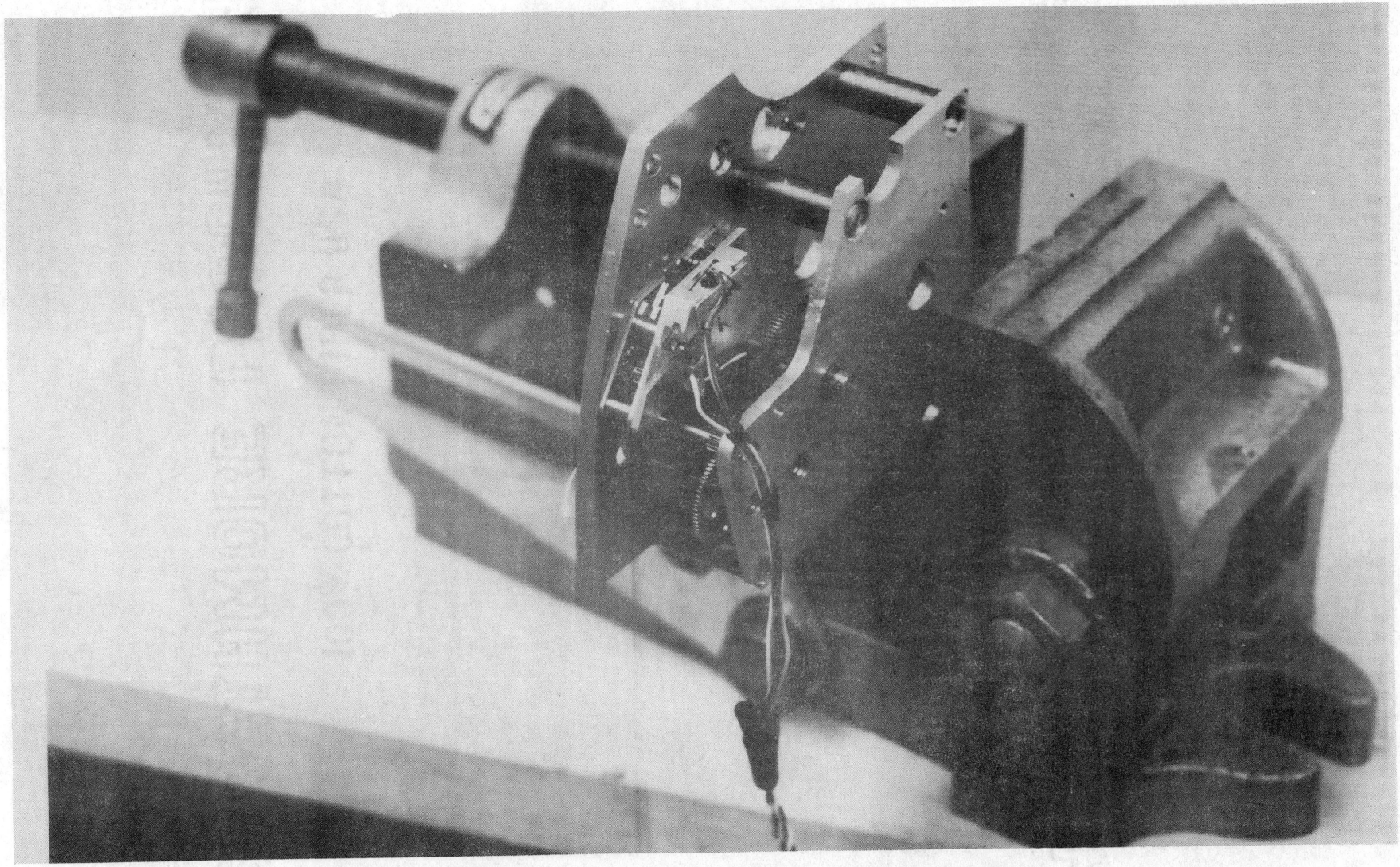

PIATE III LIGHT AND PHOTO-CELL ASSEMBLY

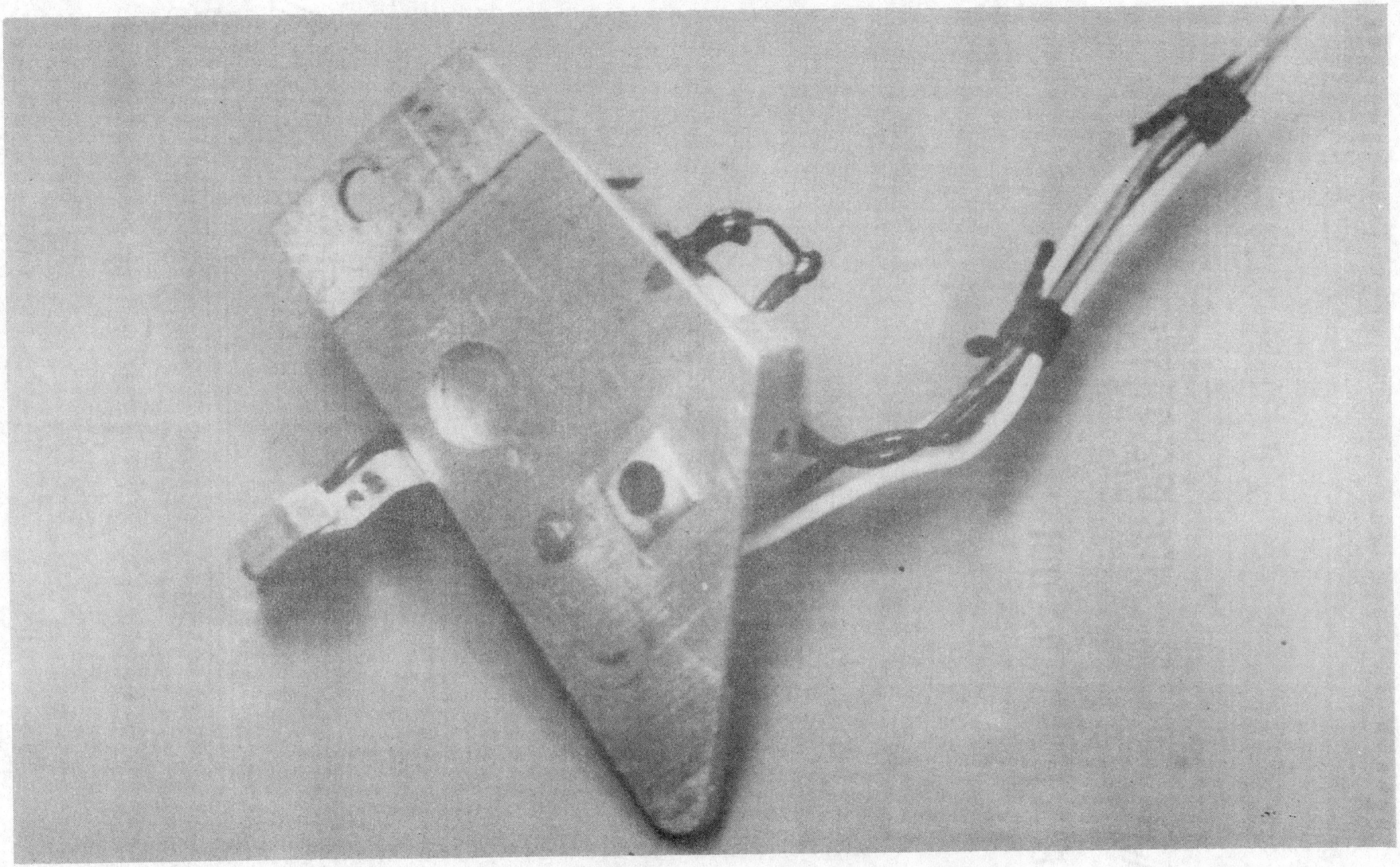

Computed Unit Curves

These curves are similar to the "unit curves" except they are generated from the solution of the equation of motion discussed in Chapter III. All of the computed unit curves used with this study and included in the Appendix C were generated with the ten-step computer program of Appendix B. This program is used to compute the positive maximum value of the oscillation at the same point in each cycle along with the number of cycles and the values of C/ω_o, R/ω_o^2, X_3/ω_o^2, and X_2/ω_o^2 and to print this information for each cycle. From this it is easy to plot the computed unit curves. Since R/ω_o^2 times some constant is equal to X_3/ω_o^2 times some other constant and is also equal to X_2/ω_o^2 times still another constant, it was expedient to combine these constants and plot a combined single value K rather than various values of each of the constants.

Thus, a "computed unit curve" with a specific C/ω_o and a certain K can be obtained by setting $R/\omega_o^2 = 0$; $X_2/\omega_o^2 = 0$; and $X_3/\omega_o^2 = A$. This same curve can also be obtained by setting $R/\omega_o^2 = -B$; $X_2/\omega_o^2 = 0$; and $X_3/\omega_o^2 = 0$. A third method of obtaining this same identical curve would be setting $R/\omega_o^2 = 0$; $X_2/\omega_o^2 = -D$; and $X_3/\omega_o^2 = 0$. Since R/ω_o^2 acts over the entire cycle and X_3/ω_o^2 and X_2/ω_o^2 act only during a short portion of the cycle (forcing and unlock), it becomes necessary to have some equivalence

factor or graph factor to convert A to B and B to C depending on the duration of X_2 and X_3. All the "computed unit curves" in this document, unless specifically noted, were computed with A = K and $R/\omega_o^2 = X_2/\omega_o^2 = 0$ with a duration of X_3 equal to plus and minus 0.2786896 radians. Thus, the graph factor on K is 3.650. This means that if K is divided by 3.65, B is obtained. Then by means of the other two types of graphs one can convert to any duration on X_2 and X_3, and thus use these computed unit curves for escapements other than the one discussed here.

Figure 8 is a diagram of a relative comparison of X_2, X_3, and R. One must adhere to the sign convention as shown or erroneous computation will result.

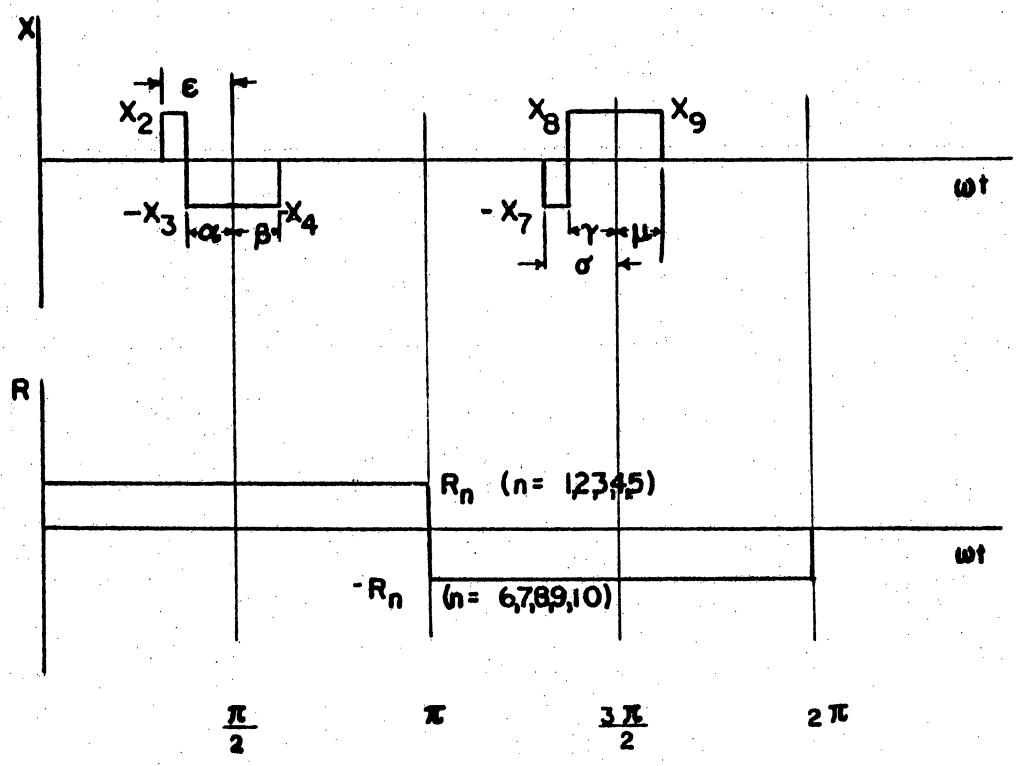

Figure 8. Ten Step Division of X and R

All computed unit curves assume

$$X_2 = -X_7, \qquad X_3 = X_4 = -X_8 = -X_9,$$

$$\mu = \sigma, \qquad \alpha = \beta = \gamma = \mu,$$

$$R_1 = R_2 = \ldots = R_5 = -R_6 = -R_7, \ldots = -R_{10},$$

and ω_o is constant over the entire range.

Estimation of Unit Parameters

Certain values over and above the "unit curves" just discussed will be required for the estimation of unit parameters by the graphical method. The method will be outlined by means of an actual example based on a test unit in this study. This method will entail the use of all the curves previously discussed in this chapter in addition to values that either can be measured from the unit or computed from the detailed drawings of the unit. These include draw angle (0.3551 radians) and power angle (plus or minus 0.2787 radians). The draw angle is defined as the angle the balance turns during unlocking the escape wheel. The power angle is defined as the angle through which the balance turns during the time the forcing functions act; this angle is measured from "0" beat position both plus and minus.

The first step after the above values have been determined is to estimate C/ω_o. This is done by matching the above "unit curves" to some "computed unit curve" as closely as possible. It would be rather unique if a

"unit curve" should fall exactly on a "computed unit curve;" therefore, good judgment must prevail in matching the curves. This is also another good reason for using several different torques when taking data for the "unit curves." This provides an opportunity that one of the curves is more likely to approximate a computed unit curve. Should it be obvious that the unit curves are out of the range of those curves available, other curves can be generated rapidly for different C/ω_o values. This was discussed under the second topic in this chapter. Figure 9 shows the match of the unit curve with a "calculated or computed unit curve" where $C/\omega_o = 0.0515$. This curve was generated especially to show a close match condition. From the time marks on the recording paper the frequency of oscillation is 2.574 cycles per second or $\omega_1 = 16.173$ rad./sec. From the solution of the equation of motion, Chapter III,

$$\omega_1 = \frac{\sqrt{4\omega_o^2 - C^2}}{2},$$

and with $C/\omega_o = 0.0515$, C and ω_o are found to be 0.833 and 16.174, respectively.

Now it is necessary to determine the K value for the curve. Although K and C are not independent, once C has been found any change in K is linear with a change in X or R. It is permissible to interpolate in the flat region of the curves without appreciable error. Thus K = 0.214 for the 100 gm load. K is a combined function consisting

of the forcing function (X_3/ω_o^2), the kinetic friction function (R/ω_o^2), and the negative forcing function (X_2/ω_o^2). This negative forcing function occurs during draw or unlock when the balance is doing work on the lever.

K_R is found by dividing K by the graph factor,

$0.214/3.65 = K_R = 0.0586$.

By measurement, the particular loading fixture which was used in these tests was found to inpart a torque of 0.007155 in-gms to the balance during unlock and 0.06215 in-gms during power for every 100 gms load on the input to the fixture. This information must be determined for each fixture.

$X_2 = M_2/I$ where M_2 is the input to the balance during the unlocking interval and I is the polar moment of inertia of the balance

$$X_2 = \frac{0.007155 \text{ in-gms} \times 2.205 \text{ lbs.}}{1000 \text{ gms } 1.10 \times 10^{-7} \text{ in \# sec}^2}$$

$X_2 = 143.41$

$X_3 = M_3/I$ where M_3 is input to balance during power or driving phase

$$X_3 = \frac{0.06215 \times 2.205}{1000 \times 1.10 \times 10^{-7}} = 1245.8$$

or $X_2/\omega_o^2 = .5\,49$ and $X_3/\omega_o^2 = 4.77$.

After determining from drawings or measurement that the draw angle is 0.3551 radians and the power is plus or minus 0.2787 radians, one refers to Figure 10 where

$\alpha = 0.2787$, $\beta = 0$, and $\varepsilon = 0.2787 + 0.3551$ or 0.6338. ε is the angular measurement to the beginning of the unlock interval. The curve of interest lies approximately on the line (0.3, 0, 0.60). The curve label sequence is $(\alpha, \beta, \varepsilon) \sim (0.3, 0, 0.6)$. Thus, at $X_2/\omega_o^2 = 0.549$, a corresponding value of R_{X_2}/ω_o^2 is 0.073.

Likewise, on the second curve (Figure 11) find at X_3/ω_o^2 is 4.77, R_{X_3}/ω_o^2 is 1.30. The curve to use in this instance is approximately one-half the distance between (0, 0.25, 0.25) and (0, 0.3, 0.3) where α is 0.2787 and β is 0.2787. Other relevant computations are

$$R_{X_3}/\omega_o^2 - R_{X_2}/\omega_o^2 - R/\omega_o^2 = K_R,$$

$$1.30 - 0.073 - R/\omega_o^2 = 0.0586,$$

or $R/\omega_o^2 = 1.168$ and $R = 305.546$.

$R_o/I = R$, $R_o = 3.36 \times 10^{-5}$ #in/rad.

$R = 305.546$, $\omega_o = 16.174$,

$X_2 = 143.41$, $\omega_1 = 16.173$,

$X_3 = 1245.8$,

$C = 0.833$.

These values substituted into the solution of the equation of motion would lead to the "computed unit curve" as shown in Figure 9. A family of curves could now be generated by changing the input load and thus varying X_2 and X_3.

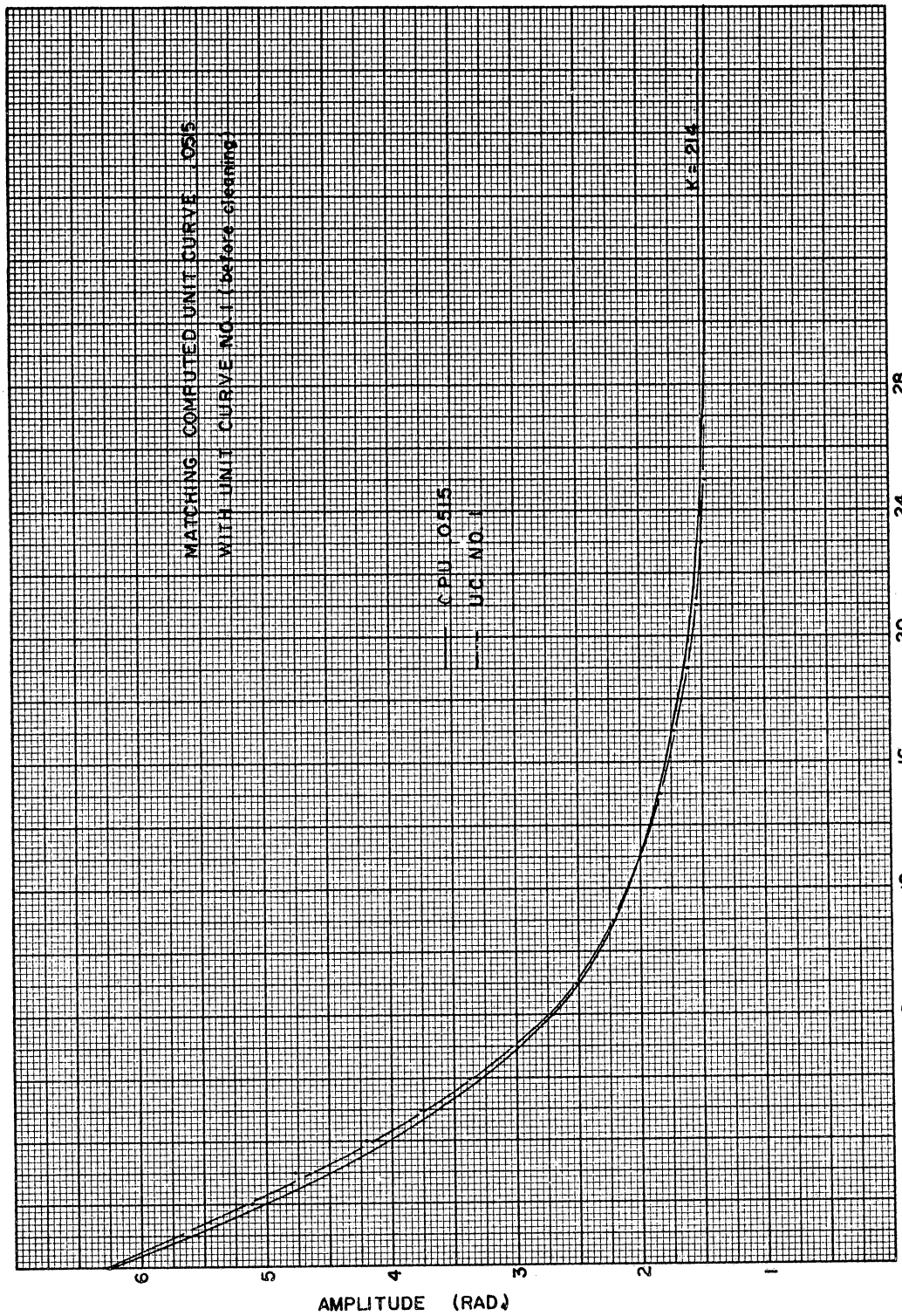

Figure 9. Matching Computed Unit Curve 0.055 with Unit Curve No. 1

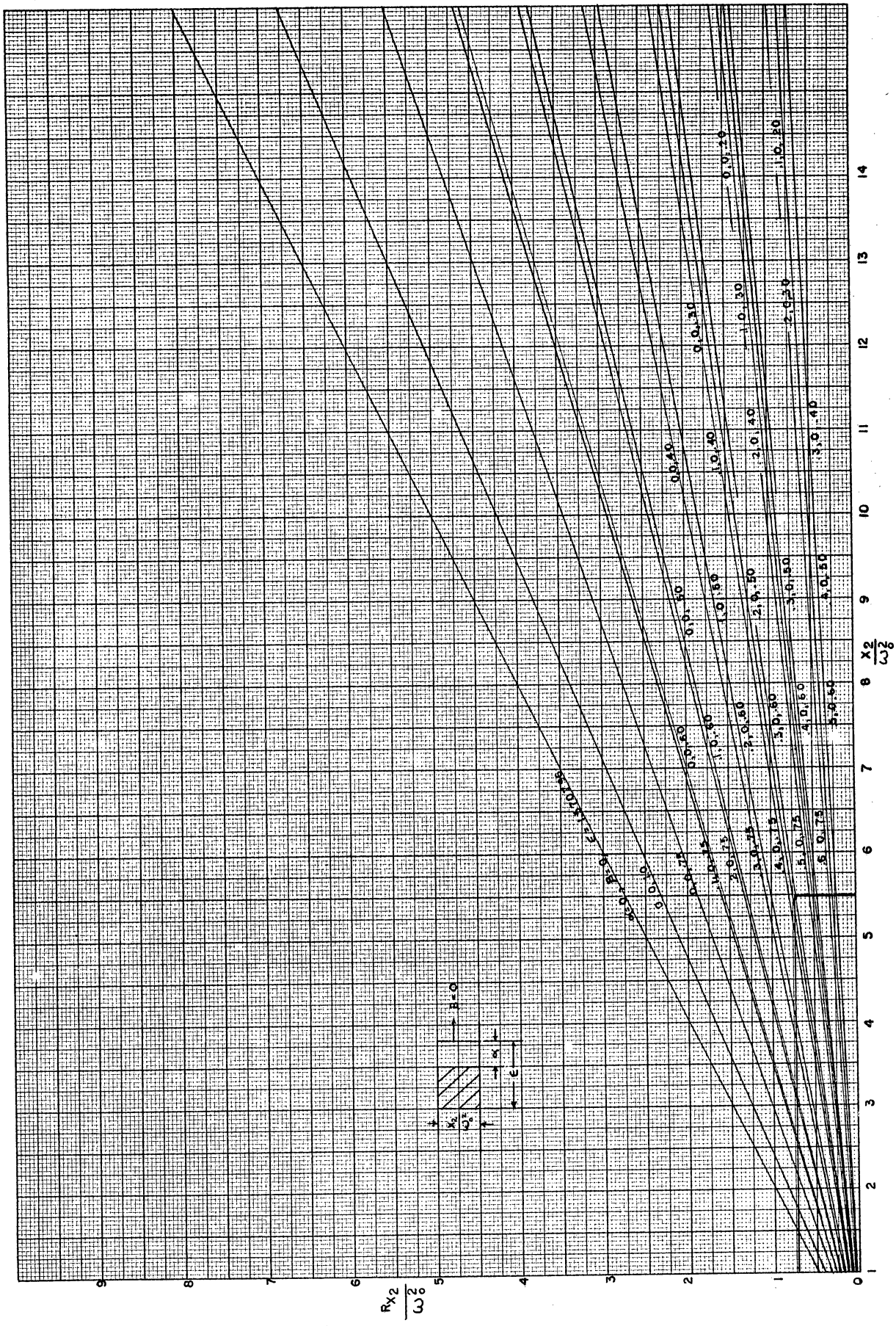

Figure 10. Conversion Chart for X_2/ω_o^2

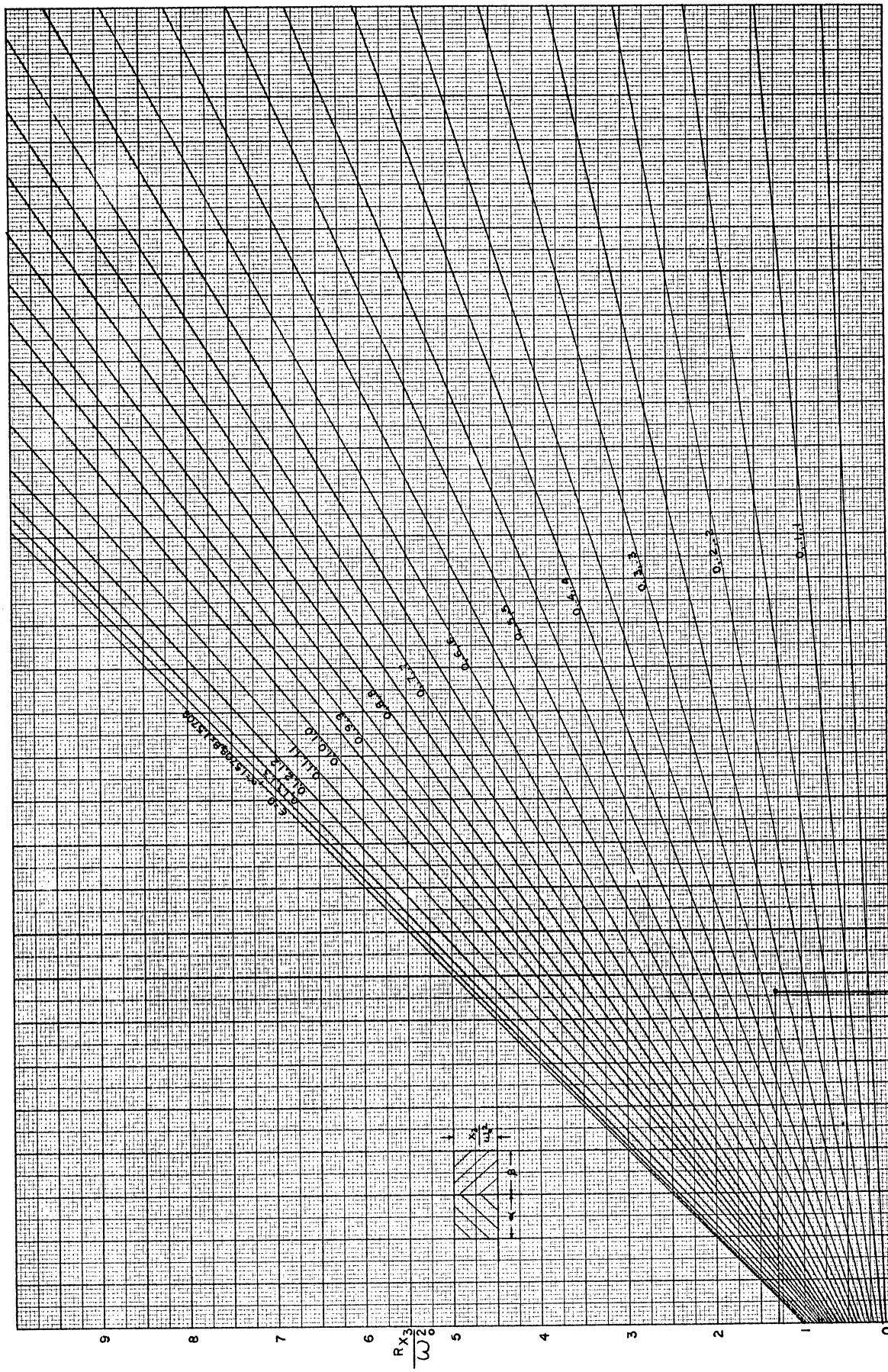

Figure 11. Conversion Chart for X_3/ω_0^2

Operational Curve Estimation

The family of curves discussed above are for a specific C and a varying input torque. Many times it will be necessary to estimate how a change in R and C will affect the resultant operation of the unit. There are two approaches to estimating this effect. The simplest, assuming computer time is available, is to put the new values in the solution to the equation of motion and compute new curves. If this method is used, five data cards need to be punched with the following values containing no more than 10 digits each:

Card 1: α, β, γ, μ, C, θ_o, ω_o;

Card 2: μ, σ;

Card 3: R_1, R_2, R_3, R_4, R_5;

Card 4: $-R_6$, $-R_7$, $-R_8$, $-R_9$, $-R_{10}$;

Card 5: X_2, $-X_3$, $-X_4$, $-X_7$, X_8, X_9.

For the sample problem they would be as follows:

.2787 .2787 .2787 .2787 .833 6.28 16.174

.6338 .6338

305.546 305.546 305.546 305.546 305.546

-305.546 -305.546 -305.546 -305.546 -305.546

143.41 -1245.8 -1245.8 -143.41 1245.8 1245.8

In some instances a program cannot be computed and yet there is need to know what should be expected with a change in a parameter. A change in R is easy to evaluate. One simply computes the new R/ω_o^2; finds the difference

between the old and new R/ω_o^2; multiplies the change by 3.65; and applies it to the known K by addition. This value will be the new condition for the unit, and the new amplitude will be the steady-state amplitude for the unit under these conditions. A change in C will not only change the decay time characteristics, but also it will change the amplitude of oscillation. By the use of Figure 12, it is possible to estimate the change in amplitude caused by a change in C. The abscissa is C/ω_o and the ordinate is a decimal multiplication factor to be applied to the amplitude for correction. For instance, if C/ω_o was previously 0.040 and the new C/ω_o was 0.060, it would be expected that the amplitude would decrease by 0.83/1.2 x old amplitude; thus, the new amplitude is 4.20 x 0.83/1.2 = 2.835.

At times the numerical values of C, X, and R will not be important but rather their relation to one another will be most important. These methods outlined herein offer a means of computing the numerical values of C, X, and R if desired. The operational characteristics of the units can be determined by the graphical means discussed without numerical computation of these values.

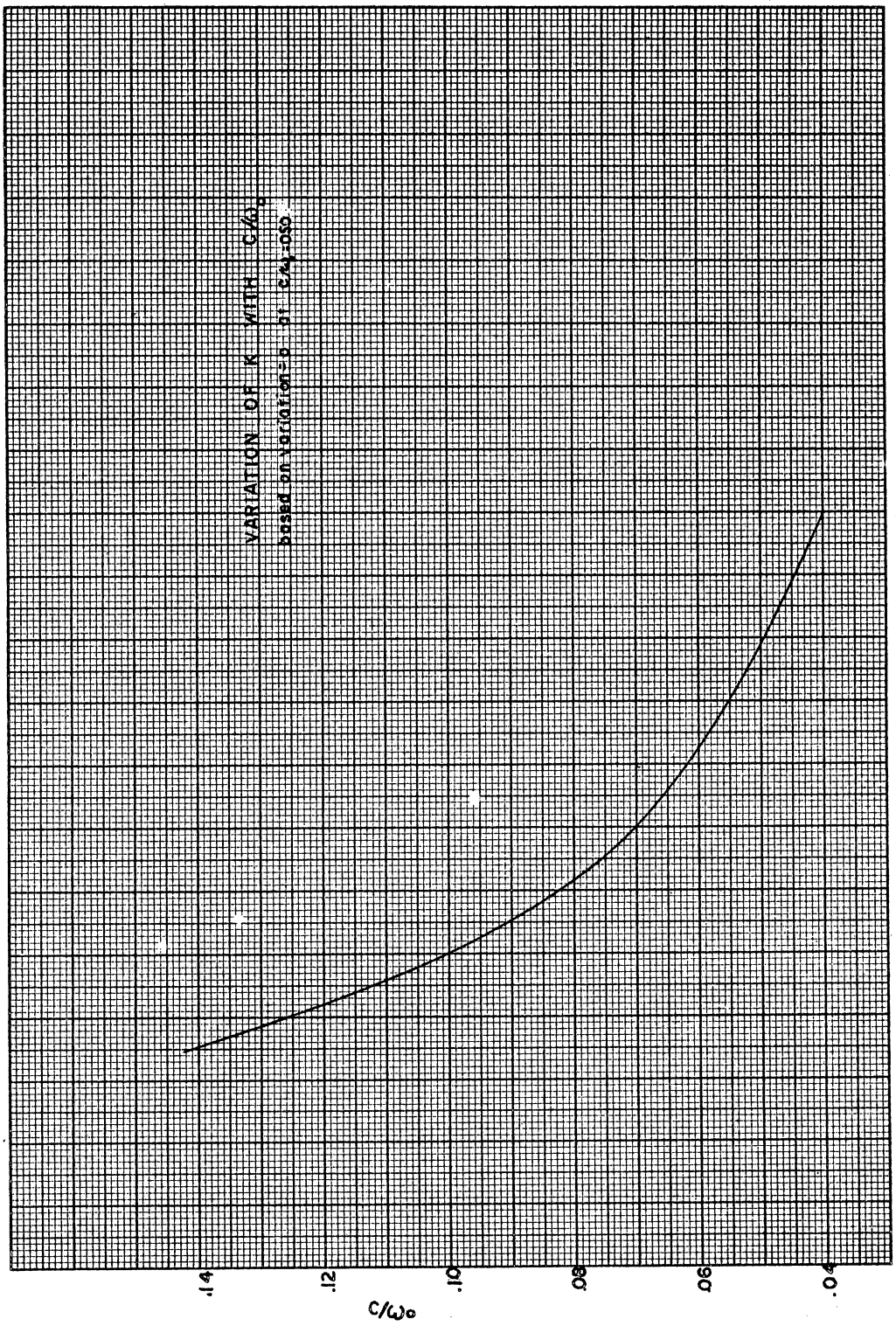

Figure 12. Variation of K with C/ω_o

CHAPTER V

COMPARISON OF RESULTS

These experimental results are based on the test data from five 1321-type escapements supplied by Sandia Corporation. These units, although packaged differently, are similar in size and construction to the jeweled-lever escapement used in a Hamilton Railroad Watch. The basic differences are an uncompensated beryllium copper balance wheel, a different hairspring, increased diameter balance and escape wheel pivots and beryllium copper balance and escape wheel bushings. The units were from obsolete timers that had different manufacturing dates and had been subjected to varying unknown environments. The units were numbered one through five. Units one through three appeared to be of similar design and construction. Unit four was of a later design and included Electrofilmed escape wheel teeth, pallet fork, and bushings. Unit five was assembled at Oklahoma State University from spare parts and, in general, seemed to exhibit freer motion than the other units. The only noticeable mechanical difference between unit five and the first three units was a decreased lock angle.

Prior to testing, the units were placed in an electrosonic watch cleaning machine and allowed to remain during a standard watch cleaning cycle using L and R watch cleaning solution. The units were then placed in the test fixture and allowed to operate without lubricant under a 200 gm load for approximately thirty minutes prior to obtaining test data. It was observed that readings obtained shortly after cleaning were not consistent with readings taken after this "run in" time had elapsed. By and large, results of early readings indicated a smaller C. After this run-in operation, readings were taken for three fixture loads. A variation in amplitude of plus or minus 0.104 radians would be considered as the same amplitude since the sensitivity of amplitude measurement was only as accurate as plus or minus one tooth on the balance wheel. This amounts to about 1.67 percent of the overbank amplitude. The matching results are shown in Figures 13, 14, 15, 16, and 17 with Table I containing the calculated values for X, R, and C.

C varies over a reasonably large range -- 0.757 to 1.431 -- but this could be expected from the non-homogeneity of the sample of units tested here. Once the amplitude of units tested reached a constant value, the difference between computed data and measured data is indistinguishable. Thus the analytical prediction of linearity with load is established and will allow

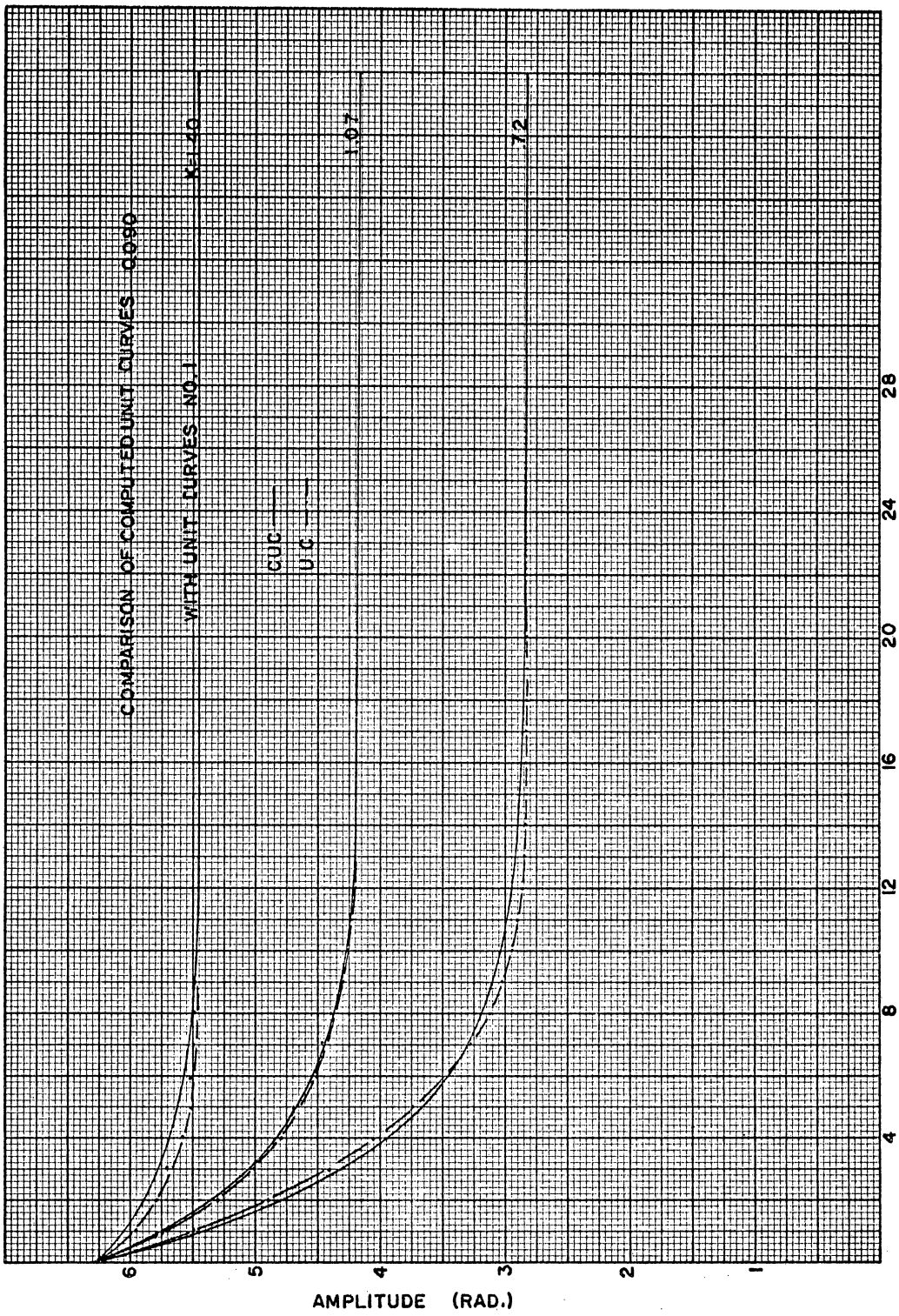

Figure 13. Comparison of Computed Unit Curves 0.090 With Unit Curves No. 1

Figure 12. Comparison of Combined Unit Curves 0.080 Mfd Unit Curves No. 1

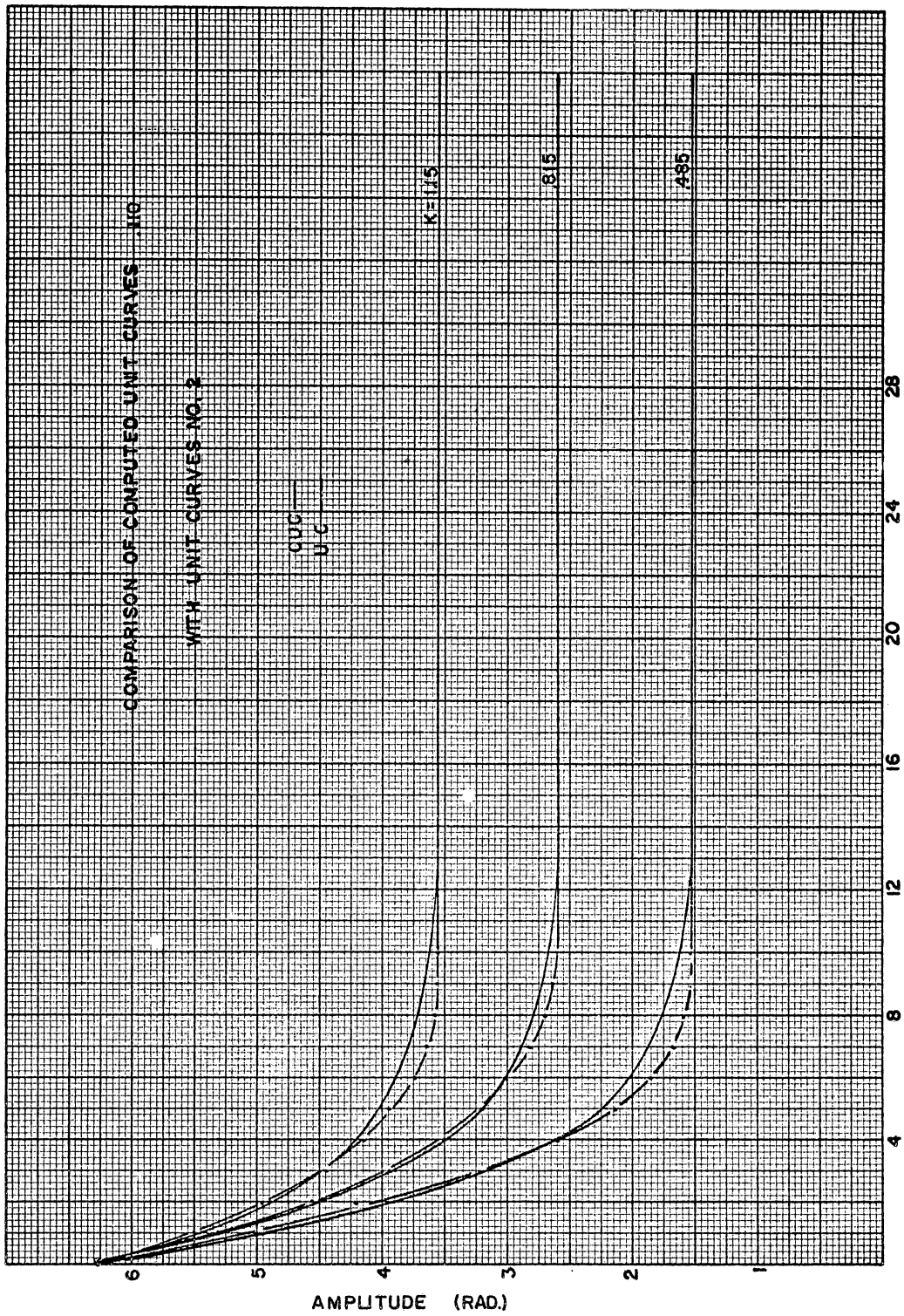

Figure 14. Comparison of Computed Unit Curves 0.110 With Unit Curves No. 2

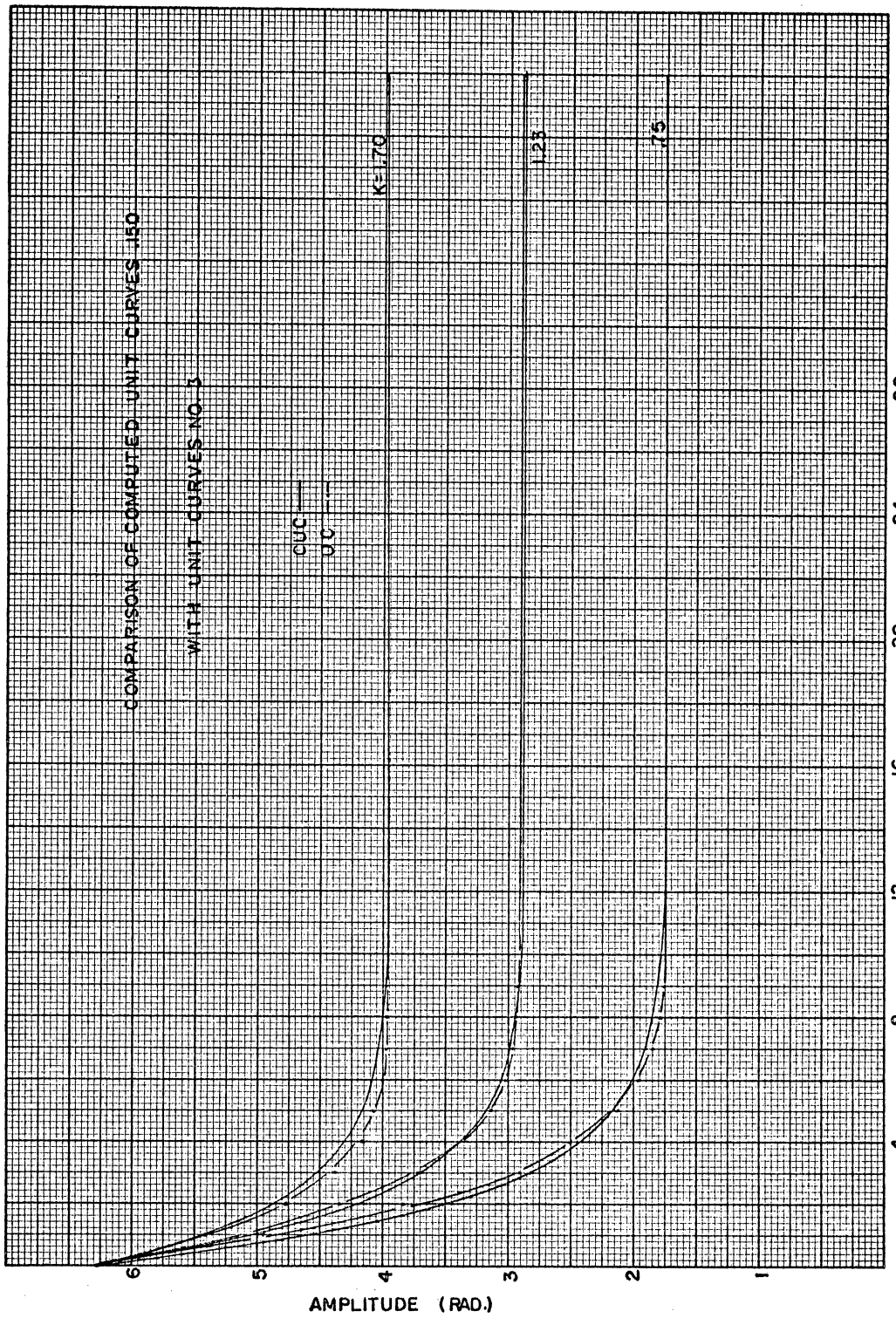

Figure 15. Comparison of Computed Unit Curves 0.150 With Unit Curves No. 3

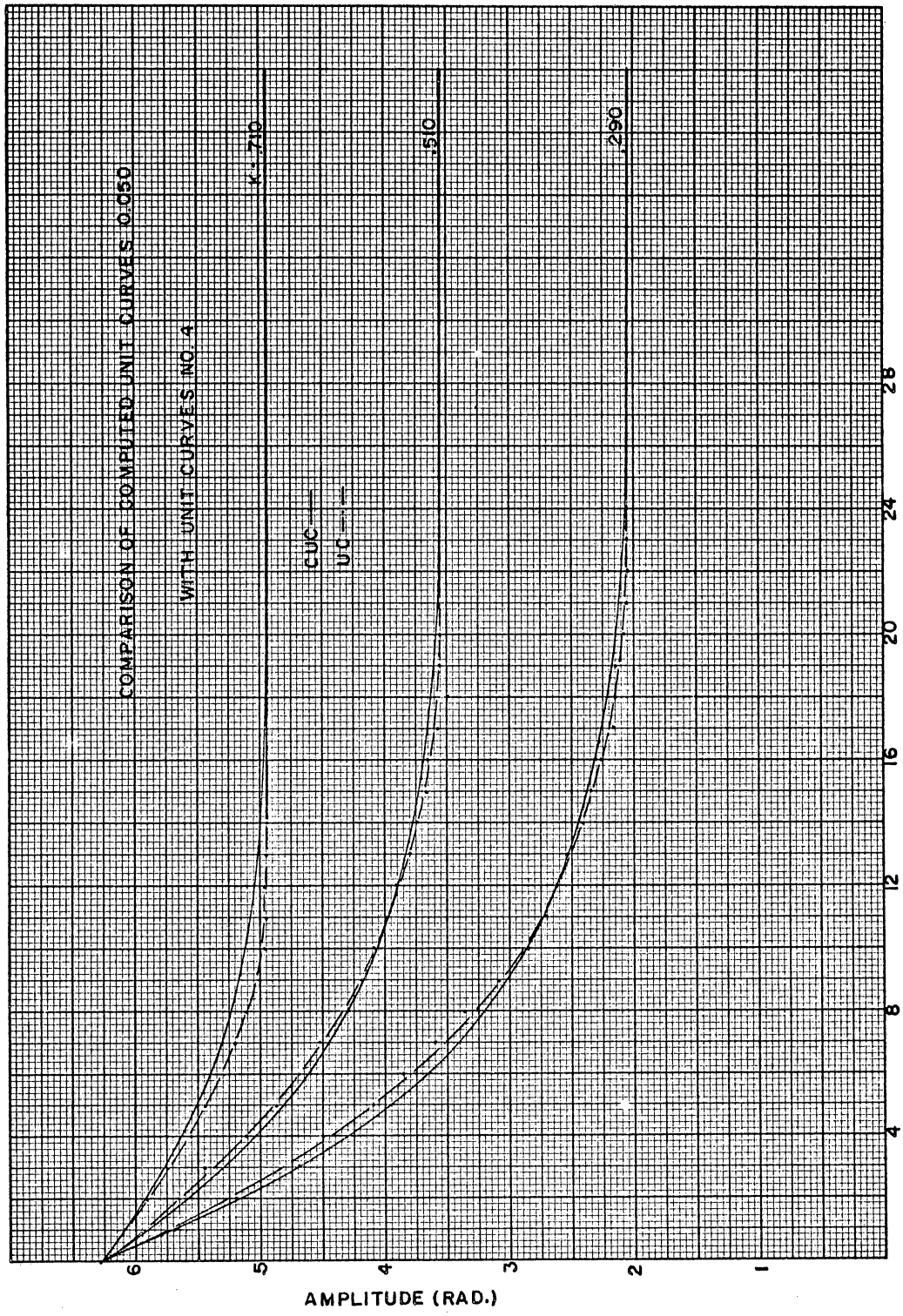

Figure 16. Comparison of Computed Unit Curves 0.050 With Unit Curves No. 4

Figure 15. Comparison of Computed Unit Curves 0.020 with Curves No. 4

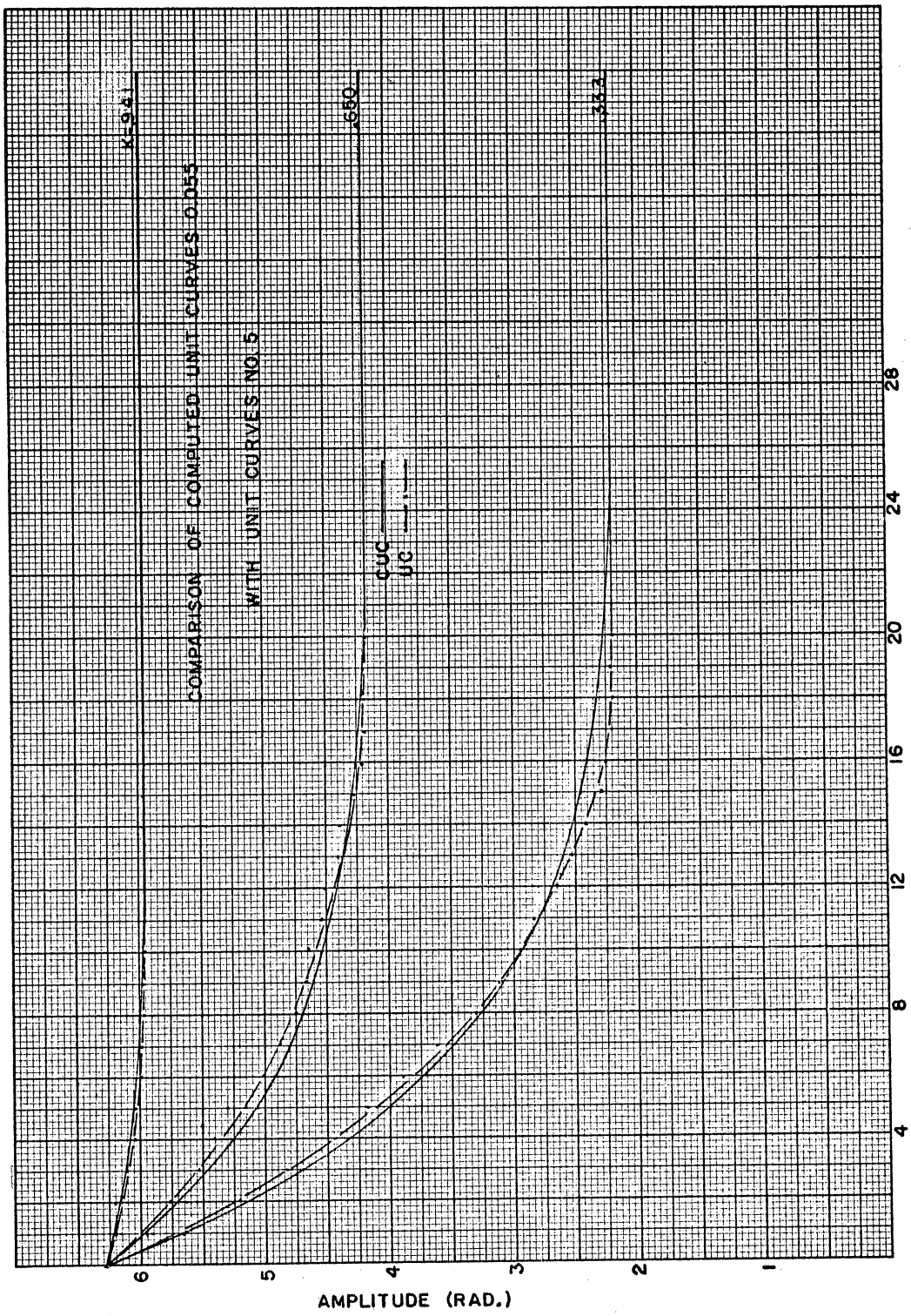

Figure 17. Comparison of Computed Unit Curves 0.055 With Unit Curves No. 5

TABLE I

UNIT CURVE COMPARISONS

Unit No.	ω_1	C/ω_o	ω_o	C	ε	α or β	R	X_2	X_3	K
1	15.707	0.090	15.90	1.431	0.633	$\pm$0.278	965.482	473.070	4,119.339	0.720
							1981.859	946.140	8,238.678	1.070
							3022.290	1419.210	12,358.017	1.400
2	15.457	0.110	15.48	1.703	0.576	$\pm$0.262	932.640	473.070	4,119.339	0.485
							1875.584	946.140	8,238.678	0.815
							2817.809	1419.210	12,358.017	1.150
3	15.707	0.150	15.78	2.367	0.612	$\pm$0.280	980.015	473.070	4,119.339	0.750
							2027.762	946.140	8,238.678	1.230
							3028.122	1419.210	12,358.017	1.700
4	15.142	0.050	15.15	0.757	0.620	$\pm$0.288	524.522	232.530	2,059.664	0.290
							1046.292	473.070	4,119.339	0.510
							1573.109	709.600	6,179.003	0.710
5	15.143	0.055	15.15	0.833	0.506	$\pm$0.244	439.167	236.530	2,059.664	0.333
							1324.385	709.600	6,179.003	0.650
							2196.290	1182.670	10,298.342	0.941

operating characteristic prediction. Prior to the time the amplitude reaches a constant, the closest match shows a certain amount of variation. The characteristic of this variation for a good match between a computed unit curve (CUC) and a unit curve (UC) is that the UC has a lower decay rate than the CUC over the first few cycles and a greater decay rate than the CUC as the unit approaches a constant amplitude. A better match can be seen in Figure 18 where C has been allowed to increase at an arbitrary preset rate depending on the value of $e^{-Ct/2}$. In the upper curve C varied from 0.151 to 0.175 and in the lower curve C varied from 0.140 to 0.163. For a value of $e^{-Ct/2}$ greater than 0.15, C increased three percent per cycle. For a value of $e^{-Ct/2}$ less than 0.150 and greater than 0.03, C increased 1.5 percent per cycle. For a value of $e^{-Ct/2}$ less than 0.03 and greater than 0.005, C increased 0.5 percent per cycle and $e^{-Ct/2}$ less than 0.005, C remained constant. Thus, there is apparently a slight nonlinearity in the damping coefficient with velocity. When the amplitude is high, the average velocity is high. As the amplitude decreases the velocity decreases and the friction increases. The explanation of the phenomena of curve seems reasonable since an increase in friction is a common occurrence in nature with a decrease in velocity in such ordinary things as a fiddle string. It also agrees with the deduction of Doctor Glaser in the article on

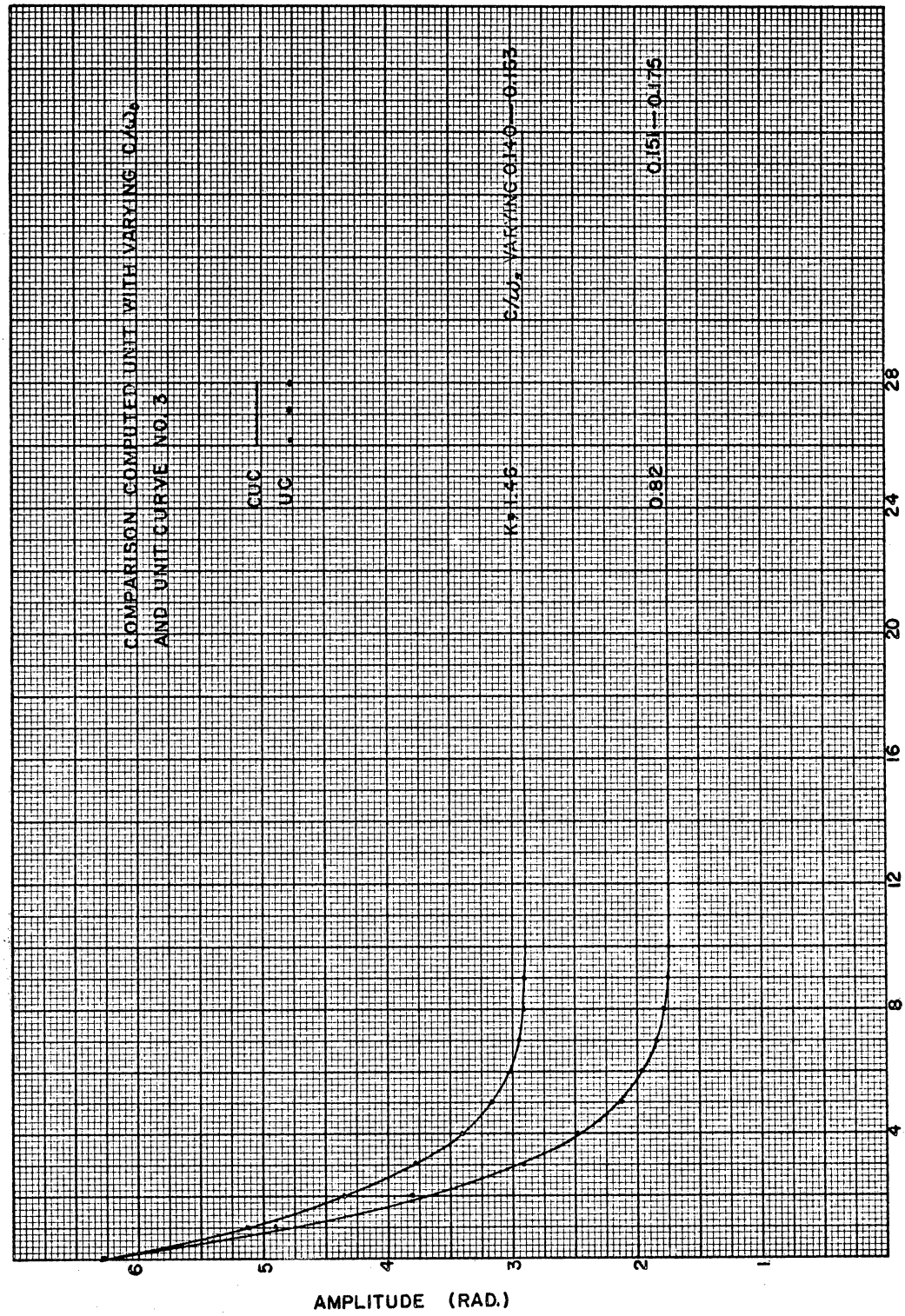

Figure 18. Comparison Computed Unit With Varying C/ω_o And Unit Curve No. 3

measuring escapement motions.[9] In general, the curves are in agreement, offering support to the analytical analysis.

CHAPTER VI

LIGHT LOAD SLIDING FRICTION TESTS

Test Approach

The friction tests were undertaken because test data are almost nonexistent and because friction magnitude and its dependence on velocity have an influence on the mathematical model as well as on the manipulation of the model.

In order to perform this test, equipment was constructed whereby the velocity could be varied and different forces could be applied. The basic apparatus is shown in Figure 19. In order not to disturb the

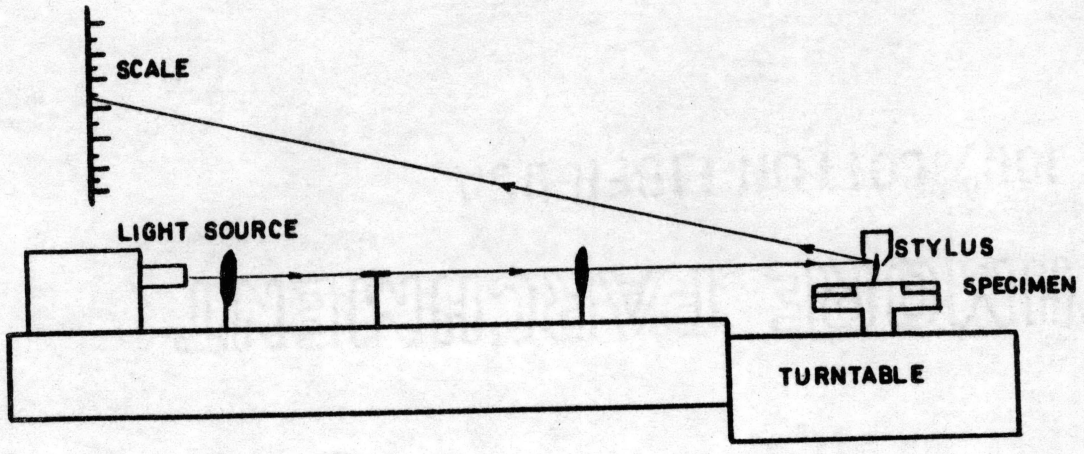

Figure 19. Friction Test Fixture

system with the measuring apparatus, an optical system of measurement was used. Details and physical features are illustrated in the drawings and photographs in the test equipment section of this chapter.

One of the two materials to be tested was formed in a round disc and the other in the shape of a pallet stone from a watch. The disc was attached to the turntable. The pallet stone was attached to a holder that was suspended on a fine torsion wire. The wire was then suspended from a supporting device that was carefully balanced and damped by a viscous damper. If a weight was applied to the supporting device, the pallet-shaped piece came into contact with the rotating disc. The more friction and weight, the more the pallet stone tended to rotate the torsion wire. As the torsion wire rotated, a mirror on the wire was rotated which in turn deflected a beam of light proportional to the amount of rotation. The amount of deflection of the beam of light was measured by a calibrated scale. By proper zero calibration while the disc was not rotating, it was possible to calculate from the light beam deflection the sliding friction force for small normal forces. The tests were performed using aluminum, stainless steel, and high carbon steel plates and a synthetic ruby pallet stone.

The results indicated (Fig. 20), with the velocities normally found in this type of device (3 to 10 f/s), that there was no appreciable variation with velocity.

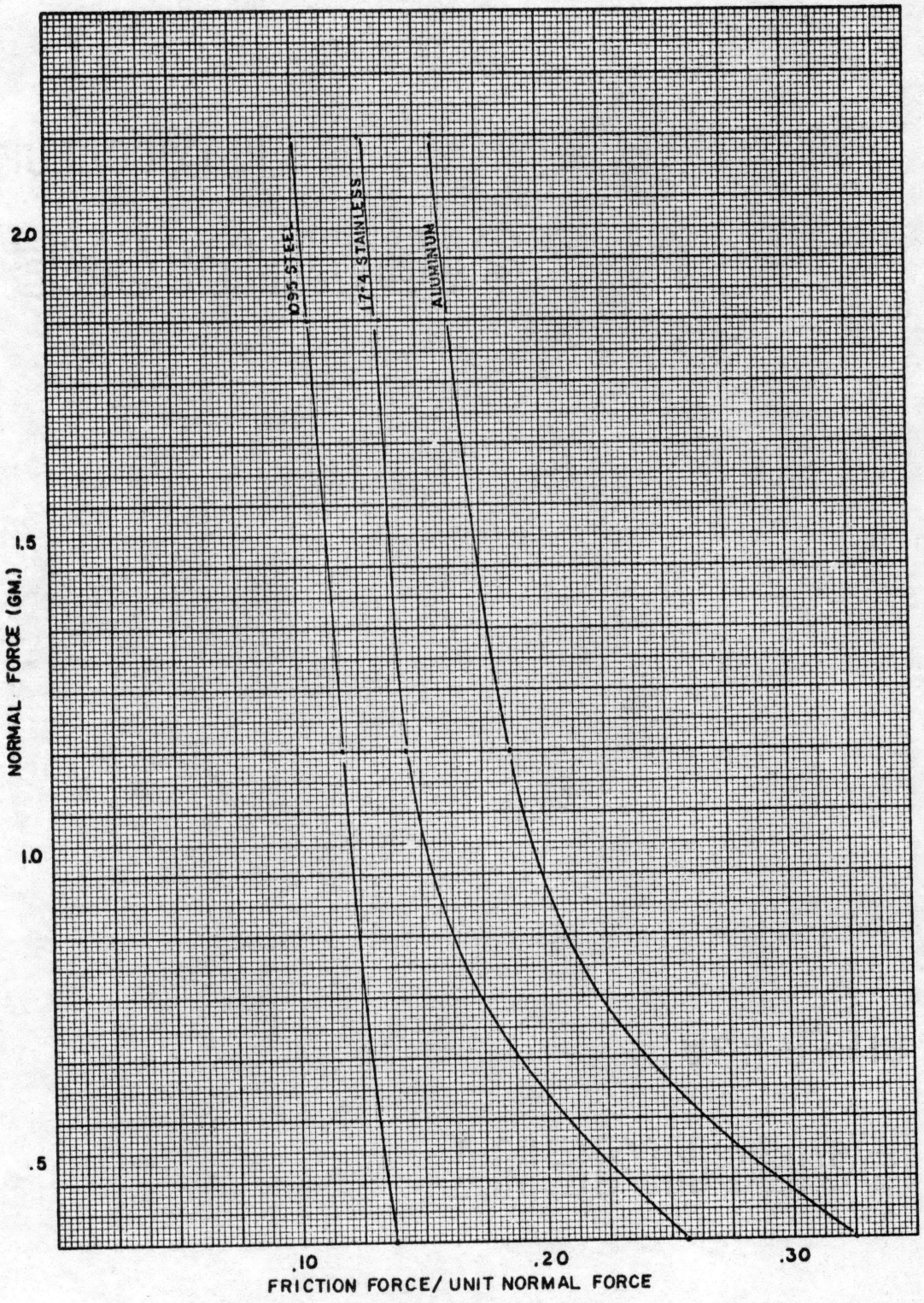

Figure 20. Sliding Friction Curves

There was, however, a slight change of the friction coefficient with a change in the normal force.

Standard data are not readily available for these combinations of materials; therefore, some interpretation must be considered. The data, at least for the hard steel, is within a reasonable approximation of steel to steel data. The actual comparisons for these tests are as follows:

	Ruby Pallet at a Load of 2.2 grams	Standard data steel-steel
1095 steel (hard)	0.100	0.15-0.4[12]
17-4 PH stainless	0.125	
aluminum	0.160	

The differences might have been caused by the high surface finish (less than 8 rms) and a difference of surface contact. Both of these can have considerable effect on the coefficient of sliding friction. The reference data tests were made using a small sphere against a plate and these tests were made using a cylindrical surface against the plate.

All tests were made with the surfaces cleaned in acetone and run dry. Surface finish was less than 8 rms on the plates and on the pallet. The pallet had a cylindrical-shaped end (line contact).

The method of arriving at the friction coefficient is based on geometry and equilibrium.

An initial calibration plot was made by loading the member without allowing a component of force, F, to develop (see test equipment section). The only force then applied would be the weight, w, counteracted by the torsion wire. This would result in a certain displacement of the reflected light beam and a corresponding d. This was repeated for various w's. Then the low friction fixture was removed and replaced by the test specimen. The specimen were allowed to rotate at varying velocities with varying loads applied. Each mirror deflection corresponding to load and speed was noted. From these measurements and the following equations it was possible to obtain information to plot the resulting graph (Figure 20).

k = the length from torsion wire to the end of the pallet stone.

F = friction force.

w = normal force.

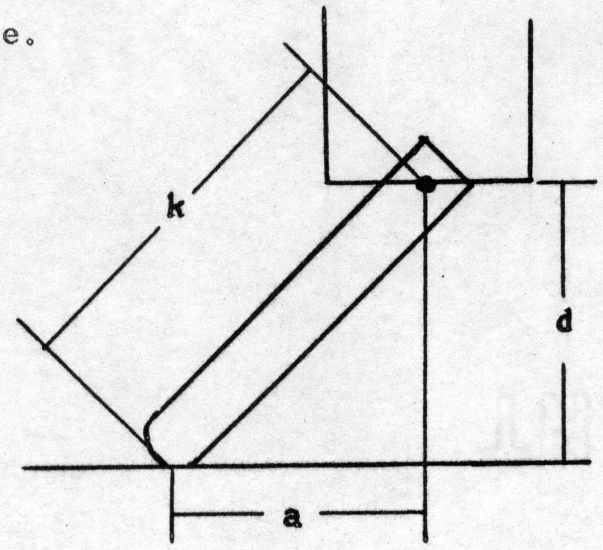

Figure 21. Stylus

At a constant light beam deflection, d is constant. Thus a w with no F will cause a certain deflection. In order to obtain the same deflection with an F value different from zero, more or less w will be needed. For any certain deflection, this difference in w which enters into the equation will be called Δw. Thus $\Delta w \cdot a = F \cdot d$ where a is the horizontal distance from a point under the torsion wire to the tip of the speciman. "a" cannot be measured easily. Instead it is eliminated by means of the equation,

$$a^2 = k^2 - d^2,$$

$$F = \Delta w\left(\frac{k^2}{d^2} - 1\right)^{1/2}.$$

The coefficient of friction is

$$F_c = \frac{F}{w}.$$

Test Equipment

For discussion, the following friction test equipment will be divided into three items; each will be discussed separately:

1. Light source
2. Turntable
3. Stylus

Light Source

The light source (Figure 22) was a Model 119 Federal

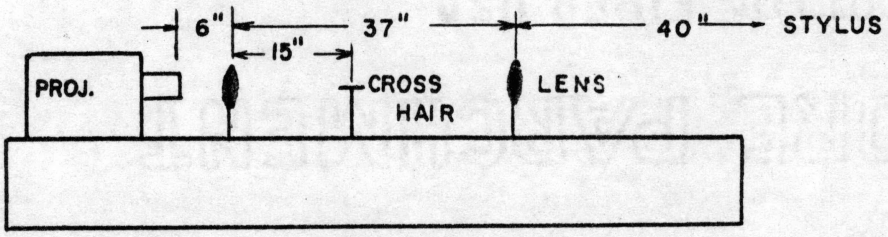

Figure 22. Light Source

Microfilm Projector. A plate with a 1/4-inch-diameter hole replaced the normal microfilm slide to reduce the spreading of the light rays. This small beam of light then was focused by sending it through two condensing lenses approximately 37 inches apart. Between these lenses a horizontal reed was placed to act as a cross-hair when reflected on the graduated scale. This beam impinged on the stylus mirror and was reflected onto a large scale. It was possible to read to 1/2 inch on the 11-and-1/2-foot scale approximately 15 feet from the source.

Turntable

The prime requisites of the turntable were rigidity, constant speed, and plane motion. Without these, calibration would have been difficult and repeatable readings next to impossible. Having this in mind, the

PIATE IV FRICTION TEST EQUIPMENT

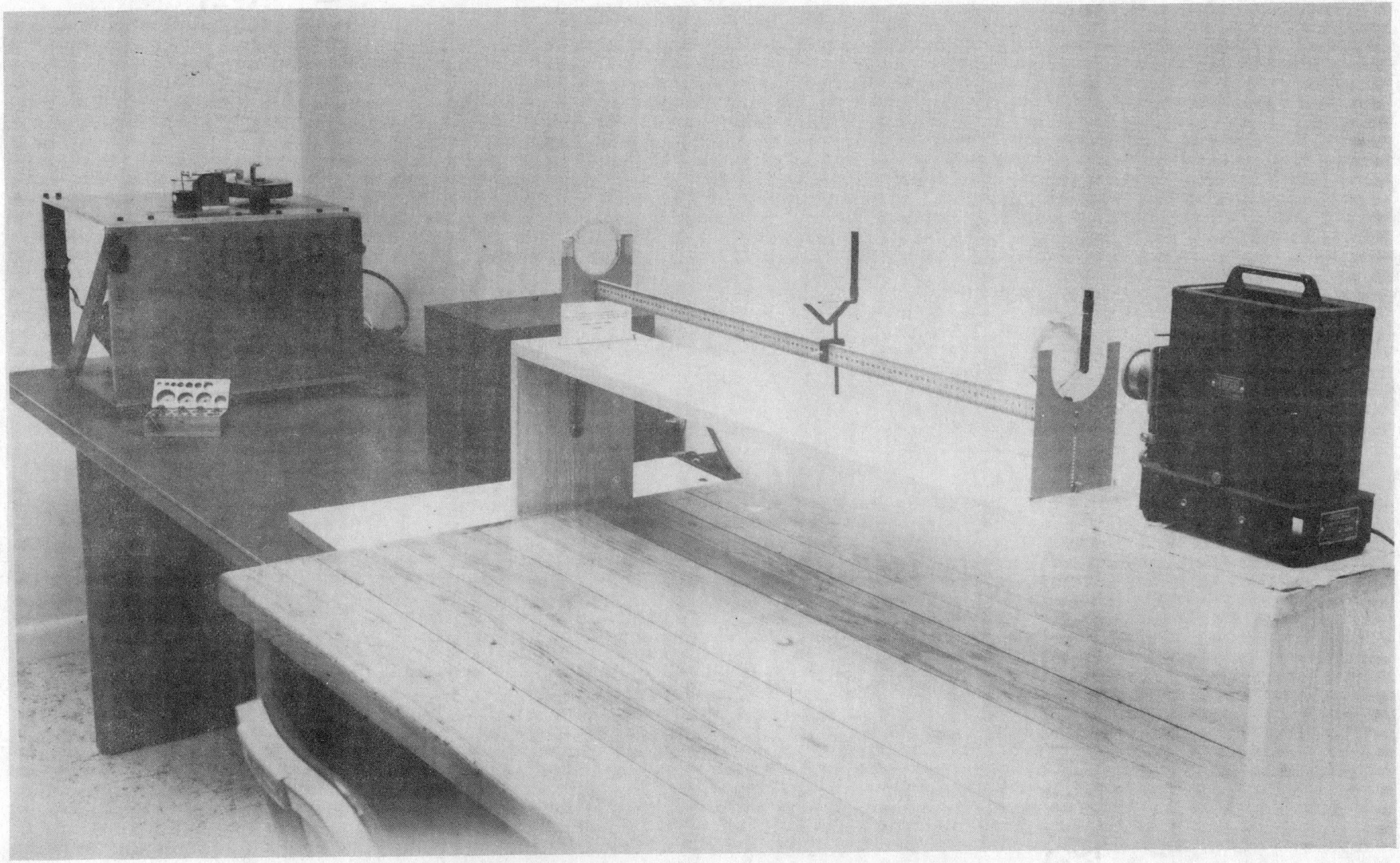

PLATE V STYLUS ASSEMBLY

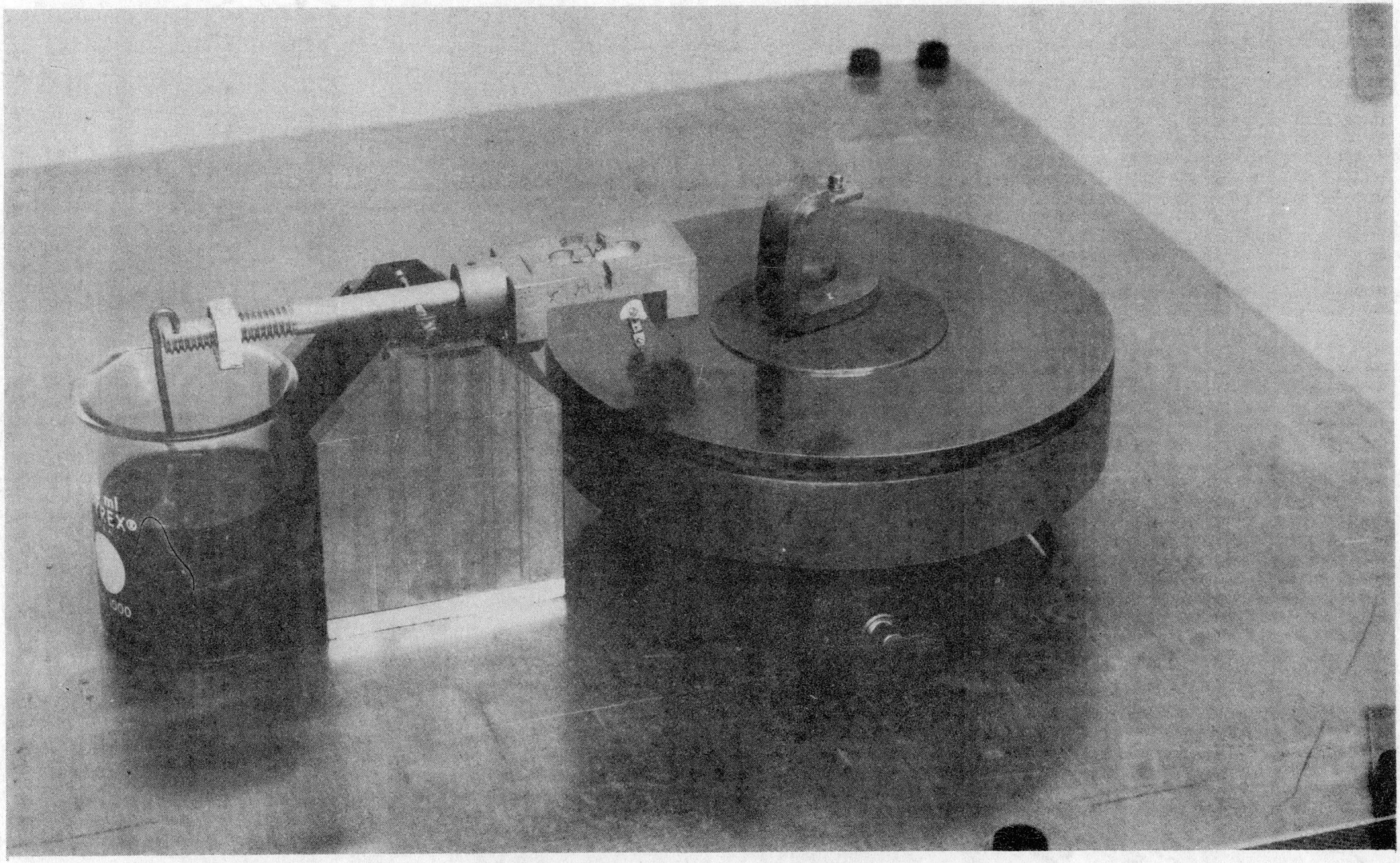

turntable was constructed from 1/2-inch plate aluminum in the form of a box (Figure 23). The drive shaft protruded through a hole in the top of the box to allow for attachment of the speciman carrying flange. All other parts of the turntable were internal to the box. To the lower end of the shaft was attached a large, heavy flange that served two purposes: to allow coupling through a rubber friction disc to the synchronous motor-drive assembly; and to assure that the speed would not be subjected to minute fluctuations of the drive train. By varying the position of the friction roller on the flange it was possible to vary the speed of rotation of the speciman between 3 and 15 ft./sec. (Figures 23, 24, 25, and 26).

Stylus

The stylus or pickup mechanism is shown in Figures 27, 28, and 29. The pickup converts the friction force into a deflection of the light beam by means of a mirror and spring arrangement. The spring consists of a stainless steel wire 0.0035 inches in diameter and one inch in length. It is held under a light tension between machine screws in the pickup head. The friction force exerts a torque on the wire spring causing a torsional deflection (α) in the spring and a resultant deflection (2α) to the reflected light beam. It was necessary to

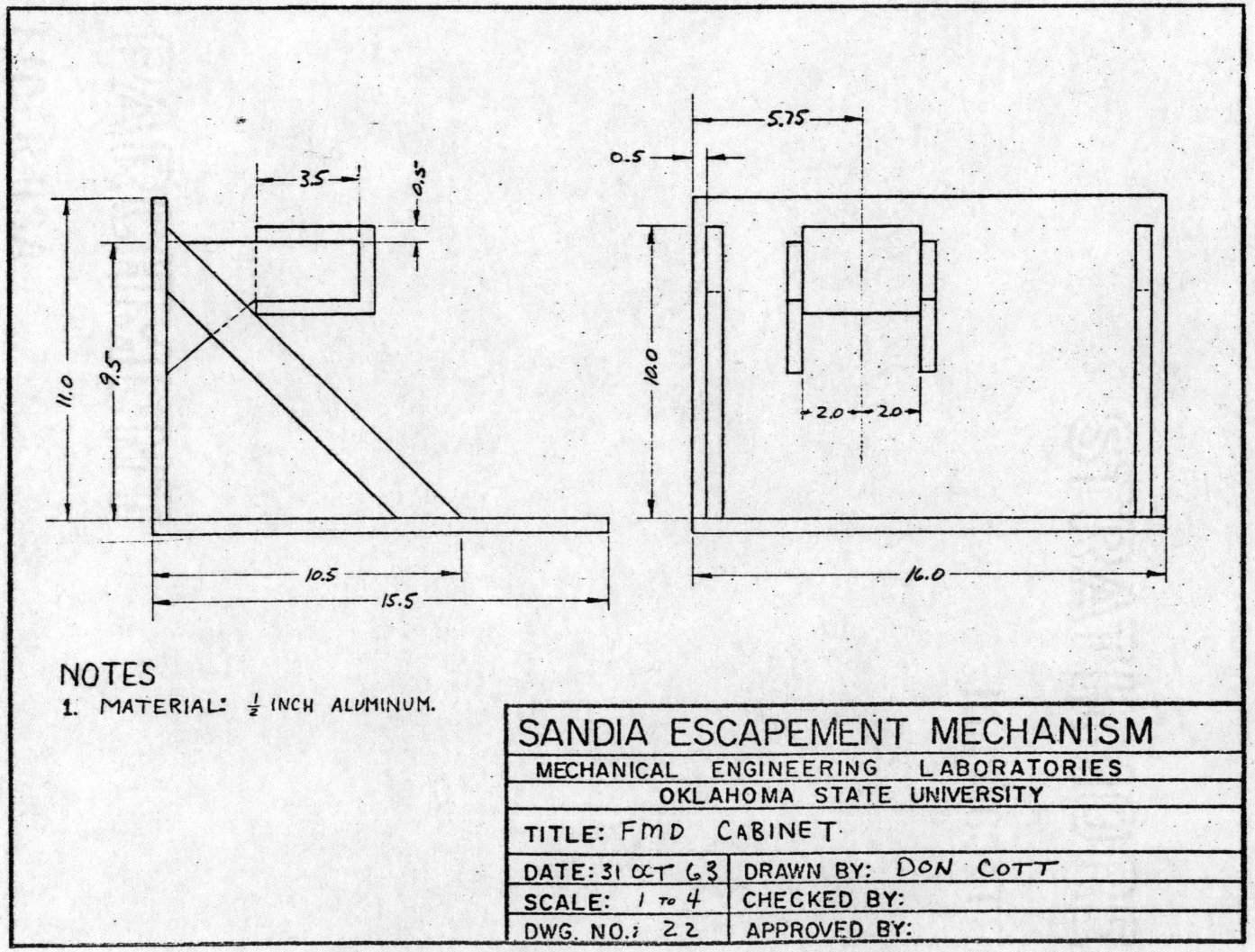

Figure 23. Friction Test Cabinet

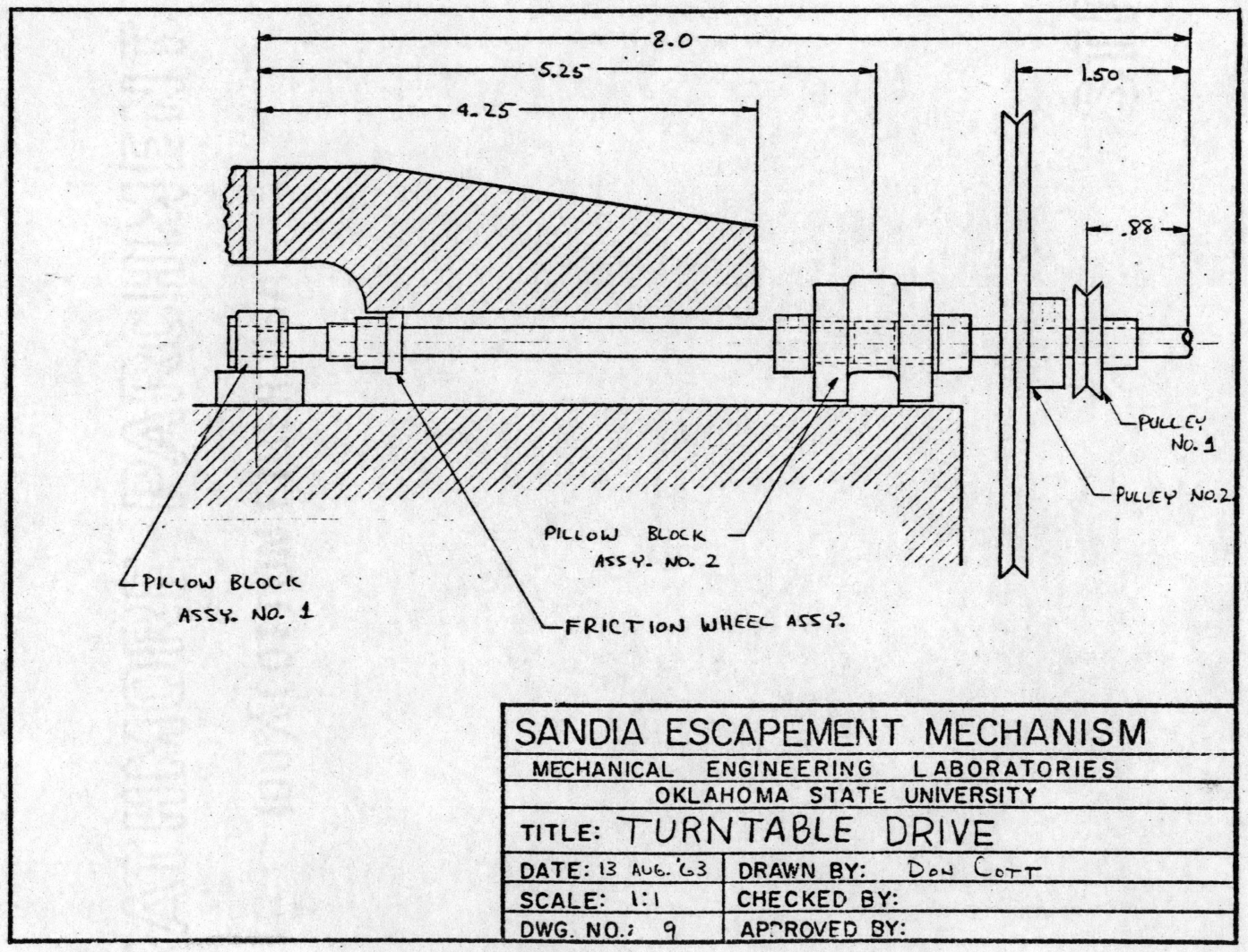

Figure 24. Turntable Drive

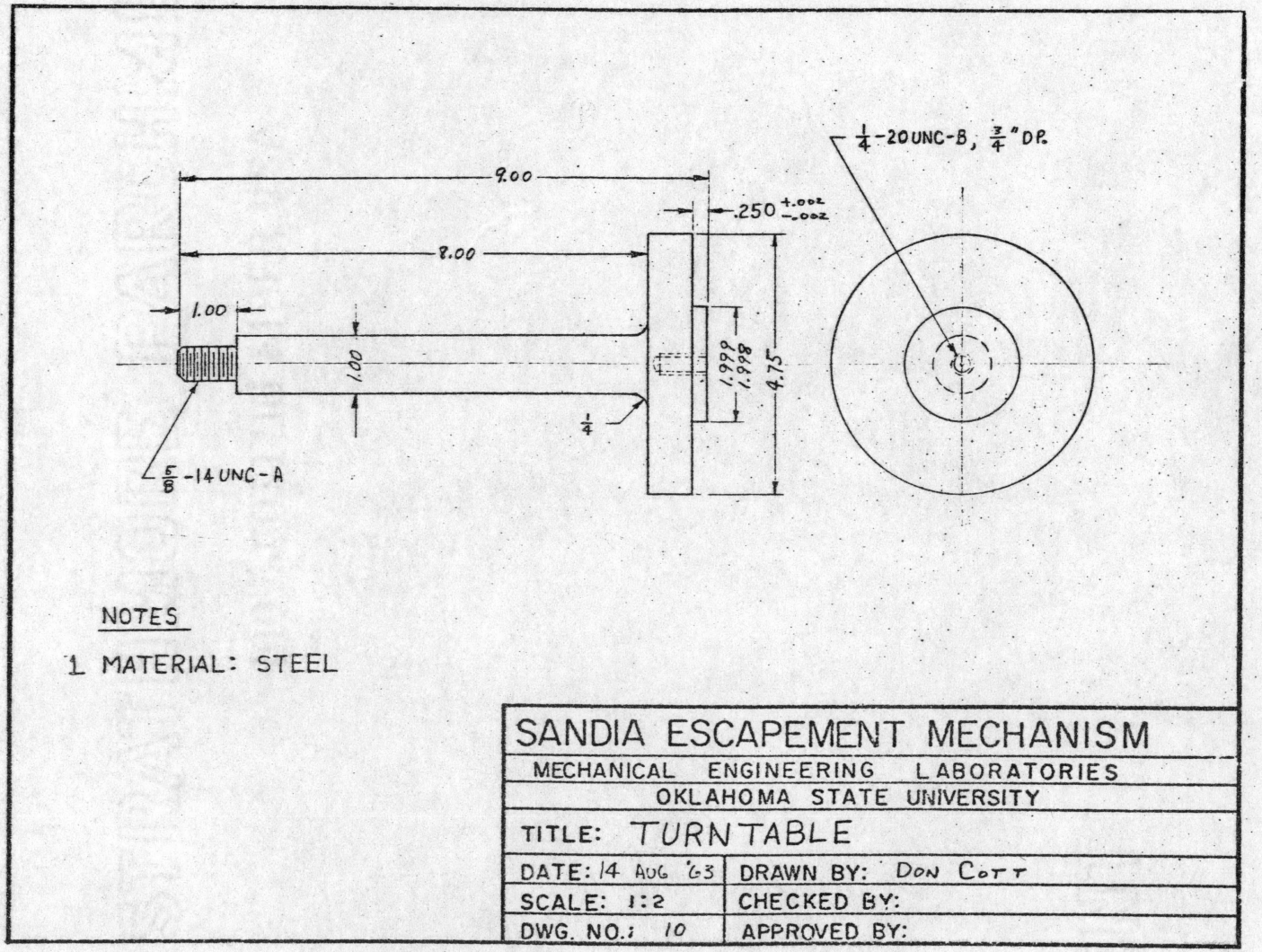

Figure 25. Turntable

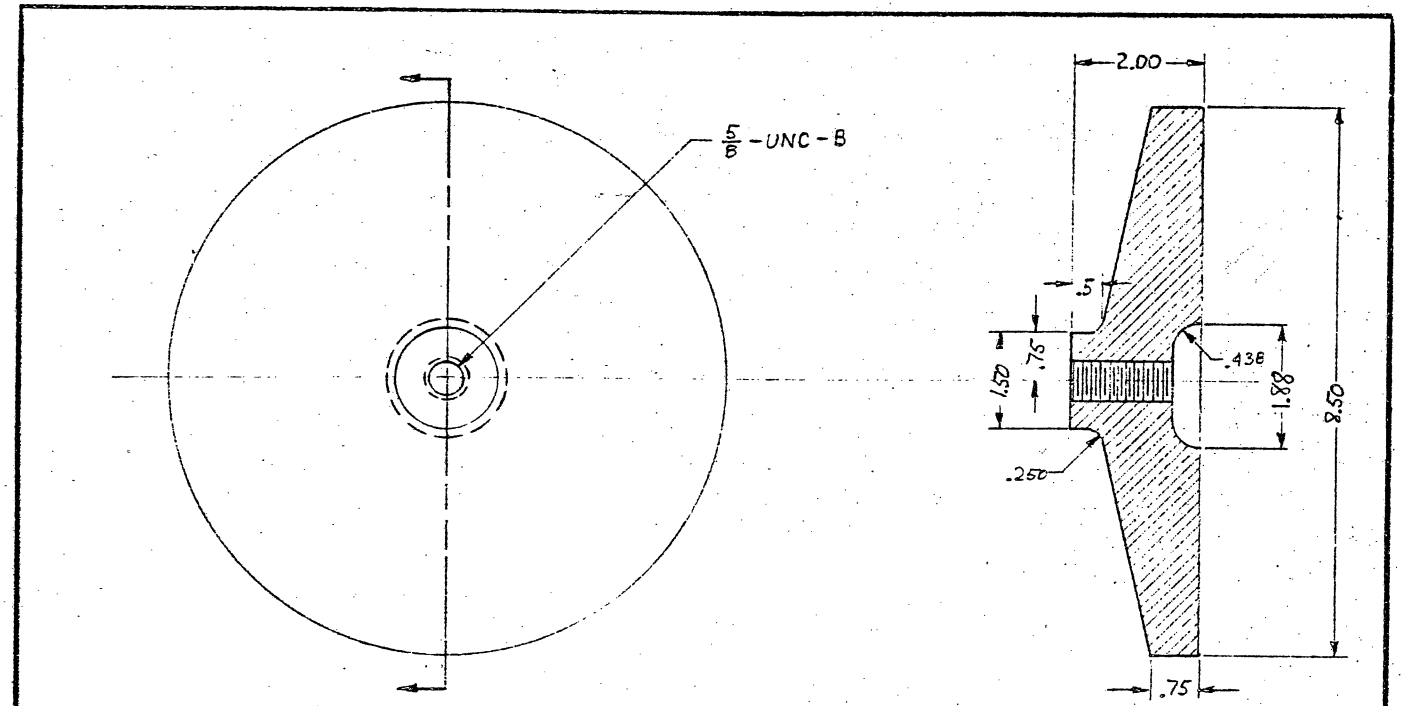

NOTES

1. MATERIAL, STEEL
2. WOBBLE ON THIS SURFACE SHOULD BE LESS THAN .001 WHEN PART IS MATED WITH TURNTABLE AND TURNED ABOUT AXIS OF TURN-TABLE.
3. DIMENSIONS IN INCHES.

SANDIA ESCAPEMENT MECHANISM	
MECHANICAL ENGINEERING LABORATORIES	
OKLAHOMA STATE UNIVERSITY	
TITLE: FLYWHEEL	
DATE: 15 AUG '63	DRAWN BY: DON COTT
SCALE: 1:2	CHECKED BY:
DWG. NO.: 12	APPROVED BY:

Figure 26. Flywheel

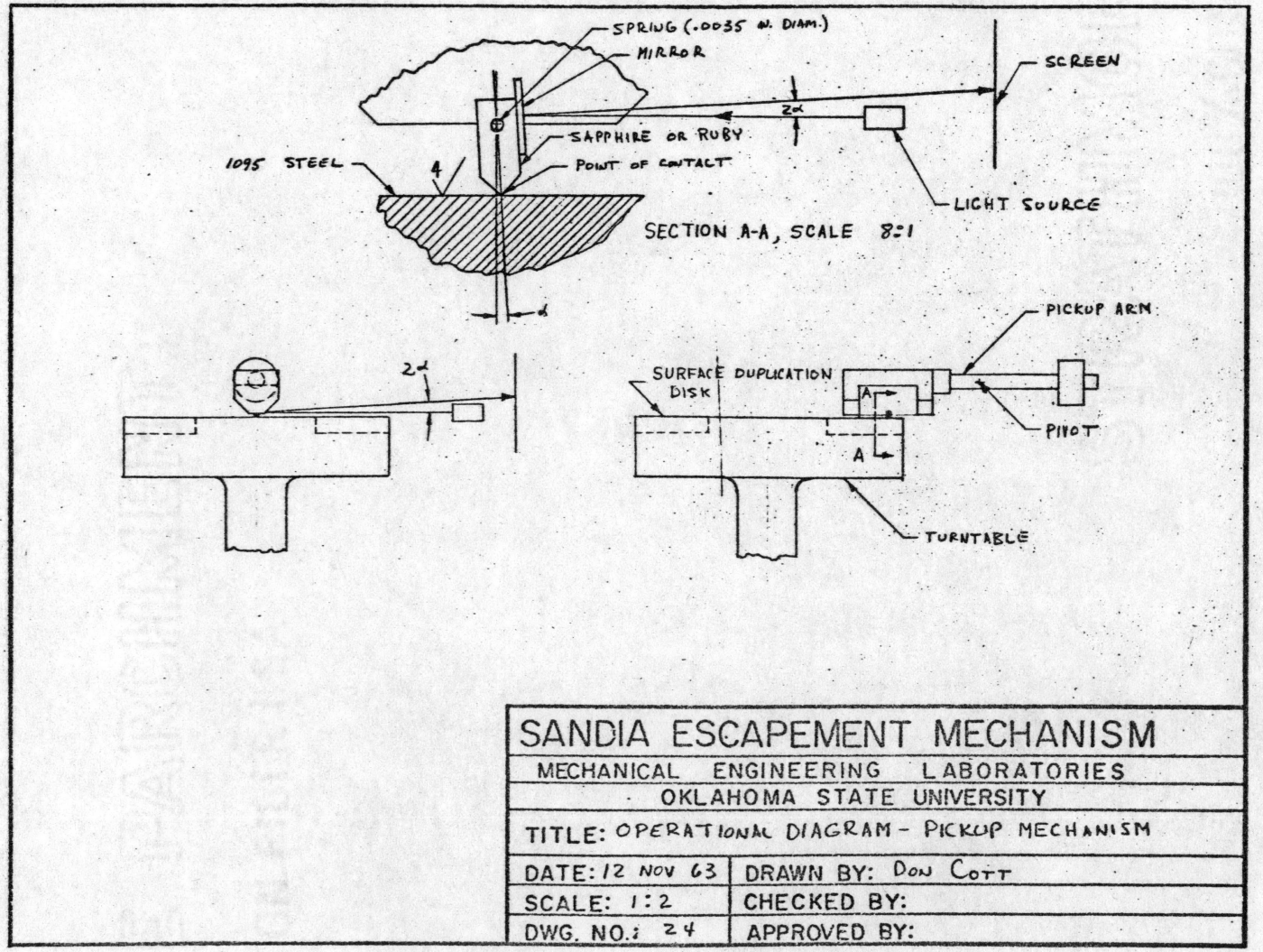

Figure 27. Pickup Mechanism

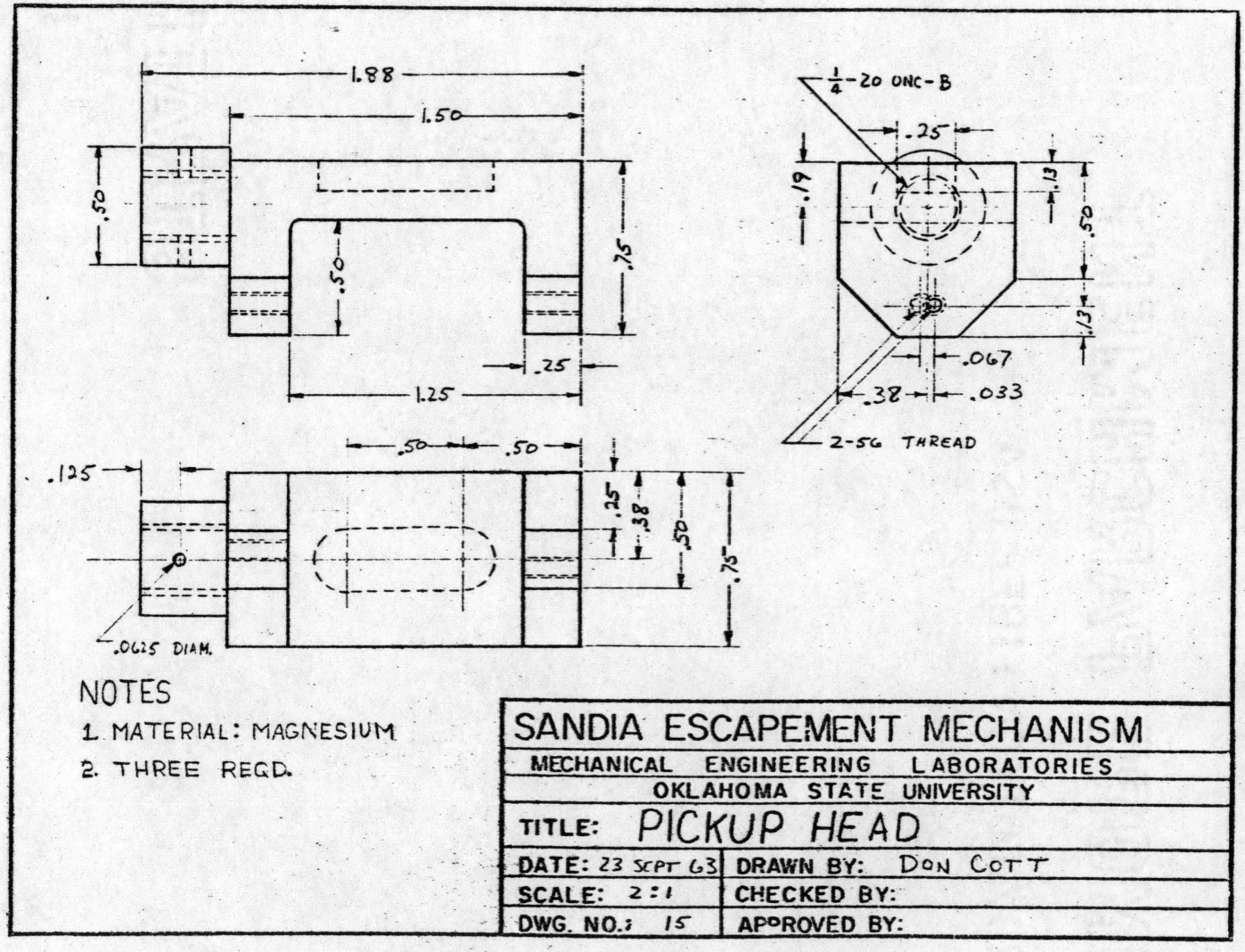

Figure 28. Pickup Head

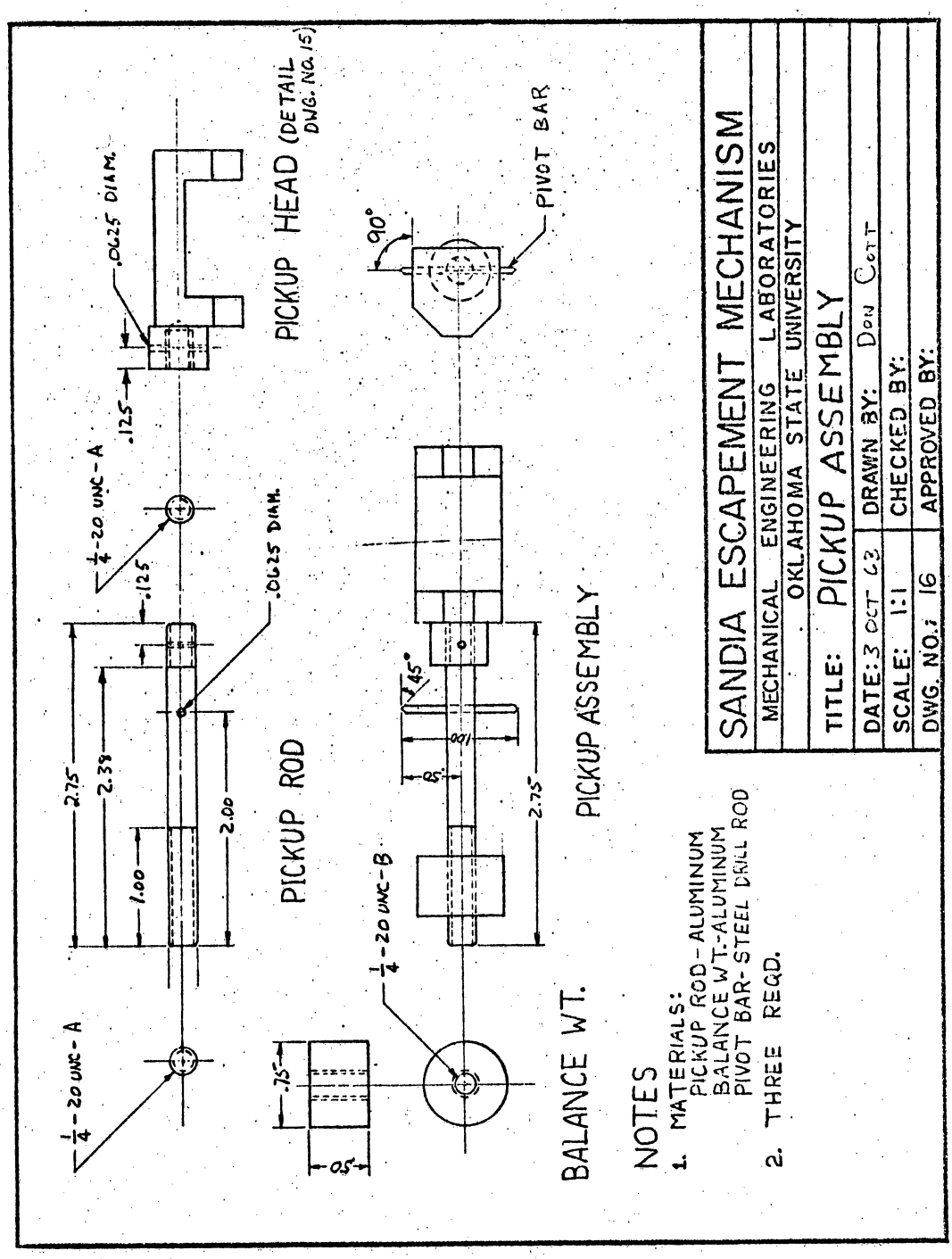

Figure 29. Pickup Assembly

attach a viscous damper to the stylus to reduce oscillation of the stylus during testing. This damper consisted of a one-and-one-half-inch circular plate immersed in a light oil and attached to the rear of the stylus.

An additional fixture had to be constructed to obtain a zero calibration reading for the light beam (Figure 30). This allowed for the rotation of the stylus about its own axis as weight was applied without developing an appreciable horizontal force.

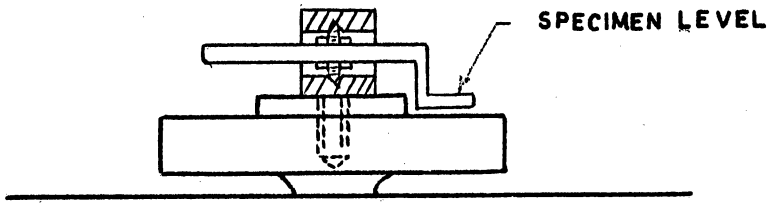

Figure 30. Zero Fixture

Figure 31 shows the stylus and turntable assembly with a portion of the cabinet removed for clarity.

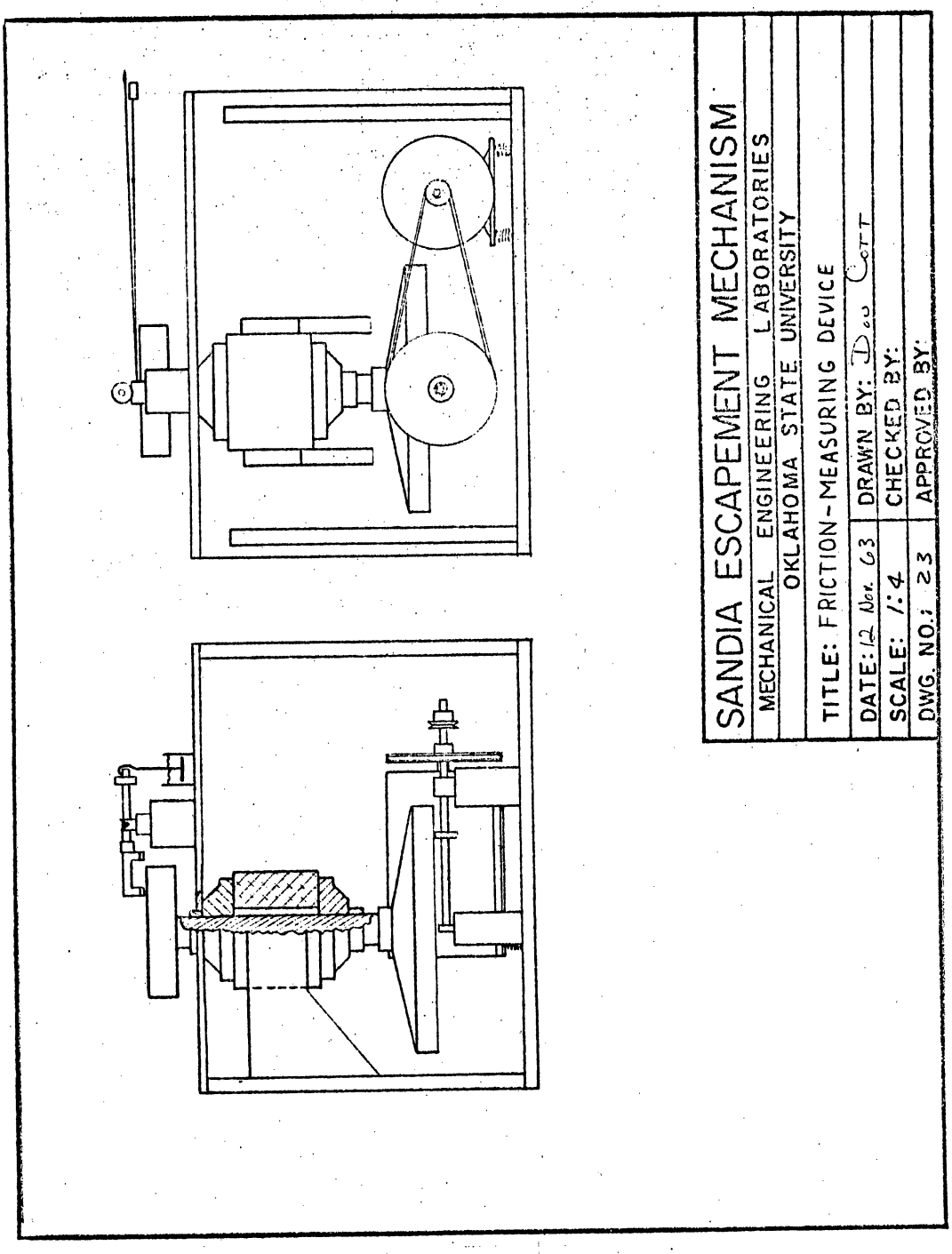

Figure 31. Friction Measuring Assembly

CHAPTER VII

A METHOD OF TORQUE CONTROL

Although the "detached" escapement offers a tremendous increase in accuracy over previous escapements for a greater variation in driving torque, it still (as with all mechanical-driven mechanisms), to some small extent, has a rate of oscillation varying with input torque (torque sensitivity). An awareness of torque sensitivity has led to a multitude of devices for giving a more constant power supply to the escapement. Two of these are: the fusee, to compensate for decay in mainspring torque during unwinding; and a remontoir, consisting of a spring rewound periodically by an electric motor in some DC-powered electric clocks. These methods, although complex, offer advantages where the load on the escapement is relatively constant and the power supply only varies slightly; whereas, ordnance and rocket timers usually are used as controlled-rate power packages rather than purely as timers. Instead of having a small fixed load such as hour, minute, and second hands to drive, the ordnance and rocket timers must throw switches, turn cams, bring rotors into alignment, etc. These functions not only impose large loads on the timing

movement but the loads are often variable throughout the cycle and from one timer operation to another. As a result, the escapement is subjected to a relatively large variation in torque which is the difference between the torque available from the power supply and that being used for external functions. Most of the previously mentioned torque compensating devices and changes in the clocks and watches were made to facilitate a constant torque load from the energy source and very little was done to keep the net power to the escapement constant.

Some methods of controlling torque to the escapement have been tried. One is a capstan-type regulator using a spring clutch arrangement that works very well in theory; but, as is pointed out in an HDL report[3], it requires extremely close tolerances on the spring clutch and would be difficult to manufacture reliably. The method presented here is another way of keeping the input torque to the escapement constant which should not cause a tolerance problem. It has several advantages which will be pointed out later. There are various configurations of this method that could be used, but only one will be discussed here.

Fundamentally, in this method a low power escapement controls the time rate output of a high-torque power source while tapping a small fraction of the torque for its operation. With this arrangement, the escapement torque is relatively constant and thus provides better

regulation. This modified escapement (Figure 32) uses a light spring coupling between the power source toothed-wheel and the timing escape wheel. The timing escapement trips the gating lever, which is engaged in a tooth of the toothed-wheel, twice per oscillation of the balance and lets the power source rotate one tooth at a time. For each swing of the escapement lever the power source wheel unwinds one tooth. As it moves this amount, it tends to wind the light spring attached to the escape wheel the same amount. This brings the torque on the escape wheel to the same level as it was prior to the last balance oscillation. Thus the torque on the escape wheel remains at the same average level. The gating lever and the power source toothed-wheel can be regarded as simply another lever and escape wheel, where the escapement lever trips the power lever in the same manner as the balance trips the escapement lever. Perhaps the greatest advantage of having the separate spring to drive the escapement is that of being able to apply compensations to this spring without effecting the power spring in the least, and thus apply a more constant torque to the oscillatory control system in almost complete independence of the power system.

In all standard detached escapements, an increase in power-source torque will increase the amplitude of balance wheel motion; but with this modified escapement, an increase in power source torque will decrease the motion

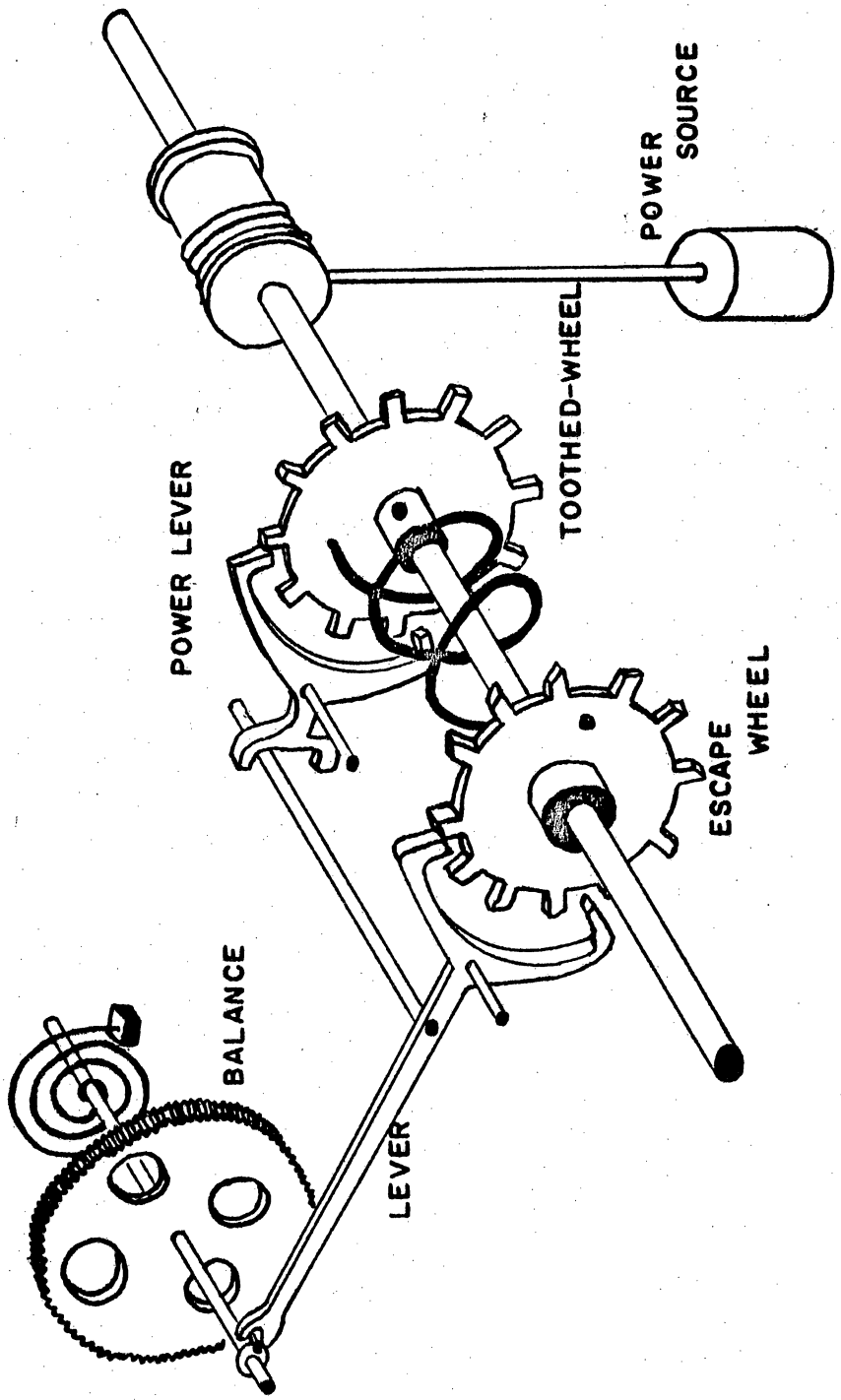

Figure 32. Modified Escapement

PLATE VI MODIFIED 1321 PARTS

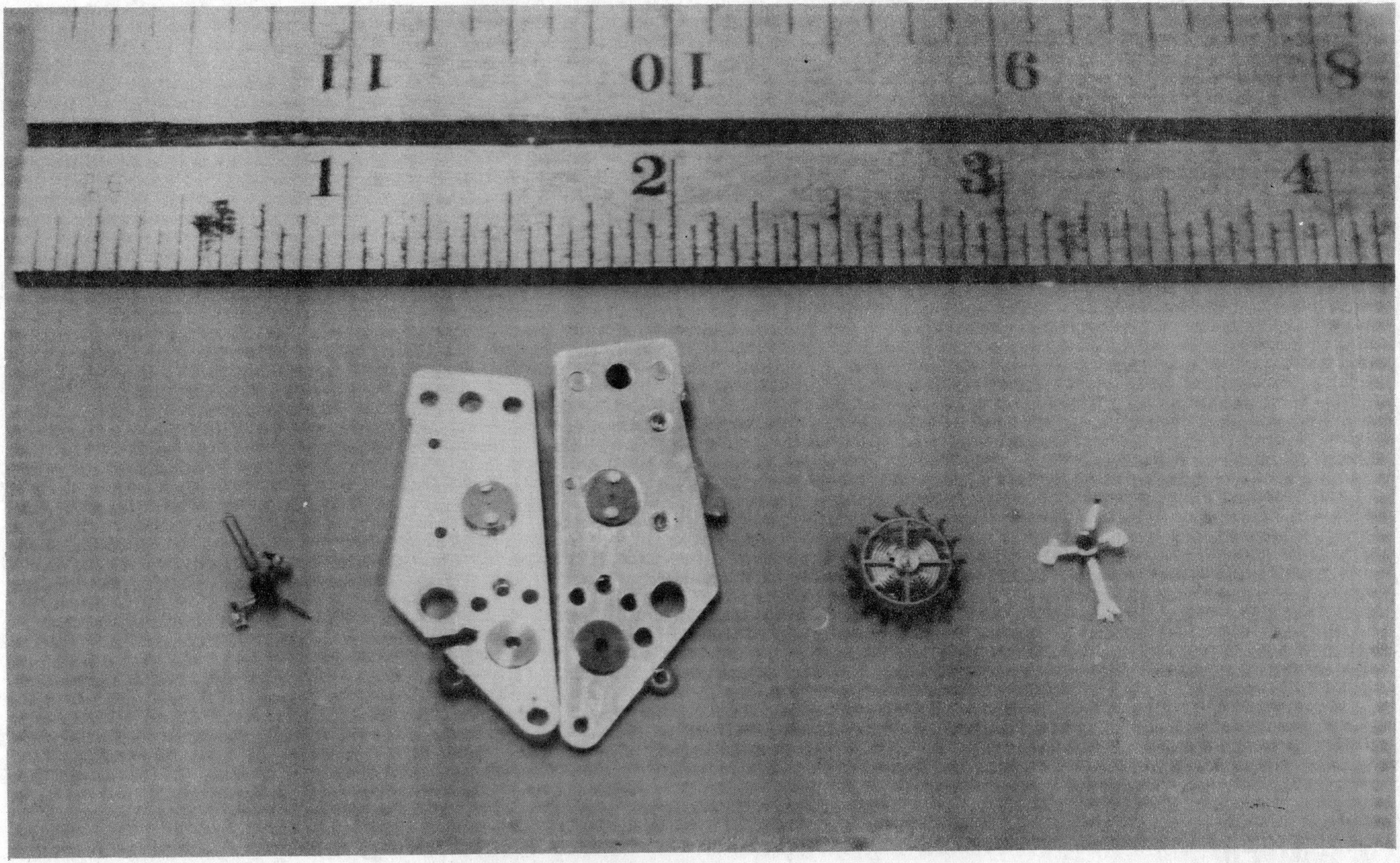

of the balance. This is brought about by the increased friction on the trip mechanism. The amplitude change can be kept to a minimum by proper design and use of polished friction surfaces on the second lever and escape wheel.

Two types of escapements were modified to this configuration and the results can be seen in Figure 33. The top of Figure 33 is a graph of the time rate vs. torque of an inexpensive Gilbert alarm clock escapement both before and after modification. The bottom of Figure 33 is the time rate vs. torque of a Sandia 1321 escapement; this escapement has parts the same size as those found in a Hamilton Railroad Watch. This is a well-made detached lever escapement and does quite well without compensation over a small variation in torque; however, the torque range is limited without exceeding the built-in stops for the balance (overbanking), as can be seen from the figure. With the modification, an increase in torque variation of about four-to-one is available without appreciable change in timing accuracy.

It is apparent from the graphs and the tests that the units require a higher minimum torque for operation after modification than they did before modification. This stems from the increased number of parts and the extra friction surfaces. However, obtaining a greater amount of torque usually is not as much a problem as being able to handle large variations of torque; and this

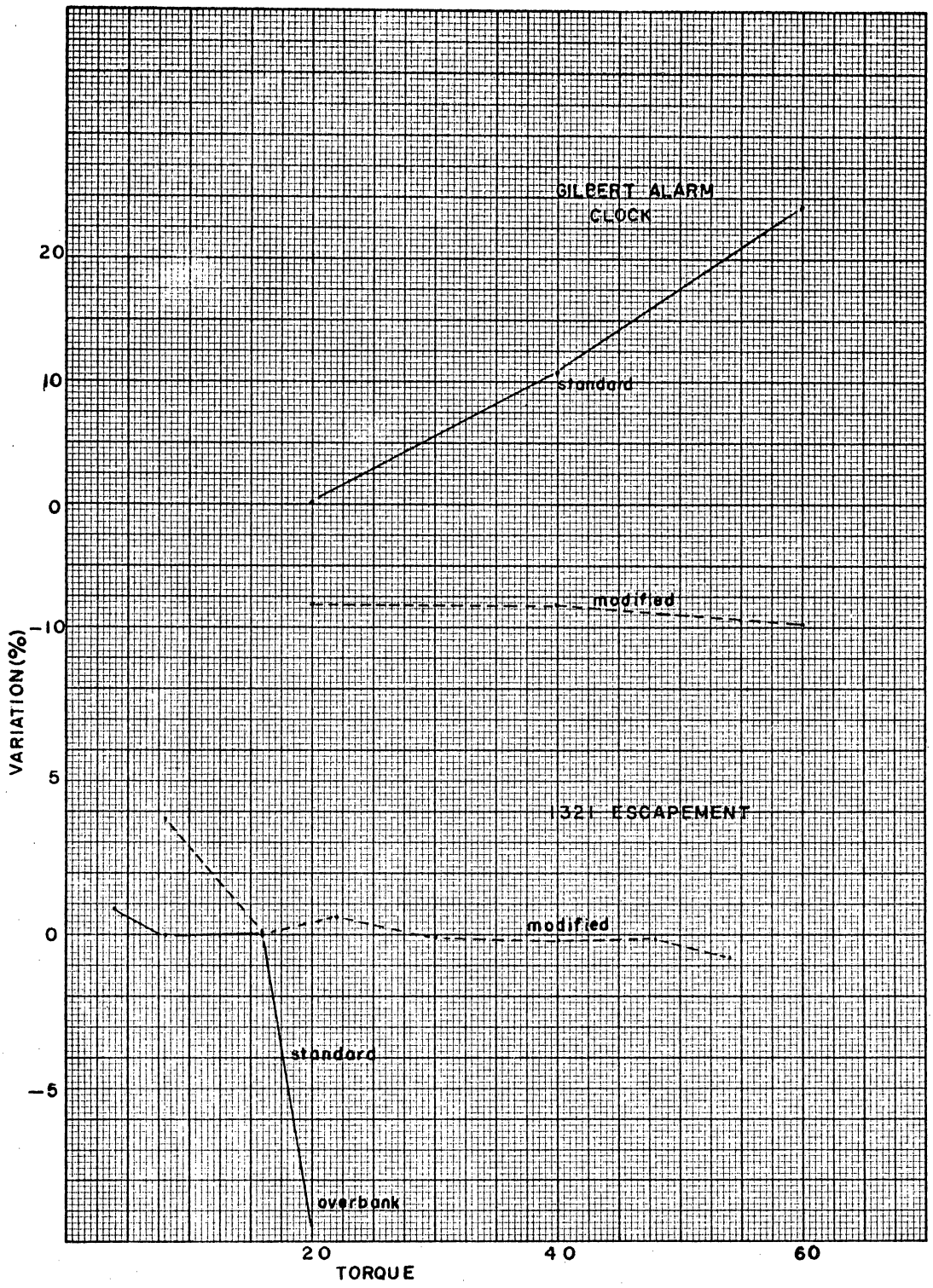

Figure 33. Modified Escapement Torque Curve

method does prove effective on the torque variation. One disadvantage is the increased complexity of the mechanism since, as was previously mentioned, it is essentially a dual escapement. But if greater accuracy is of primary importance, the increased complexity could be justified. The design was not taken beyond a three shop-built-model phase since this was a side issue to the research problem; however, the results show enough promise that this should bear further consideration if the need arises for extreme accuracy coupled with large torque variations.

CHAPTER VIII

SUMMARY AND CONCLUSIONS

Throughout the history of timing devices little has been done in the area of theoretical study of escapement mechanisms. The major efforts have developed along the cut and try procedures without having guide lines to predict the results. This study has attempted to alleviate some of these problems by providing a theoretical study of the escapement as a continuous entity; where values could not be reasonably determined theoretically (such as viscous and kinetic friction), this study has coupled the analytical with the experimental. This has a twofold purpose. First, it allows a reasonable estimate of those coefficients that could be "educated guesses" otherwise; and second, it allows one to predict the magnitude and direction of shift in characteristics of an operating unit if one changes these parameters.

It is felt that this study offers an approach which heretofore has not been available to those interested in better timing devices, particularly in the ordnance and rocket field.

Although specifically derived for the detached lever escapement, the equations presented have universal applications to escapement mechanisms by a change of the shape and duration of the forcing and friction functions.

In conclusion, the five units tested and compared with the theoretical data give excellent correlation in both expected predictions and shape of the curves. Since the units tested were not homogeneous, it is felt that these five units give reasonable proof that the method outlined herein will give satisfactory results. "C" appears to be slightly nonlinear during the transient phase of operation, and it is during this phase that the curves do not match identically. This nonlinearity creates no problem to the use of the equations and solution of this study unless one is interested in timing during the first few cycles after starting. Should this be the case, one could approximate the increase in C by adding a simple program to those of Appendix B and letting C increase a small amount each cycle.

This study provides an analytical tool for preliminary estimates of performance and for estimates of a change of timing characteristics to achieve a change in performance. The success of the analysis also offers promise of developing transfer functions for mechanical timers when they become part of a larger system.

CHAPTER IX

RECOMMENDATIONS FOR FUTURE STUDY

During the research work on this project, certain aspects arose that would directly add information of value to the field of horology. The more important of these are presented here.

Perhaps of primary importance is the effect of friction in the gear train and its effect on the motion of the escapement. Since the gear train is continually being reversed, started, and stopped twice each cycle it is important to know this effect and its interaction with the inertia effects. It is understood that Sandia Corporation, Albuquerque, New Mexico, is doing some work in this area and that one of the references[9] included a portion on small gearing friction; however, it is believed that much greater depth must be explored in this area before the action and reaction of the escapement to a change in parameter is fully understood and analytically definable. This research is able to circumvent this area by the combination of the experimental and analytical approaches, but it would be extremely advantageous to have an analytical definition of the reaction of the gear train.

There is no present provision in the equations for compensation due to temperature and environmental changes or any compensation for positional variations due to a change in pivot friction when changing the orientation of the assembly. This is a second area that would be of great interest and probably could be integrated into the basic solutions of this report by means of subprograms.

The basic equations of motion set forth could apply to any type of escapement mechanism. The forcing function and friction functions were formed specifically for the detached-lever escapement. It is believed that by careful choice of these functions, the operational characteristics of any escapement could be predicted. This application to other timing devices is another area that would be of great interest to the timing-device field.

A fourth area of interest is in the refinement and application of new techniques to the measurement of the parameters of small devices, without interference in their operation. This becomes extremely important for small, low-torque devices such as escapements. For instance the photo-cell amplitude measurement device worked well, but its accuracy was no greater than plus or minus one tooth or 6°. A variation of this amount in the amplitude could have occured during the tests without detection. An accuracy of ten times this would have been desirable but a 600-tooth wheel, 1/2-inch in diameter is rather difficult to attain.

A fifth area of interest for future study might be the statistical comparison of a sufficient quantity of unit curves with computed unit curves. This could only be done with data from a large quantity of units; perhaps commercial watches could be used.

Any of the above would be a research project in itself and, of course, the ultimate objective of these would be to arrive at a complete definition of the operation of mechanical escapement devices analytically.

BIBLIOGRAPHY

1. Baillie, G. H. Clocks and Watches. 1st. ed. London: N.A.G. Press Ltd., 1951.

2. Bercot, P., and P. Altenburger. "The Amplitude Variations in a Clock (Timepiece)" Report Book of VI International Congress for Chronometry, II. Munich: (June 19-23, 1959). Translated from the French by M. I. Weinrich, Albuquerque: Sandia Corporation SCLT-458 (1963).

3. Bettwy, D. S. "A Capstan-type Torque Regulator for Timing Movements." Report of Harry Diamond Laboratories, No. TR-1130. Washington, D.C.: Army Materiel Command, 1963.

4. Britten, F. J. Watch and Clock Makers' Handbook. 15th ed. New York: D. Van Nostrand Co., Inc., 1955.

5. Fried, H. B. The Watch Escapement. New York: B. Jadow, Inc., 1959.

6. Gazeley, W. J. Clock and Watch Escapements. New York: D. Van Nostrand Co., Inc., 1956.

7. Giebel, K. "Einfluss der Hemmung auf den Gang der Uhr." Unpublished dissertation, Göttingen, 1905.

8. Glaser, G. "Concerning New Methods for Understanding the Function of the Balance Oscillating Systems." Report Book of VI International Congress for Chronometry, I. Munich: (June 19-23, 1959). Translated from the German by M. I. Weinreich, Albuquerque: Sandia Corporation SCLT-463 (1963).

9. _____. "Concerning the Causes of the Balancer-Amplitude Oscillations." Seventh Yearbook of the German Society for Chronometry, (1956), pp. 23-31. Translated from the German by M. I. Weinreich, Albuquerque: Sandia Corporation. (1964).

10. _____. "The Dynamics of the Pallet Escapement." Seventh Yearbook of the German Society for Chronometry, (1956), pp. 49-64. Translated from the German by M. I. Weinreich, Albuquerque: Sandia Corporation (1964).

11. Grossman, Moritz. A Practical and Theoretical Treatise on Detached Lever Escapement for Watches and Time Pieces. Leiptzig: G. Kreysing, 1866.

12. Marks, L. S. Marks' Handbook. 4th ed. New York: McGraw-Hill, 1941.

13. Milham, W. I. Time and Timekeepers. New York: Macmillan Co., 1951.

14. Rawlings, A. L. The Science of Clocks and Watches. New York: Pitman Publishing Co., 1948.

15. Saunier, Claudius. A Treatise on Modern Horology in Theory and Practice. Translated from the French by J. Tripplin and E. Rigg. London: W. and G. Foyle Ltd., 1878.

16. Swineburne, J. The Mechanism of the Watch. London: N.A.G. Press Ltd., 1950.

APPENDIX A

SOLUTION TO THE EQUATION OF MOTION

The solution to the equation of motion for the balance wheel is presented here. All previous sign conventions discussed in Chapter III apply.

The equation to be solved is

$$\ddot{\theta} + \omega_o^2\theta + C\dot{\theta} + R\frac{\dot{\theta}}{|\dot{\theta}|} - X_{(\theta)} = 0.$$

If the nonlinear terms are transferred to the right side giving

$$\ddot{\theta} + \omega_o^2\theta + C\dot{\theta} = -R\frac{\dot{\theta}}{|\dot{\theta}|} + X_{(\theta)},$$

the complementary solution for the equation becomes

$$\theta = e^{-Ct/2}(A \cos \omega t + B \sin \omega t),$$

where

$$\omega = \frac{\sqrt{4\omega_o^2 - C^2}}{2}.$$

To obtain the particular solution, one must examine the nonlinear terms. $X_{(\theta)}$ would appear as shown in Figure 34. When the balance wheel is rotating clockwise, the power added is negative and the power dissipated is positive; when the balance reverses, the power added is positive and power dissipated is negative. Since the point of application of $X_{(\theta)}$ is dependent upon θ, and

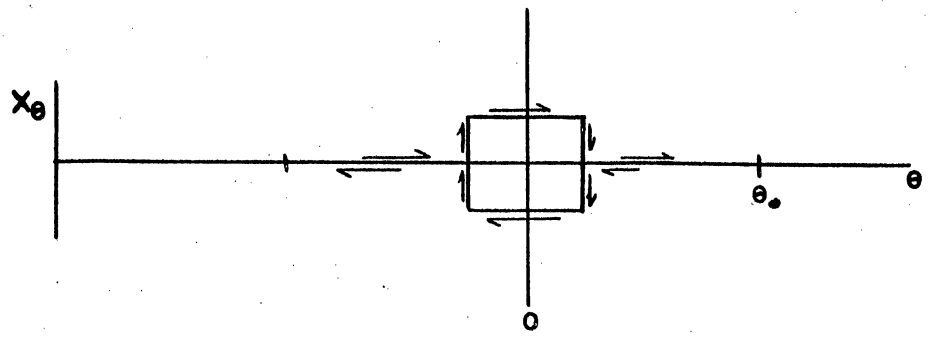

Figure 34. Force as a Function of Theta (Simplified)

θ for a specific frequency of oscillation can be converted to a time function. $X_{(\theta)}$ would then appear as shown in Figure 35.

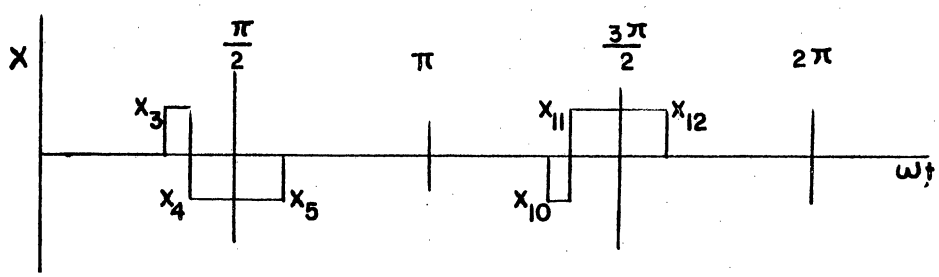

Figure 35. Complete Force Function

It should be noted that X_3 and X_{10} were omitted from the θ curve for clarity. X_3 and X_{10} are energies involved in unlocking the escapement.

It appears that $X_{(\theta)}$ can be separated into a series of pulses of a certain constant magnitude (X_1, ---,X_{14}) and duration (α, β, γ, μ, σ, ε, ϕ, δ). The term $R\frac{\dot{\theta}}{|\dot{\theta}|}$ is a constant term multiplied by the sign of $\dot{\theta}$. Differentiating the complementary solution, one obtains

$$\dot{\theta} = e^{-Ct/2}((-\omega A + \frac{BC}{2})\sin \omega t - (\frac{AC}{2} - \omega B)\cos \omega t).$$

The initial condition of $\theta = \theta_o$ and $\dot{\theta} = 0$, when $t = 0$ lead to $A = \theta_o$ and $B = \frac{\theta_o C}{2\omega}$

and $\dot{\theta} = e^{-Ct/2}((-\omega\theta_o + \frac{\theta_o C^2}{2\omega})\sin \omega t)$.

From 0 to π the sign of the sin ωt is positive and from π to 2π the sign of sin ωt is negative, and since $C < 1$ and $\omega > \theta_o$, the quantity $(-\omega\theta + \frac{\theta_o C^2}{2\omega})$ is negative. $\omega\theta_o > \frac{\theta_o C^2}{2\omega}$ since ω and θ_o are always positive. Thus $\dot{\theta}$ is negative from 0 to π and positive from π to 2π. A plot of R versus ωt resembles Figure 31.

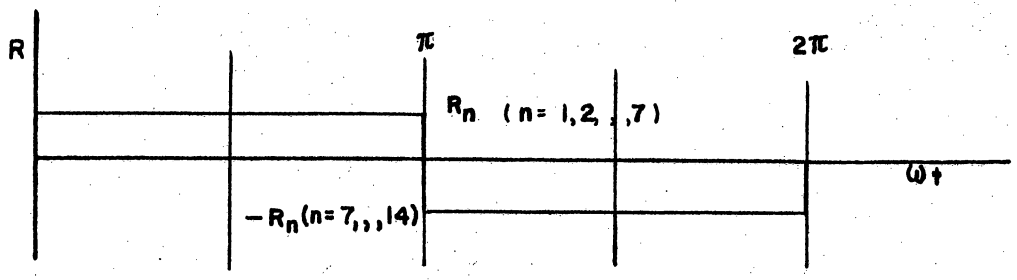

Figure 36. Sliding Friction

Using this and the previously established sign convention, the particular solution becomes

$$\frac{R_n}{\omega_o^2} + \frac{X_n}{\omega_o^2}; \quad n = 1, - - - -, 14$$

The combination of the complementary and particular solution produces

$$\theta_n = e^{-Ct/2}(A_n \cos \omega t + B_n \sin \omega t) + \frac{R_n}{\omega_o^2} + \frac{X_n}{\omega_o^2};$$

Thus, the solution to the one nonlinear equation has been reduced to a set of fourteen linear equations with constants A_n and B_n which must be determined by matching boundary conditions at the beginning and end of each interval of θ_n.

Should the hairspring constant be nonlinear and could be represented by straight-line segments, then ω_o could have a subscript also. In this analysis, there was an allowance for four such straight-line segments; thus ω_o also must be subscripted, i.e., ω_{oi}. Since ω is a function of ω_o and C, it will carry the same subscript as ω_{oi}, ω_i.

The solution then becomes

$$\theta_n = e^{-Ct/2}(A_n \cos \omega_i t + B_n \sin \omega_i t) + \frac{R_n}{\omega_{oi}^2} + \frac{X_n}{\omega_{oi}^2};$$

$n = 1, 14 \qquad i = 1$

$n = 2, 3, 4, 12, 13 \qquad i = 2$

$n = 5, 6, 9, 10, 11 \qquad i = 3$

$n = 7, 8 \qquad i = 4$

The solution for A_n and B_n are as follows:

$$\theta_1 = e^{-Ct/2}(A_1 \cos \omega_1 t + B_1 \sin \omega_1 t) + \frac{R_1}{\omega_{o1}^2} + \frac{X_1}{\omega_{o1}^2},$$

$$\dot{\theta}_1 = -\frac{C}{2} e^{-Ct/2}(A_1 \cos \omega_1 t + B_1 \sin \omega_1 t) + e^{-Ct/2}(-\omega_1 A \sin \omega_1 t + B_1 \cos \omega_1 t),$$

$$\dot{\theta}_1 = e^{-Ct/2}\left(\left(-\omega_1 A_1 - \frac{C}{2} B_1\right) \sin \omega_1 t + \left(B_1 \omega_1 - \frac{A_1 C}{2}\right) \cos \omega_1 t\right).$$

If $\frac{C}{2\omega_i} = BL_i$ the differentiation leads to

$$\dot{\theta}_1 = -\omega_1 e^{-Ct/2}((A_1 + B_1 BL_1)\sin \omega_1 t - (B_1 - A_1 BL_1)\cos \omega_1 t).$$

Boundary conditions at $t = 0, \theta = \theta_o$ and $\dot{\theta} = 0$ simplify the results to

$$\dot{\theta}_1 = 0 = \omega_1(B_1 - A_1 BL_1),$$

or

$$B_1 = A_1 BL_1,$$

$$\theta = \theta_o = A_1 + \frac{R_1}{\omega_{o1}^2} + \frac{X_1}{\omega_{o1}^2},$$

$$A_1 = \theta_o - (\frac{R_1}{\omega_{o1}^2} + \frac{X_1}{\omega_{o1}^2}),$$

with $X_1 = 0$ the coefficients are

$$A_1 = \theta_o - \frac{R_1}{\omega_{o1}^2},$$

$$B_1 = (\theta_o - \frac{R_1}{\omega_{o1}^2})BL_1.$$

Also the angle is

$$\theta_1 = e^{-CT/2}(A_1 \cos \omega_1 t + B_1 \sin \omega_1 t) + \frac{R_1}{\omega_{o1}^2}.$$

The solution for A_2 and B_2 proceeds in a manner similar to that for A_1 and B_1:

$$\theta_2 = e^{-Ct/2}(A_2 \cos \omega_2 t + B_2 \sin \omega_2 t) + \frac{R_2}{\omega_{o2}^2} + \frac{X_2}{\omega_{o2}^2},$$

and

$$\dot{\theta}_2 = -\omega_2 e^{-Ct/2}((A_2+B_2BL_2)\sin \omega_2 t-(B_2-A_2BL_2)\cos \omega_2 t).$$

From boundary conditions $\theta_2 = \theta_1$ and $\dot{\theta}_2 = \dot{\theta}_1$;

$$\omega_1 t_x = \frac{\pi}{2} - \delta = \omega_2 t_y.$$

Defining

$$TT_2 = \frac{\pi/2 - \delta}{\omega_1} \quad \text{and} \quad \omega_1 t_x = E$$

and consequently

$$\theta_1 = e^{-CTT_2/2}(A_1\cos E + B_1\sin E) + \frac{R_1}{\omega_{o1}^2} = \theta_2$$

$$\theta_2 = e^{-CTT_2/2}(A_2\cos E + B_2\sin E) + \frac{R_2}{\omega_{o2}^2},$$

$$B_2\sin E = (A_1 - A_2)\cos E + B_1\sin E + \frac{R_1}{\omega_{o1}^2 e^{-CTT_2/2}}$$

$$- \frac{R_2}{\omega_{o2}^2 e^{-CTT_2/2}},$$

$$B_2 = (A_1-A_2)\frac{\cos E}{\sin E} + B_1 + \left(\frac{R_1}{\omega_{o1}^2} - \frac{R_2}{\omega_{o2}^2}\right)\frac{1}{e^{-CTT_2/2}\sin E};$$

also

$$\dot{\theta}_1=-\omega_1 e^{-CTT_2/2}((A_1+B_1BL_1)\sin E-(B_1-A_1BL_1)\cos E)= \dot{\theta}_2$$

$$\dot{\theta}_2=-\omega_2 e^{-CTT_2/2}((A_2+B_2BL_2)\sin E-(B_2-A_2BL_2)\cos E),$$

$$\omega_2 B_2(BL_2 \sin E - \cos E) = \omega_1 B_1(BL_1 \sin E - \cos E)$$
$$+ \omega_1 A_1(\sin E + BL_1 \cos E)$$
$$- \omega_2 A_2(\sin E + BL_2 \cos E),$$

$$B_2 = \frac{\omega_1 B_1(BL_1 \sin E - \cos E)}{\omega_2 \ (BL_2 \sin E - \cos E)} + \frac{\omega_1 A_1(\sin E + BL_1 \cos E)}{\omega_2 \ (BL_2 \sin E - \cos E)}$$
$$- \frac{\omega_2 A_2(\sin E + BL_2 \cos E)}{\omega_2 \ (BL_2 \sin E - \cos E)},$$

$$B_1\left(1 - \frac{\omega_1(BL_1 \sin E - \cos E)}{\omega_2(BL_2 \sin E - \cos E}\right) + A_1\left(\frac{\cos E}{\sin E}\right)$$
$$- \frac{\omega_1 A_1(\sin E + BL_1 \cos E)}{\omega_2 \ (BL_2 \sin E - Cos E)} - \left(\frac{R_2}{\omega_{o2}^2} - \frac{R_1}{\omega_{o1}^2}\right)\frac{1}{e^{-CTT_2/2} \sin E}$$
$$= A_2\left(\frac{\cos E}{\sin E} - \frac{(\sin E + BL_2 \cos E)}{(BL_2 \sin E - \cos E)}\right),$$

$$\left(\frac{\cos E}{\sin E} - \frac{\sin E + BL_2 \cos E}{BL_2 \sin E - \cos E}\right) = \frac{-1}{\sin E(BL_2 \sin E - \cos E)};$$

and

$$A_2 = -\frac{B_1}{\omega_2}(\omega_2 \sin E(BL_2 \sin E - \cos E)$$
$$-\omega_1 \sin E(BL_1 \sin E - \cos E))$$
$$+ \frac{A_1}{\omega_2}(\omega_2 \cos E(\cos E - BL_2 \sin E)$$
$$+ \omega_1 \sin E(\sin E + BL_1 \cos E))$$
$$- \left(\frac{R_1}{\omega_{o1}^2} - \frac{R_2}{\omega_{o2}^2}\right)\left(\frac{BL_2 \sin E - Cos E}{e^{-CTT_2/2}}\right),$$

$$B_2 = \frac{\omega_1}{\omega_2}\left(\frac{B_1(BL_1\sin E - \cos E) + A_1(\sin E + BL_1\cos E)}{(BL_2\sin E - \cos E)}\right)$$

$$- A_2\left(\frac{\sin E + BL_2\cos E}{BL_2\sin E - \cos E}\right).$$

The sequential equations in resolving the third group of angles are

$$\theta_2 = \theta_3,$$

$$TT_3 = \frac{\pi/2 - \delta}{\omega_1} + \frac{\delta - \varepsilon}{\omega_2},$$

$$\omega_2 TT_3 = F,$$

$$\theta_2 = e^{-CTT_3/2}(A_2\cos F + B_2\sin F) + \frac{R_2}{\omega_{o2}^2},$$

$$\theta_3 = e^{-CTT_3/2}(A_3\cos F + B_3\sin F) + \frac{R_3}{\omega_{o2}^2} + \frac{X_3}{\omega_{o2}^2},$$

$$\dot{\theta}_2 = \dot{\theta}_3$$

$$\dot{\theta}_2 = -\omega_2 e^{-CTT_3/2}((A_2+B_2BL_2)\sin F - (B_2-A_2BL_2)\cos F),$$

$$\dot{\theta}_3 = -\omega_2 e^{-CTT_3/2}((A_3+B_3BL_2)\sin F - (B_3-A_3BL_2)\cos F),$$

$$B_3\sin F = (A_2 - A_3)\cos F + B_2\sin F + \frac{R_2 - R_3 - X_3}{\omega_{o2}^2 e^{-CTT_3/2}},$$

$$B_3 = (A_2 - A_3)\frac{\cos F}{\sin F} + B_2 + \frac{R_2 - R_3 - X_3}{\omega_{o2}^2 e^{-CTT_3/2}\sin F},$$

$$B_3(BL_2\sin F - \cos F) = B_2(BL_2\sin F - \cos F)$$

$$+ (A_2 - A_3)(\sin F + BL_2\cos F),$$

$$B_3 = B_2 + (A_2 - A_3)\left(\frac{\sin F + BL_2 \cos F}{BL_2 \sin F - \cos F}\right),$$

$$0 = (A_2 - A_3)\left(\frac{\cos F}{\sin F} - \frac{\sin F + BL_2 \cos F}{BL_2 \sin F - \cos F}\right) + \frac{R_2 - R_3 - X_3}{\omega_{o2}^2 e^{-CTT_3/2}} \sin F,$$

$$0 = (A_2 - A_3)\left(\frac{-1}{\sin F(BL_2 \sin F - \cos F)}\right) + \frac{R_2 - R_3 - X_3}{\omega_{o2}^2 e^{-CTT_3/2}} \sin F,$$

$$A_3 = A_2 - \left(\frac{R_2 - R_3 - X_3}{\omega_{o2}^2 e^{-CTT_3/2}}\right)(BL_2 \sin F - \text{Cos } F),$$

$$B_3 = B_2 + \left(\frac{R_2 - R_3 - X_3}{\omega_{o2}^2 e^{-CTT_3/2}}\right)(\sin F + BL_2 \cos F).$$

The resolution of the remaining equations follow the same pattern. It is almost possible to infer the information which is listed in Chapter III. The detailed steps are therefore omitted.

APPENDIX B

COMPUTER PROGRAMS

The resulting solution of the equation of motion for the escapement, by dividing the solution into fourteen segments and matching boundary condition, necessitated the use of a computer since a solution of one cycle by hand could take an hour or more. These programs presented are in "Fortran with Format" and the monitor cards are for the OSU-IBM-1410 computer; other computers may require different monitor and/or some program statements. Three programs are presented here. The basic difference is that the first program allows four changes in the hairspring constant "ω_o" during a cycle. This is a relatively long program since there are 60 to 70 constants which must be computed and stored during each cycle. The other two programs use a constant "ω_o" and are considerably shorter. The number of steps per cycle can be reduced from fourteen to ten or twelve and there is no need to compute the B's if "ω_o" is constant. In the last two programs the computer needs to calculate only 10 to 15 constants per cycle and takes less time. The 12-step program allows more versatility than the 10-step program. All the curves for use in estimating

operating conditions are computed with a constant ω_o. The program's input statements are in the form of seven-column, ten-digit format and the output statements are in the form of twelve column, eleven-digit format for an on-line printer, printing one line per cycle. Block diagrams are shown in Figures 37 and 38. Figure 37 depicts the program with a changeable ω_o and Figure 38 depicts the shorter program with a constant ω_o. The first cards for the program input statements are identical. The input-output language for the programs is defined below:

Input

Long Program	Short Program	Symbol	Definition
ALPHA	ALPHA	α	Angle of power stroke before "o" beat, balance moving clockwise.
BETA	BETA	β	Angle of power stroke after "o" beat, balance moving clockwise.
GAMA	GAMA	γ	Same as α except balance moving counterclockwise.
AMU	AMU	μ	Same as β except balance moving counterclockwise.
EPIL	EPIL	ε	$\varepsilon-\alpha$ = unlock angle movement clockwise.
SIGMA	SIGMA	σ	$\sigma-\gamma$ = unlock angle movement counterclockwise.
FE	not used	ϕ	Angle counterclockwise from "o" to the first ω_o change.

Input (cont.)

Long Program	Short Program	Symbol	Definition
not used	PHI (12)	ϕ	Angle clockwise from "o" to the second change of the forcing function.
DELT	not used	δ	Same as ϕ except clockwise.
not used	DELT (12)	δ	Same as ϕ except counter-clockwise.
not used	OMEGA	ω_o	Hairspring constant.
OMn	not used	ω_{on}	Hairspring constant n = 1, 2, 3, 4.
C	C	C	Viscous damping constant.
THETO	THETO	θ_o	Initial displacement at t = 0.
Rn	R(n)	R_n	Kinetic damping constant.
Xn	X(n)	X_n	Magnitude of the forcing function in that segment.

Output

Long Program	Short Program	Definition
THETA(14)	THETA(10)	Amplitude at the end of the cycle.
T	T	Time corresponding to above amplitude.
TB	TB	Number of cycles.
TA	TA	Intermediate calculation.
TC	TC	C/ω_{o1} or C/ω_o.
XS	XS	$R14/\omega_{o1}^2$ or $R(10)/\omega_o^2$.
XT	XT	$X4/\omega_{o2}^2$ or $X(3)/\omega_o^2$.

Output (cont.)

Long Program	Short Program	Definition.
XU	XU	$X3/\omega_{o2}^2$ or $X(2)/\omega_o^2$.
THETB	THETB	θ_{14}/θ_o or θ_{10}/θ_o.
OMEGn	OMEG1	$\sqrt{4\omega_{on}^2 - C^2}/2$ or $\sqrt{4\omega_o^2 - C^2}/2$.
XIT	XIT	$1.0 - (\theta_o - \theta_{14})$ or $1.0 - (\theta_o - \theta_{10})$.
XP	XP	$e^{-Ct/2}$.

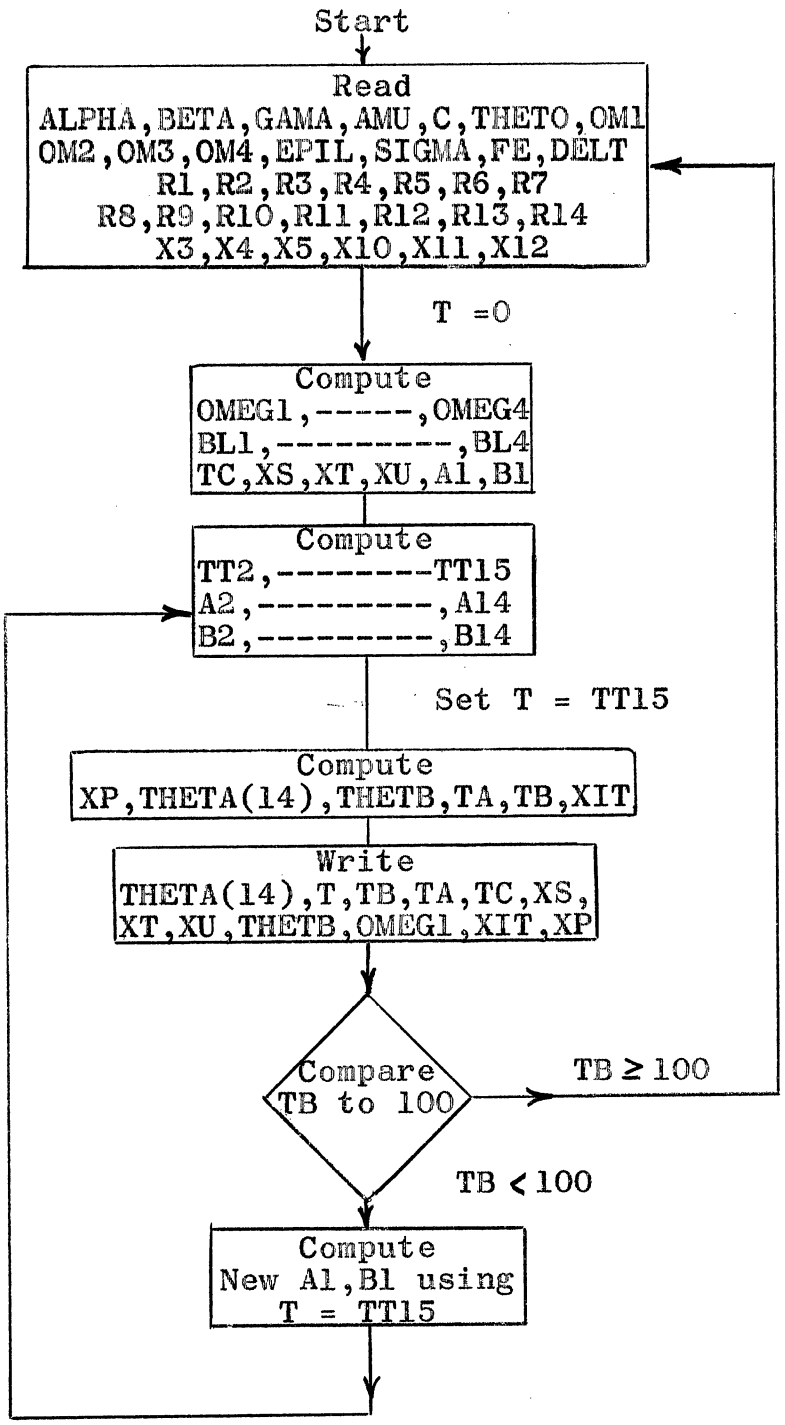

Figure 37. Diagram for Nonlinear ω_o

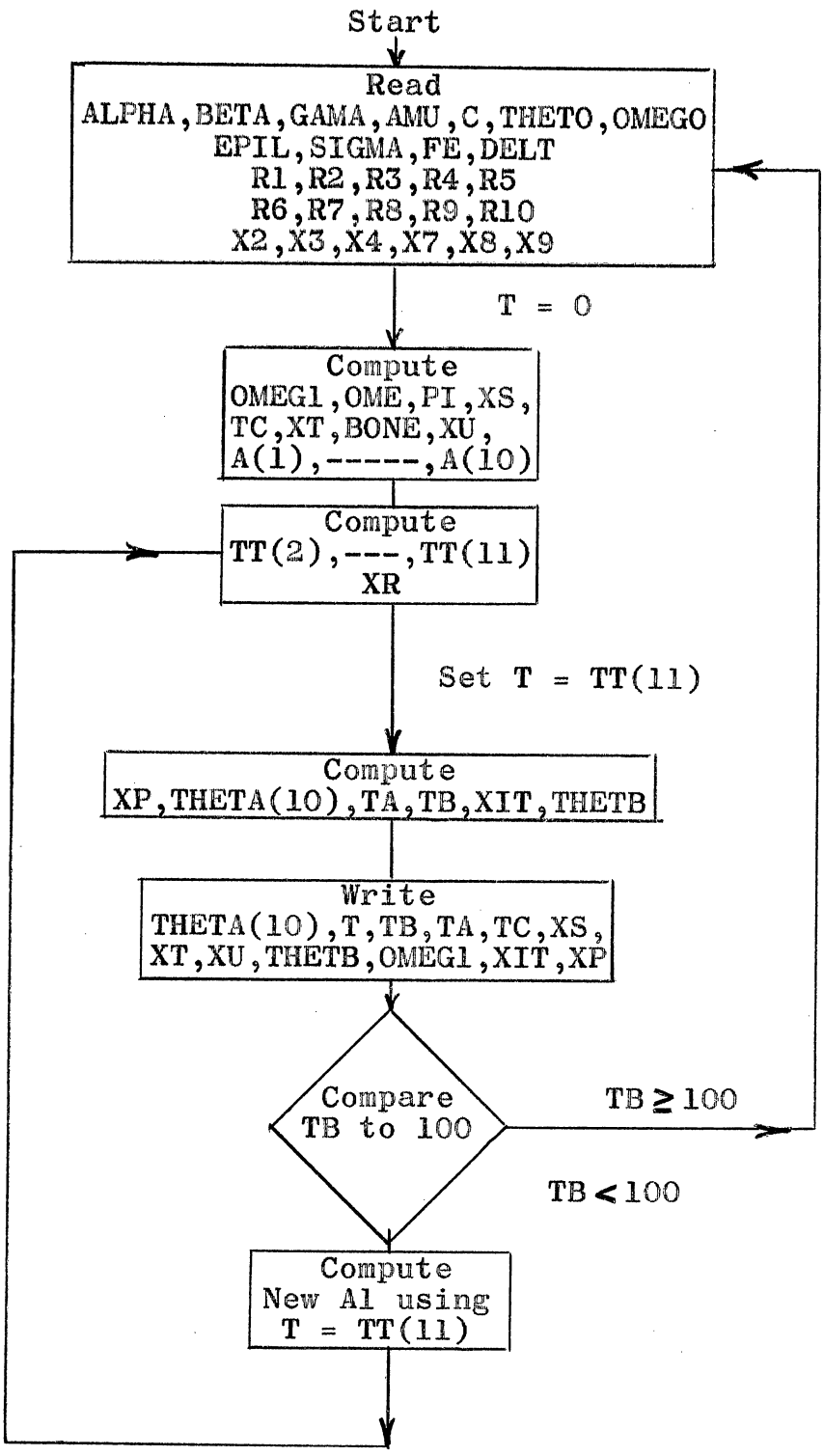

Figure 38. Diagram for Linear ω_o

TABLE II

```
C               PROGRAM WITH VARIABLE OMEGO

      MON$$       JOB  735261001          MONDAY
      MON$$       ASGN MGO,A2
      MON$$       ASGN MJB,A3
      MON$$       ASGN MW1,A4
      MON$$       ASGN MW2,A5
      MON$$       MODE GO,TEST
      MON$$       EXEQ FORTRAN
  900  FORMAT(7F10.6)
  901  FORMAT(1X,12F11.6)
  100  READ(1,900)ALPHA,BETA,GAMA,AMU,C,THETO,OM1
       READ(1,900)OM2,OM3,OM4,EPIL,SIGMA,FE,DELT
       READ(1,900)R1,R2,R3,R4,R5,R6,R7
       READ(1,900)R8,R9,R10,R11,R12,R13,R14
       READ(1,900)X3,X4,X5,X10,X11,X12
       T=0.0
       OMEG1=((SQRT(4.0*OM1*OM1-C*C))/2.0)
       OMEG2=((SQRT(4.0*OM2*OM2-C*C))/2.0)
       OMEG3=((SQRT(4.0*OM3*OM3-C*C))/2.0)
       OMEG4=((SQRT(4.0*OM4*OM4-C*C))/2.0)
       BL1=C/(2.0*OMEG1)
       BL2=C/(2.0*OMEG2)
       BL3=C/(2.0*OMEG3)
       BL4=C/(2.0*OMEG4)
       TC=C/OM2
       XS=R14/(OM1**2)
       XT=X4/(OM2**2)
       XU=X3/(OM2**2)
       PI=3.1415926536/2.0
       A1=THETO-R1/(OM1**2)
       B1=A1*BL1
   20  TT2=(PI-DELT)/OMEG1+T
       TT3=TT2+(DELT-EPIL)/OMEG2
       TT4=TT2+(DELT-ALPHA)/OMEG2
       TT5=TT2+DELT/OMEG2
       TT6=TT5+BETA/OMEG3
       TT7=TT5+FE/OMEG3
       TT8=TT7+(PI-FE)/OMEG4
       TT9=TT7+2.0*(PI-FE)/OMEG4
       TT10=TT9+(FE-SIGMA)/OMEG3
       TT11=TT9+(FE-GAMA)/OMEG3
       TT12=TT9+FE/OMEG3
       TT13=TT12+AMU/OMEG2
       TT14=TT12+DELT/OMEG2
       TT15=TT14+(PI-DELT)/OMEG1
```

TABLE II (CONTINUED)

```
E=OMEG1*TT2
F=OMEG2*TT3
G=OMEG2*TT4
H=OMEG2*TT5
HL=OMEG3*TT6
HM=OMEG3*TT7
HN=OMEG4*TT8
P=OMEG4*TT9
Q=OMEG3*TT10
R=OMEG3*TT11
S=OMEG3*TT12
W=OMEG2*TT13
U=OMEG1*TT14
V=OMEG1*TT15
A2=B1*(OMEG2*SIN(E)*(BL2*SIN(E)-COS(E)))/OMEG2
A2=-A2+B1*(OMEG1*SIN(E)*(BL1*SIN(E)-COS(E)))/OMEG2
A2=A2+A1*(OMEG2*COS(E)*(COS(E)-BL2*SIN(E)))/OMEG2
A2=A2+A1*(OMEG1*SIN(E)*(SIN(E)+BL1*COS(E)))/OMEG2
A2=A2-(R1/(OM1**2)-R2/(OM2**2))*(BL2*SIN(E)-COS(E))/EXP(-C*TT2/2.)
B2=OMEG1*(A1*(SIN(E)+BL1*COS(E))+B1*(BL1*SIN(E)-COS(E)))
B2=B2/OMEG2*(BL2*SIN(E)-COS(E))
B2=B2-A2*(SIN(E)+BL2*COS(E))/(BL2*SIN(E)-COS(E))
A3=A2-(R2-R3-X3)*(BL2*SIN(F)-COS(F))/(OM2**2.)*EXP(-C*TT3/2.0)
B3=B2+(R2-R3-X3)*(SIN(F)+BL2*COS(F))/(OM2**2)*(EXP(-C*TT3/2.0))
A4=A3-(R3-R4+X3-X4)*(BL2*SIN(G)-COS(G))/(OM2**2)*(EXP(-C*TT4/2.0))
B4=B3+(R3-R4+X3-X4)*(SIN(G)+BL2*COS(G))/(OM2**2)*(EXP(-C*TT4/2.0))
A5=B4*(OMEG3*SIN(H)*(BL3*SIN(H)-COS(H)))/OMEG3
A5=-A5+B4*(OMEG2*SIN(H)*(BL2*SIN(H)-COS(H)))/OMEG3
A5=A5+A4*(OMEG3* COS(H)*(COS(H)-BL3*SIN(H)))/OMEG3
A5=A5+A4*(OMEG2*SIN(H)*(SIN(H)+BL2*COS(H)))/OMEG3
A5=A5-((R4+X4)/OM2**2)*(BL3*SIN(H)-COS(H))/EXP(-C*TT5/2.0)
B5=OMEG2*(A4*(SIN(H)+BL2*COS(H))+B4*(BL2*SIN(H)-COS(H)))
B5=B5/OMEG3*(BL3*SIN(H)-COS(H))
A6=A5-(R5-R6+X5)*(BL3*SIN(HL)-COS(HL))/(OM3**2)*EXP(-C*TT6/2.0)
B6=B5+(R5-R6+X5)*(SIN(HL)+BL2*COS(HL))/(OM3**2)*EXP(-C*TT6/2.0)
A7=B6*(OMEG4*SIN(HM)*(BL4*SIN(HM)-COS(HM)))/OMEG4
A7=-A7+B6*(OMEG3*SIN(HM)*(BL3*SIN(HM)-COS(HM)))/OMEG4
A7=A7+A6*(OMEG4*COS(HM)*(COS(HM)-BL4*SIN(HM)))/OMEG4
A7=A7+A6*(OMEG3*SIN(HM)*(SIN(HM)+BL3*COS(HM)))/OMEG4
A7=A7-(R6/(OM3**2))*(BL4*SIN(HM)-COS(HM))/EXP(-C*TT7/2.0)
A7=A7+(R7/(OM4**2))*(BL4*SIN(HM)-COS(HM))/EXP(-C*TT7/2.0)
B7=OMEG3*(A6*(SIN(HM)+BL3*COS(HM))+B6*(BL3*SIN(HM)-COS(HM)))
B7=B7/OMEG4*(BL4*SIN(HM)-COS(HM))
B7=B7-A7*(SIN(HM)+BL4*COS(HM))/(BL4*SIN(HM)-COS(HM))
A8=A7-(R7-R8)*(BL4*SIN(HN)-COS(HN))/EXP(-C*TT8/2.0)*(OM4**2)
B8=B7+(R7-R8)*(SIN(HN)+BL4*COS(HN))/EXP(-C*TT8/2.0)*(OM4**2)
A9=B8*(OMEG3*SIN(P)*(BL3*SIN(P)-COS(P)))/OMEG3
A9=-A9+B8*(OMEG4*SIN(P)*(BL4*SIN(P)-COS(P)))/OMEG3
A9=A9+A8*(OMEG3*COS(P)*(COS(P)-BL3*SIN(P)))/OMEG3
A9=A9+A8*(OMEG4*SIN(P)*(SIN(P)+BL4*COS(P)))/OMEG3
A9=A9-(R8/(OM4**2)-R9/(OM3**2)*(BL3*SIN(P)-COS(P)))/EXP(-C*TT9/2.)
B9=OMEG4*(A8*(SIN(P)+BL4*COS(P))+B8*(BL4*SIN(P)-COS(P)))/OMEG3
B9=(B9-A9*(SIN(P)+BL3*COS(P)))/(BL3*SIN(P)-COS(P))
A10=-(R9-R10-X10)*(BL3*SIN(Q)-COS(Q))/(OM3**2)*EXP(-C*TT10/2.0)+A9
B10=B9+(R9-R10-X10)*(SIN(Q)+BL3*COS(Q))/(OM3**2)*EXP(-C*TT10/2.0)
```

TABLE II (CONTINUED)

```
A11=(R10-R11+X10-X11)*(BL3*SIN(R)-COS(R))/(OM3**2)*EXP(-C*TT11/2.)
A11=-A11+A10
B11=(R10-R11+X10-X11)*(SIN(R)+BL3*COS(R))/(OM3**2)*EXP(-C*TT11/2.)
B11=B11+B10
A12=B11*(OMEG2*SIN(S)*(BL2*SIN(S)-COS(S)))/OMEG2
A12=-A12+B11*(OMEG3*SIN(S)*(BL3*SIN(S)-COS(S)))/OMEG2
A12=A12+A11*(OMEG2*COS(S)*(COS(S)-BL2*SIN(S)))/OMEG2
A12=A12+A11*(OMEG3*SIN(S)*(SIN(S)+BL3*COS(S)))/OMEG2
A12=A12-(R11+X11)*(BL2*SIN(S)-COS(S))/(OM2**2)*EXP(-C*TT12/2.0)
A12=A12+(R12+X12)*(BL2*SIN(S)-COS(S))/(OM2**2)*EXP(-C*TT12/2.0)
B12=OMEG3*(A11*(SIN(S)+BL3*COS(S))+B11*(BL3*SIN(S)-COS(S)))/OMEG2
B12=(B12-A12*(SIN(S)+BL2*COS(S)))/(BL2*SIN(S)-COS(S))
A13=-(R12-R13+X12)*(BL2*SIN(W)-COS(W))/(OM2**2)*EXP(-C*TT13/2.0)
A13=A13+A12
B13=(R12-R13+X12)*(BL2*SIN(W)-COS(W))/(OM2**2)*EXP(-C*TT13/2.0)
B13=B13+B12
A14=B13*(OMEG1*SIN(U)*(BL1*SIN(U)-COS(U)))/OMEG1
A14=-A14+B13*(OMEG2*SIN(U)*(BL2*SIN(U)-COS(U)))/OMEG1
A14=A14+A13*(OMEG1*COS(U)*(COS(U)-BL1*SIN(U)))/OMEG1
A14=A14+A13*(OMEG2*SIN(U)*(SIN(U)+BL2*COS(U)))/OMEG1
A14=A14-(R13/(OM2**2)*(BL1*SIN(U)-COS(U)))/EXP(-C*TT14/2.0)
A14=A14+(R14/(OM1**2))*(BL1*SIN(U)-COS(U))/EXP(-C*TT14/2.0)
B14=OMEG2*(A13*(SIN(U)+BL2*COS(U))+B13*(BL2*SIN(U)-COS(U)))/OMEG1
B14=(B14-A14*(SIN(U)+BL1*COS(U)))/(BL1*SIN(U)-COS(U))
T=TT15
XP=EXP(-C*T/2.0)
TH14      =(XP*A14)+XS
TA=(TT15*OMEG1)/4.0*PI
TB=TA*OMEG1/OM1
WRITE(3,901)TH14      ,T,TB,TA,TC,XS,XT,XU,       OMEG1,    XP
IF(TB.GE. 50.0)GO TO 100
A1=A14-(R14-R1)*(BL1*SIN(V)-COS(V))/(OM1**2)*EXP(-C*TT15/2.0)
B1=B14+(R14-R1)*(SIN(V)-BL1*COS(V))/(OM1**2)*EXP(-C*TT15/2.0)
GO TO 20
END
MON$$      EXEQ LINKLOAD
           PHASEMAINPGM
           CALLNIBINTRP
           CALL MAINPGM
MON$$      EXEQ MAINPGM,MJB
```

TYPICAL DATA

```
.2786896   .2786896   .2786896   .2786896   1.570796   6.28       31.4159265
31.41592   31.41592   31.41592   .6337686   .6337686   1.00       1.00
 600.0      600.0      600.0      600.0      600.0      600.0      600.0
-600.0     -600.0     -600.0     -600.0     -600.0     -600.0     -600.0
123.0      -759.96    -759.96    -123.0      759.96     759.96
```

TABLE III

PROGRAM WITH CONSTANT OMEGO TEN PARTS

```
    MON$$      JOB  735261001         MONDAY
    MON$$      ASGN MGO,A2
    MON$$      ASGN MJB,A3
    MON$$      ASGN MW1,A4
    MON$$      ASGN MW2,A5
    MON$$      MODE GO,TEST
    MON$$      EXEQ FORTRAN
     DIMENSION  TT(11),A(10),B(10),R(10),THETA(10),X(10)
900  FORMAT(7F10.6)
901  FORMAT(1X,12F11.6)
100  READ(1,900)ALPHA ,BETA,GAMA,AMU,C,THETO,OMEGO
     READ(1,900)EPIL,SIGMA
     READ(1,900)R(1),R(2),R(3),R(4),R(5)
     READ(1,900)R(6),R(7),R(8),R(9),R(10)
     READ(1,900)X(2),X(3),X(4),X(7),X(8),X(9)
     T=0.0
     A(1) =THETO-R(1)/(OMEGO*OMEGO)
 10  OMEG1=((SQRT(4.0*OMEGO*OMEGO-C*C))/2.0)
     OME= (OMEGO**2)
     TC= C/OMEGO
     BONE=C/(2.0*OMEG1)
     PI=3.1415926536/2.0
     XS=R(10)/(OMEGO**2)
     XT=X(3)/(OMEGO**2)
     XU=X(2)/(OMEGO**2)
     A(2)=-(R(1)-R(2)-X(2))*(BONE*COS(EPIL )-SIN(EPIL ))/OME
     A(3)=-(R(2)+X(2)-R(3)-X(3))*(BONE*COS(ALPHA)-SIN(ALPHA)) /OME
     A(4)=-(R(3)+X(3)-R(4)-X(4))*BONE/OME
     A(5)= -(R(4)+X(4)-R(5))*(BONE*COS(BETA)+SIN(BETA))/OME
     A(6)=-(R(5)-R(6))/OME
     A(7)=-(-R(6)+R(7)+X(7))*(BONE*COS(SIGMA)-SIN(SIGMA))/OME
     A(8 )=-(-R(7)-X(7)+R(8)+X(8))*(BONE*COS(GAMA)-SIN(GAMA))/OME
     A(9 )=-(-R(8 )-X(8 )+R(9 )+X(9 ))*BONE/OME
     A(10)=-(-R(9)-X(9)+R(10))*(BONE*COS(AMU)+SIN(AMU))/OME
 20  TT(2)=(PI-EPIL )/OMEG1+T
     TT(3)=(PI-ALPHA)/OMEG1+T
     TT(4)=(PI)/OMEG1 +T
     TT(5)=(PI+BETA)/OMEG1 +T
     TT(6)=(2.0*PI)/OMEG1 +T
     TT(7)=(3.0*PI-SIGMA)/OMEG1+T
     TT(8 )=(3.0*PI-GAMA)/OMEG1+T
```

TABLE III (CONTINUED)

```
      TT(9 )=(3.0*PI      )/OMEG1+T
      TT(10)=(3.0*PI+AMU  )/OMEG1+T
      TT(11)=(4.0*PI)/OMEG1+T
      XR=A(1)+A(2)/EXP(-C*TT(2)/2.0)+A(3)/EXP(-C*TT(3)/2.0)
      XR=XR+A(4)/EXP(-C*TT(4)/2.0)+A(5)/EXP(-C*TT(5)/2.0)
      XR=XR+A(6)/EXP(-C*TT(6)/2.0)+A(7)/EXP(-C*TT(7)/2.0)
      XR=XR+A(8)/EXP(-C*TT(8)/2.0)+A(9)/EXP(-C*TT(9)/2.0)
      XR=XR+A(10)/EXP(-C*TT(10)/2.0)
      T=TT(11)
      XP=EXP(-C*T/2.0)
      THETA(10)=(XP*XR)+XS
      THETB=THETA(10)/THETO
      TA=(TT(11)*OMEG1)/(4.0*PI)
      TB= TA*OMEG1/OMEGO
      TX=THETA(10)-XP*XR
      XIT=1.00-(THETO -THETA(10))
      WRITE(3,901)THETA(10),T,TB,TA,TC,XS,XT,XU,THETB,OMEG1,XIT,XP
      IF(TB.GE.040.0)GO TO 100
    7 A(1) =XR    -(-R(10)+R(1))/((OMEGO**2)*EXP(-C*TT(11)/2.0))
      GO TO 10
      END
     MON$$      EXEQ LINKLOAD
                CALL MAINPGM
     MON$$      EXEQ MAINPGM,MJB
```

TYPICAL DATA

```
.2786896  .2786896  .2786896  .2786896  4.40000   6.28      31.4159265
.6337686  .6337686
 600.0     600.0     600.0     600.0     600.0
-600.0    -600.0    -600.0    -600.0    -600.0
123.0     -759.96   -759.96   -123.0     759.96    759.96
```

TABLE IV

PROGRAM WITH CONSTANT OMEGO TWELVE PARTS

```
    MON$$      JOB  735261001         MONDAY
    MON$$      ASGN MGO,A2
    MON$$      ASGN MJB,A3
    MON$$      ASGN MW1,A4
    MON$$      ASGN MW2,A5
    MON$$      MODE GO,TEST
    MON$$      EXEQ FORTRAN
     DIMENSION  TT(13),A(12),B(12),R(12),THETA(12),X(12)
900  FORMAT(7F10.6)
901  FORMAT(1X,12F11.6)
100  READ(1,900)ALPHA ,BETA,GAMA,AMU,C,THETO,OMEGO
     READ(1,900)DELT ,PHI   ,  EPIL,SIGMA
     READ(1,900)R(1),R(2),R(3),R(4),R(5)
     READ(1,900)R(6),R(7),R(8),R(9),R(10),R(11),R(12)
     READ(1,900)X(1),X(2),X(3),X(4),X(5),X(6)
     READ(1,900)X(7),X(8),X(9),X(10),X(11),X(12)
     T=0.0
     OMEG1=((SQRT(4.0*OMEGO*OMEGO-C*C))/2.0)
     OME= (OMEGO**2)
     TC= C/OMEGO
     BONE=C/(2.0*OMEG1)
     PI=3.1415926536/2.0
     XS=R(12)/(OMEGO**2)
     XT=X(4)/(OMEGO**2)
     XU=X(2)/(OMEGO**2)
     A(1) =THETO-R(1)/(OMEGO*OMEGO)
     A(2)=-(R(1)-R(2)-X(2))*(BONE*COS(EPIL )-SIN(EPIL ))/OME
     A(3)=-(R(2)+X(2)-R(3)-X(3))*(BONE*COS(DELT )-SIN(DELT )) /OME
     A(4)=-(R(3)+X(3)-R(4)-X(4))*(BONE*COS(ALPHA)-SIN(ALPHA)) /OME
     A(5)=-(R(4)+X(4)-R(5)-X(5))*BONE/OME
     A(6)= -(R(5)+X(5)-R(6))*(BONE*COS(BETA)+SIN(BETA))/OME
     A(7)=-(R(6)-R(7))/OME
     A(8)=-(-R(7)+R(8)+X(8))*(BONE*COS(SIGMA)-SIN(SIGMA))/OME
     A(9 )=-(-R(8)-X(8)+R(9)+X(9))*(BONE*COS(PHI )-SIN(PHI ))/OME
     A(10)=-(-R(9)-X(9)+R(10)+X(10))*(BONE*COS(GAMA)-SIN(GAMA))/OME
     A(11)=-(-R(10)-X(10)+R(11)+X(11))*BONE/OME
     A(12)=-(-R(11)-X(11)+R(12))*(BONE*COS(AMU)+SIN(AMU))/OME
 20  TT(2)=(PI-EPIL )/OMEG1+T
     TT(3)=(PI-DELT)/OMEG1+T
     TT(4)=(PI-ALPHA)/OMEG1+T
     TT(5)=(PI)/OMEG1 +T
```

TABLE IV (CONTINUED)

```
      TT(6)=(PI+BETA)/OMEG1 +T
      TT(7)=(2.0*PI)/OMEG1 +T
      TT(8)=(3.0*PI-SIGMA)/OMEG1+T
      TT(9)=(3.0*PI-PHI)/OMEG1+T
      TT(10)=(3.0*PI-GAMA)/OMEG1+T
      TT(11)=(3.0*PI      )/OMEG1+T
      TT(12)=(3.0*PI+AMU  )/OMEG1+T
      TT(13)=(4.0*PI)/OMEG1+T
      XR=A(1)+A(2)/EXP(-C*TT(2)/2.0)+A(3)/EXP(-C*TT(3)/2.0)
      XR=XR+A(4)/EXP(-C*TT(4)/2.0)+A(5)/EXP(-C*TT(5)/2.0)
      XR=XR+A(6)/EXP(-C*TT(6)/2.0)+A(7)/EXP(-C*TT(7)/2.0)
      XR=XR+A(8)/EXP(-C*TT(8)/2.0)+A(9)/EXP(-C*TT(9)/2.0)
      XR=XR+A(10)/EXP(-C*TT(10)/2.0)
      XR=XR+A(11)/EXP(-C*TT(11)/2.0)+A(12)/EXP(-C*TT(12)/2.0)
      T=TT(13)
      XP=EXP(-C*T/2.0)
      THETA(12)=(XP*XR)+XS
      THETB=THETA(12)/THETO
      TA=(TT(13)*OMEG1)/(4.0*PI)
      TB= TA*OMEG1/OMEGO
      TX=THETA(12)-XP*XR
      XIT=1.00-(THETO -THETA(12))
      WRITE(3,901)THETA(12),T,TB,TA,TC,XS,XT,XU,THETB,OMEG1,XIT,XP
      IF(TB.GE.050.0)GO TO 100
    7 A(1) =XR    -(-R(12)+R(1))/((OMEGO**2)*EXP(-C*TT(13)/2.0))
      GO TO 20
      END
     MON$$      EXEQ LINKLOAD
                CALL MAINPGM
     MON$$      EXEQ MAINPGM,MJB
```

TYPICAL DATA

```
.2786896   .2786896   .2786896   .2786896   4.40000    6.28        31.4159265
.6636      .6636      1.300      1.352
 600.0      600.0      600.0      600.0      600.0      600.0
-600.0     -600.0     -600.0     -600.0     -600.0     -600.0
123.0      -759.96    -759.96    -123.0      759.96     759.96
```

APPENDIX C

ADDITIONAL SOLUTION CURVES

This section contains 15 "computed unit curves" with a C/ω_o from 0.040 to 0.150. These curves can be used as outlined in Chapter IV to estimate the equation constants. The curves were solved with an initial displacement of 6.28 radians using the solution to the equations presented in Chapter III and a constant ω_o.

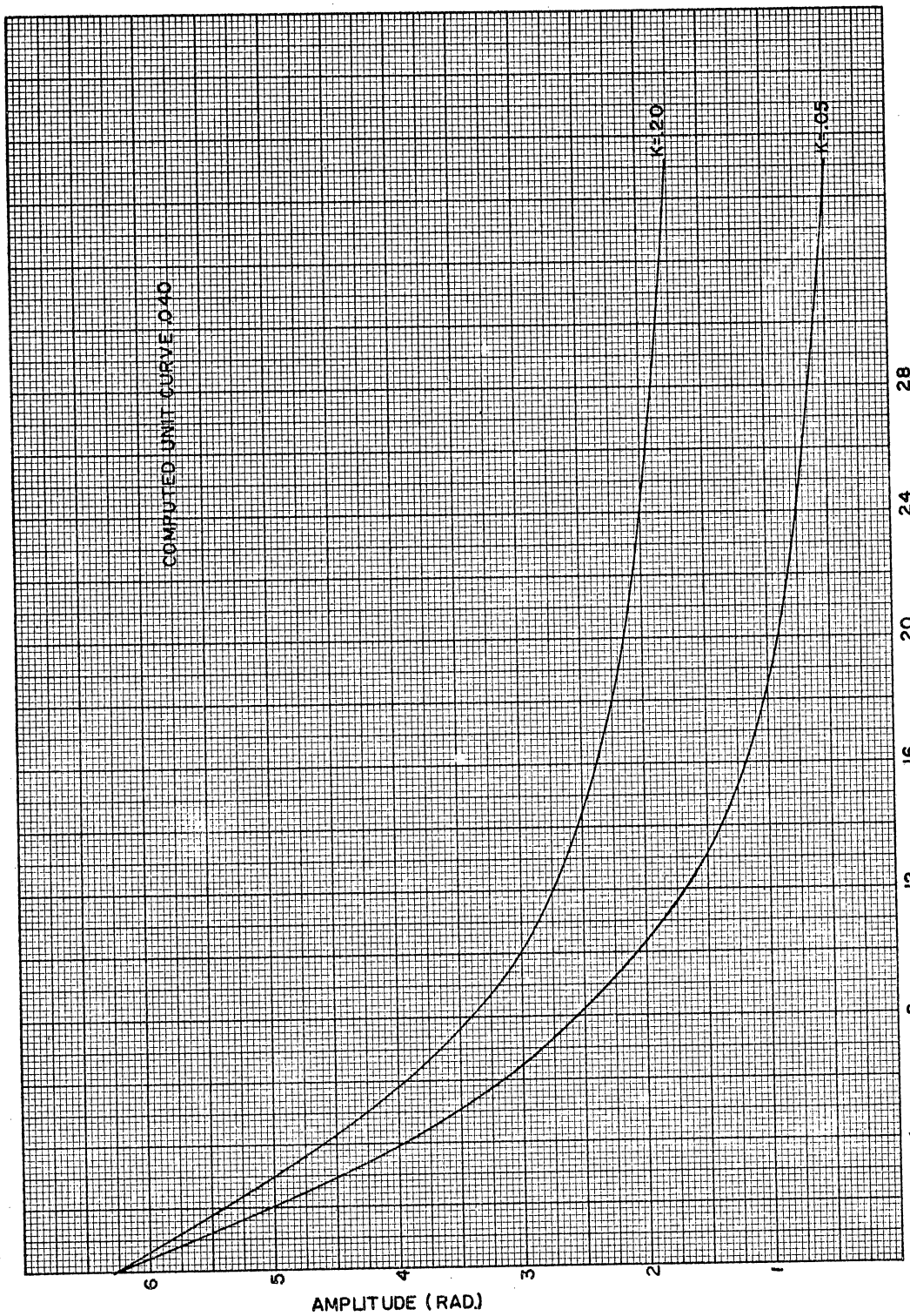

Figure 39. Computed Unit Curve 0.040

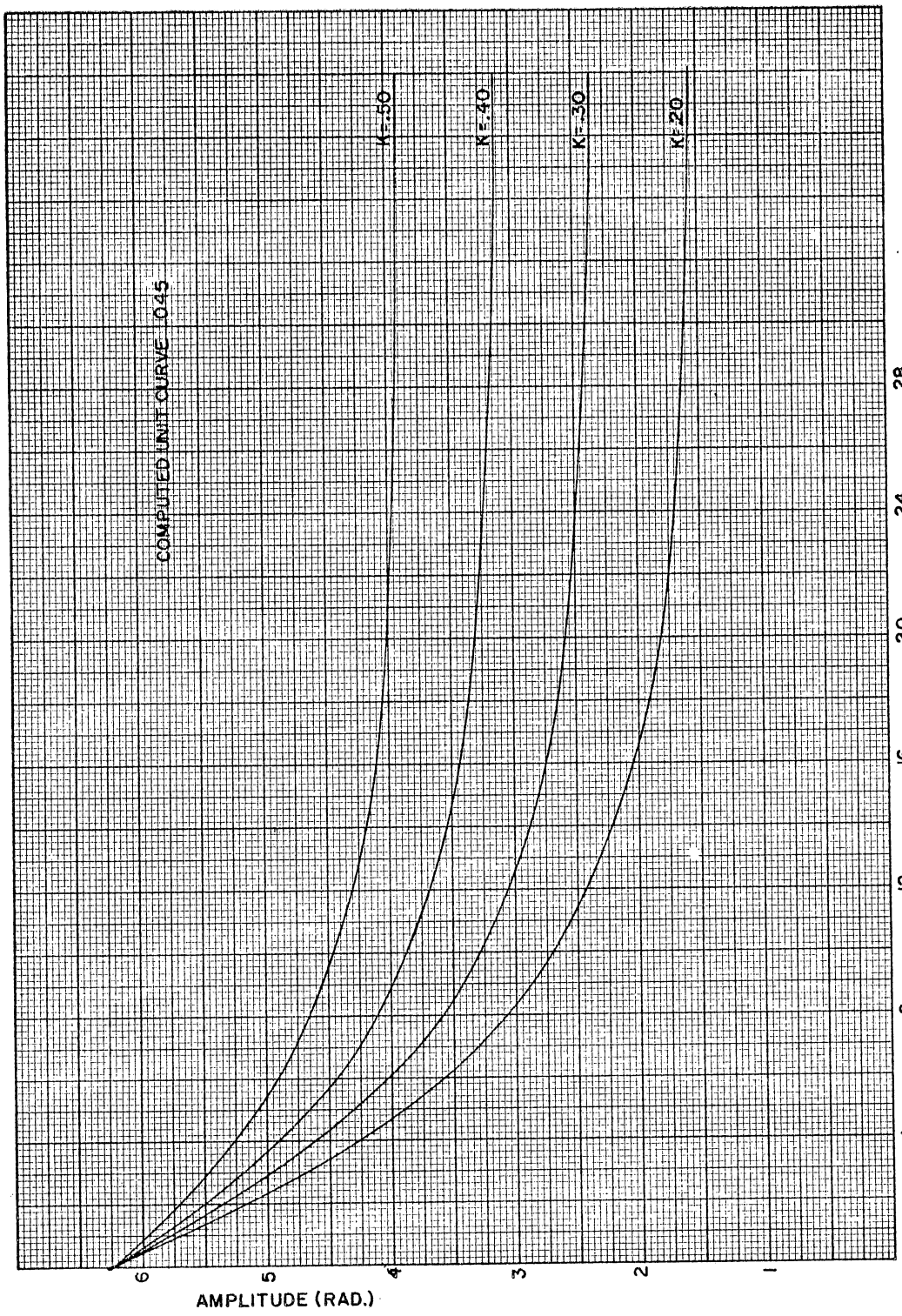

Figure 40. Computed Unit Curve 0.045

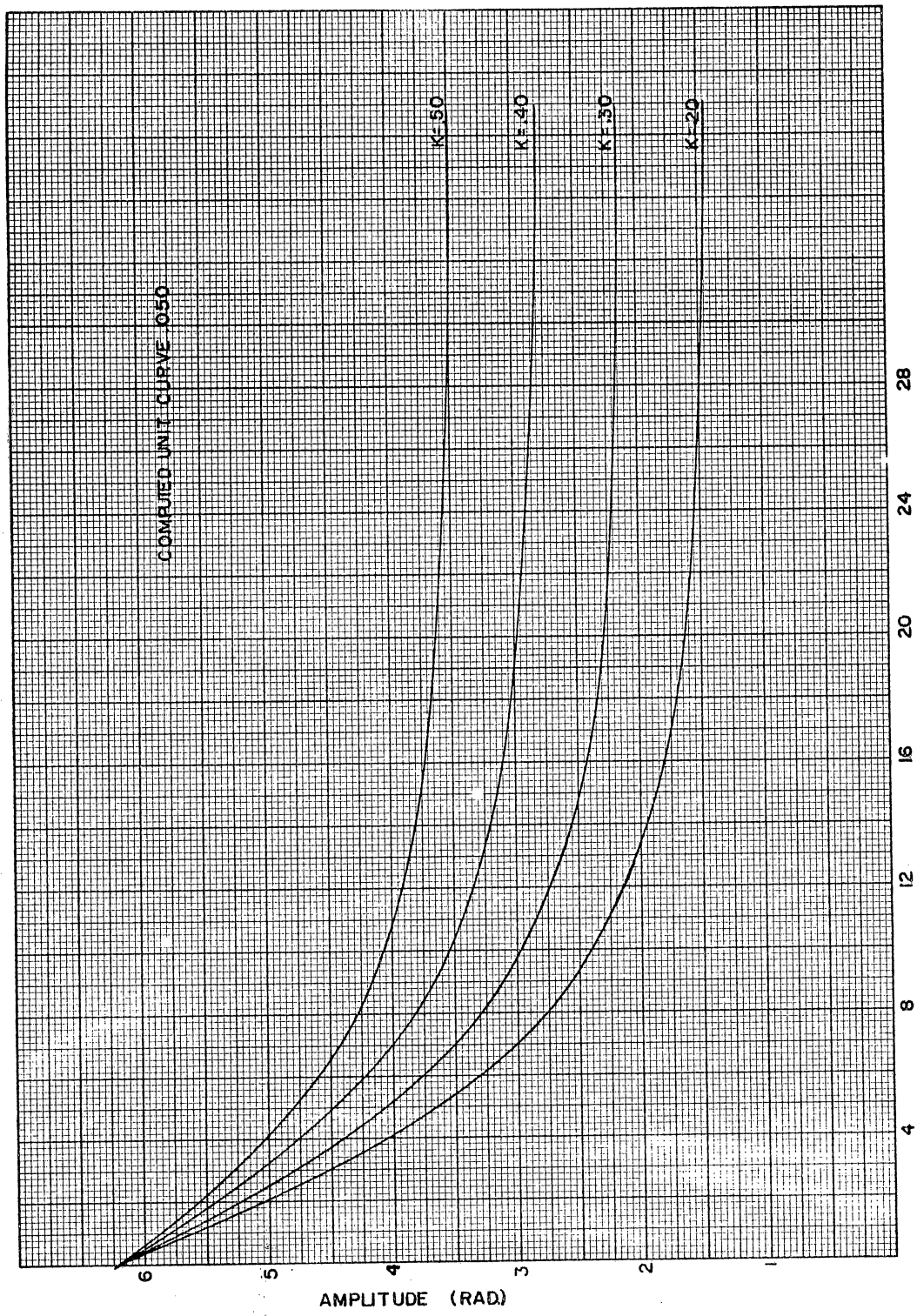

Figure 41. Computed Unit Curve 0.050

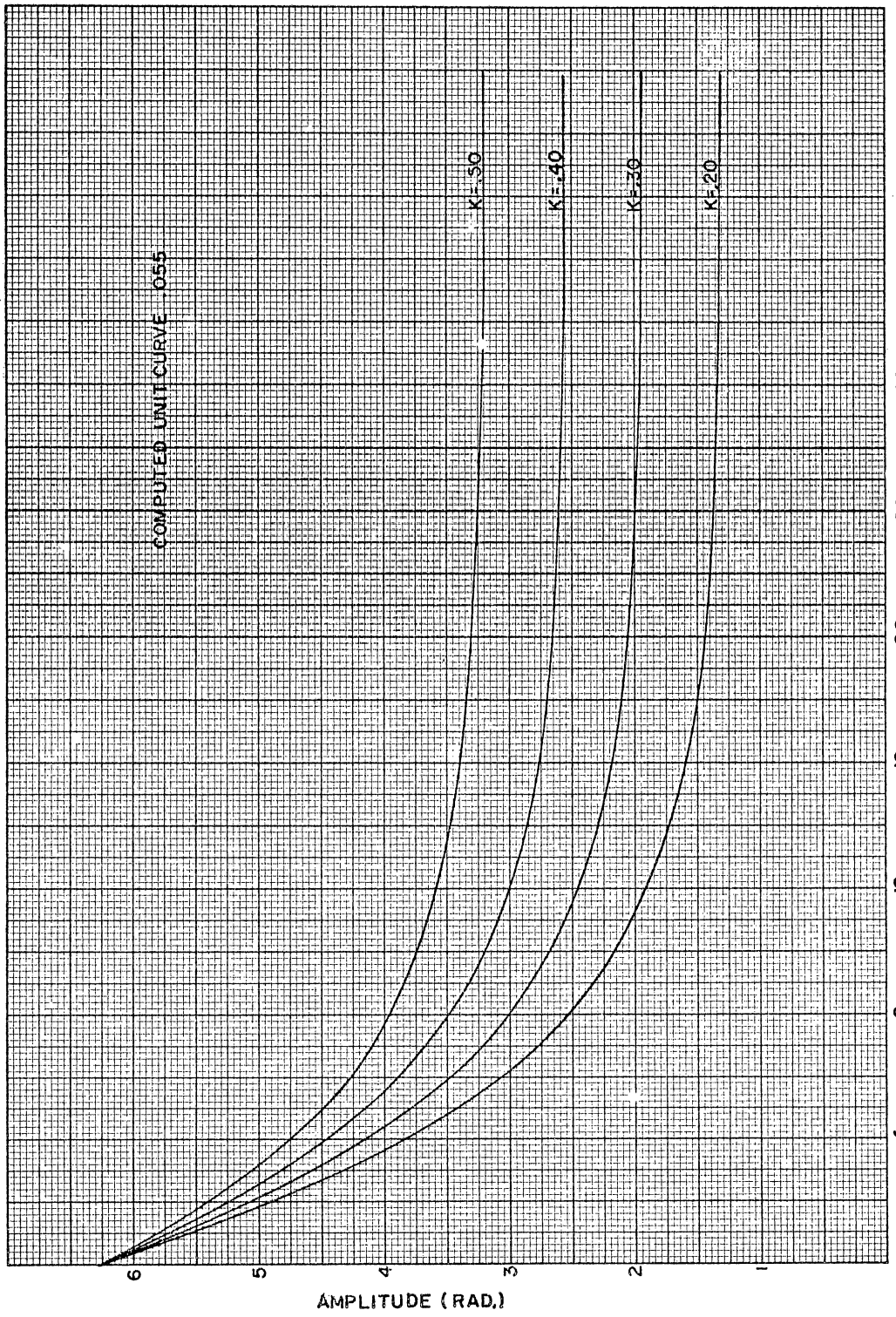

Figure 42. Computed Unit Curve 0.055

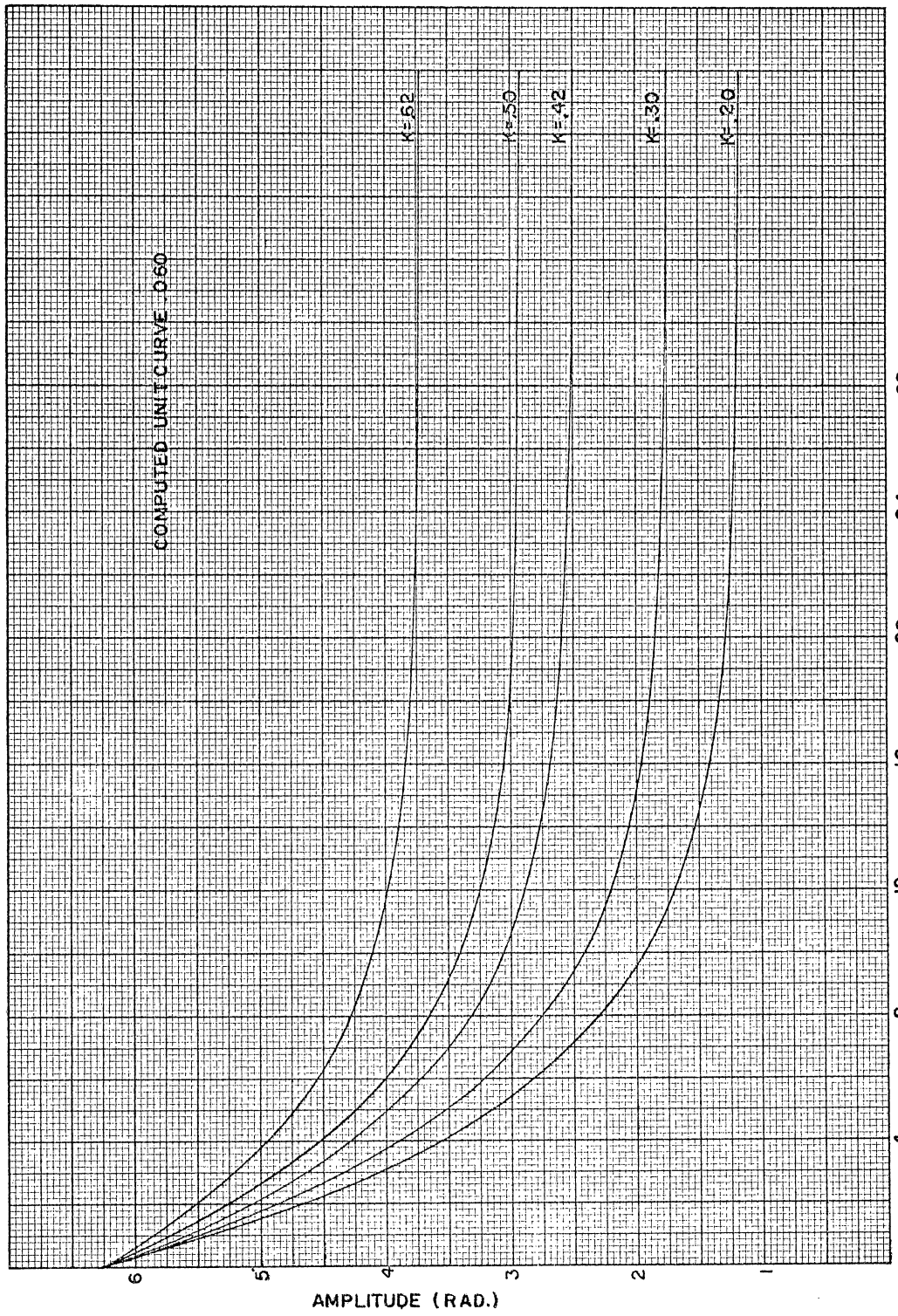

Figure 43. Computed Unit Curve 0.060

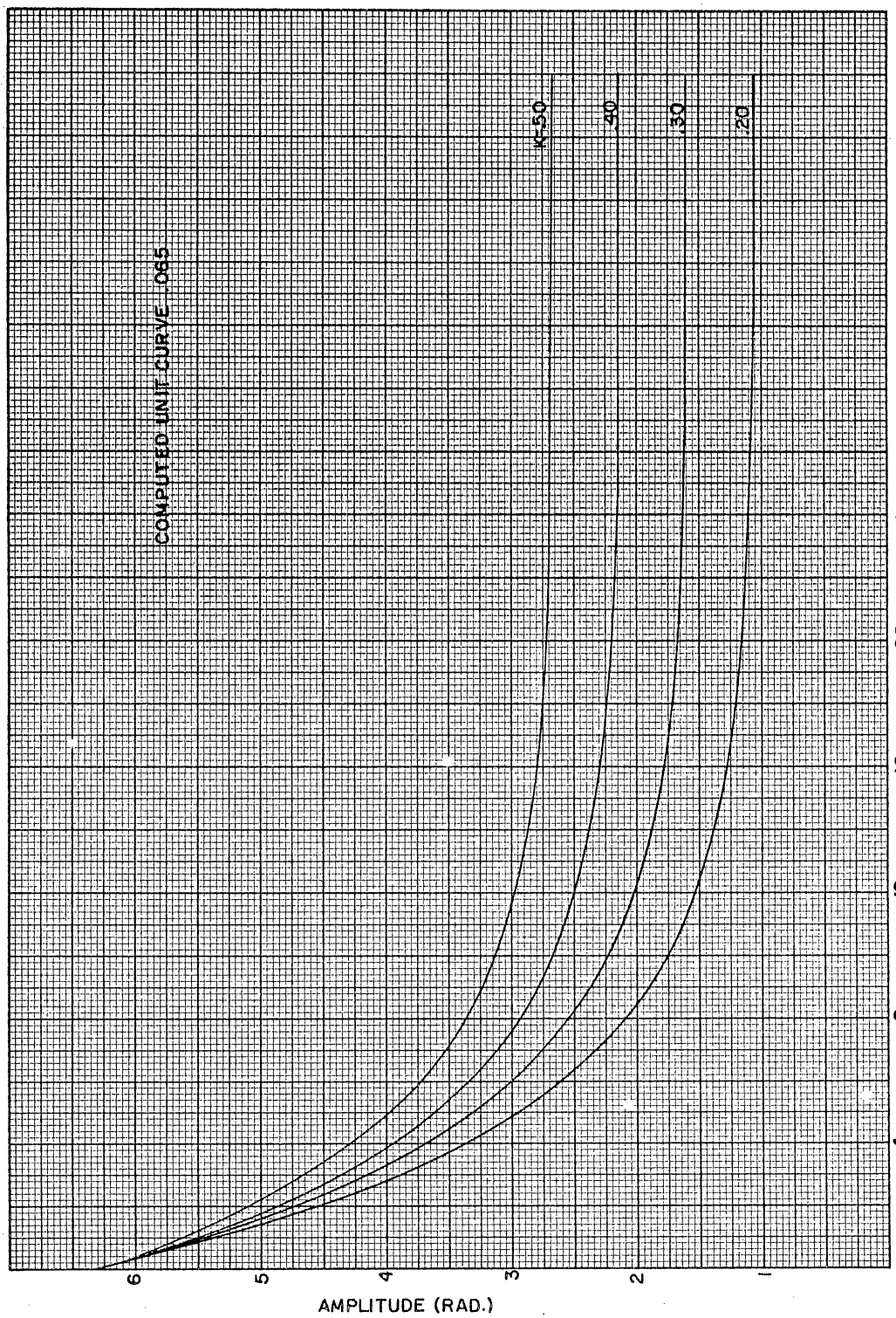

Figure 44. Computed Unit Curve 0.065

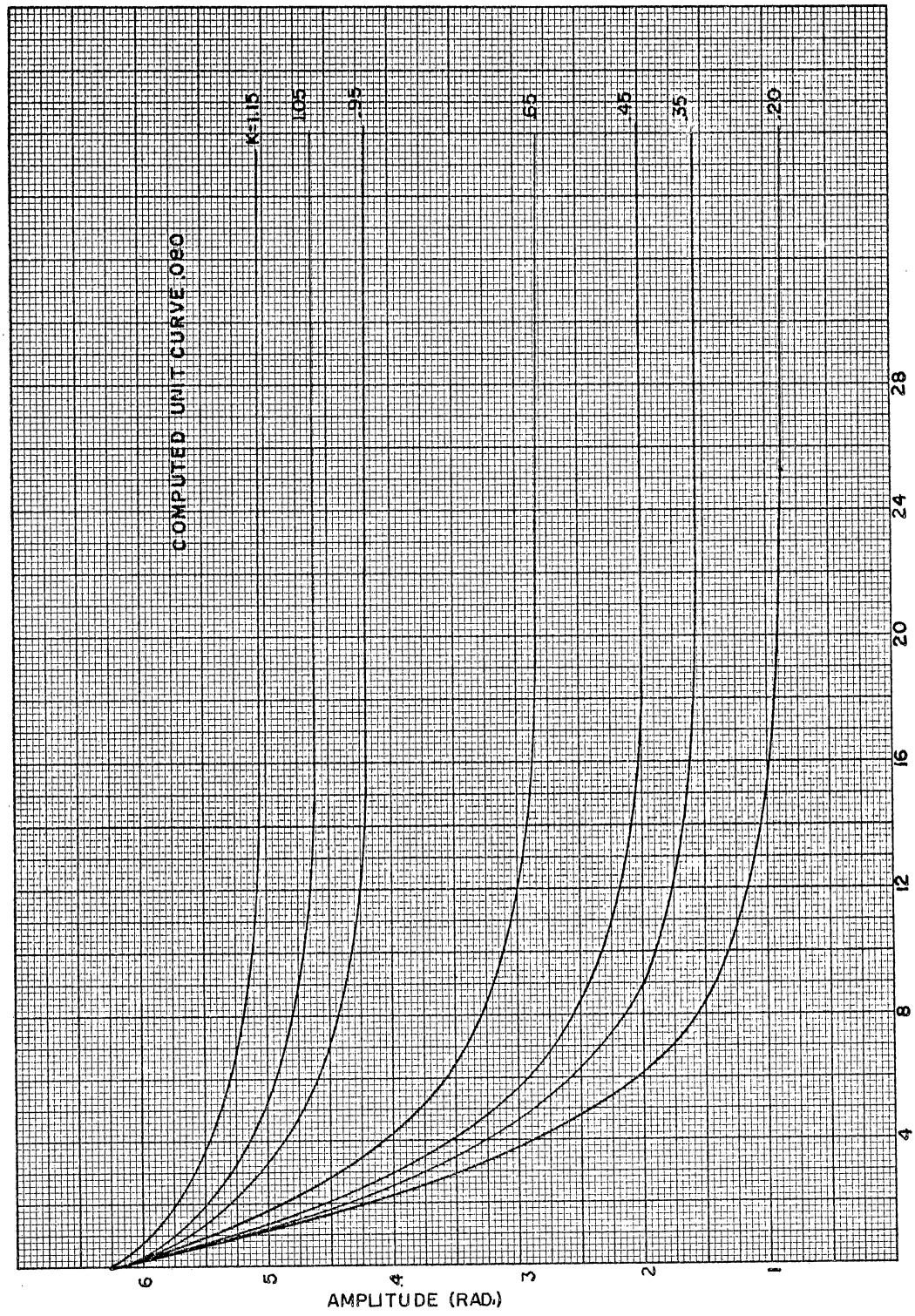

Figure 45. Computed Unit Curve 0.080

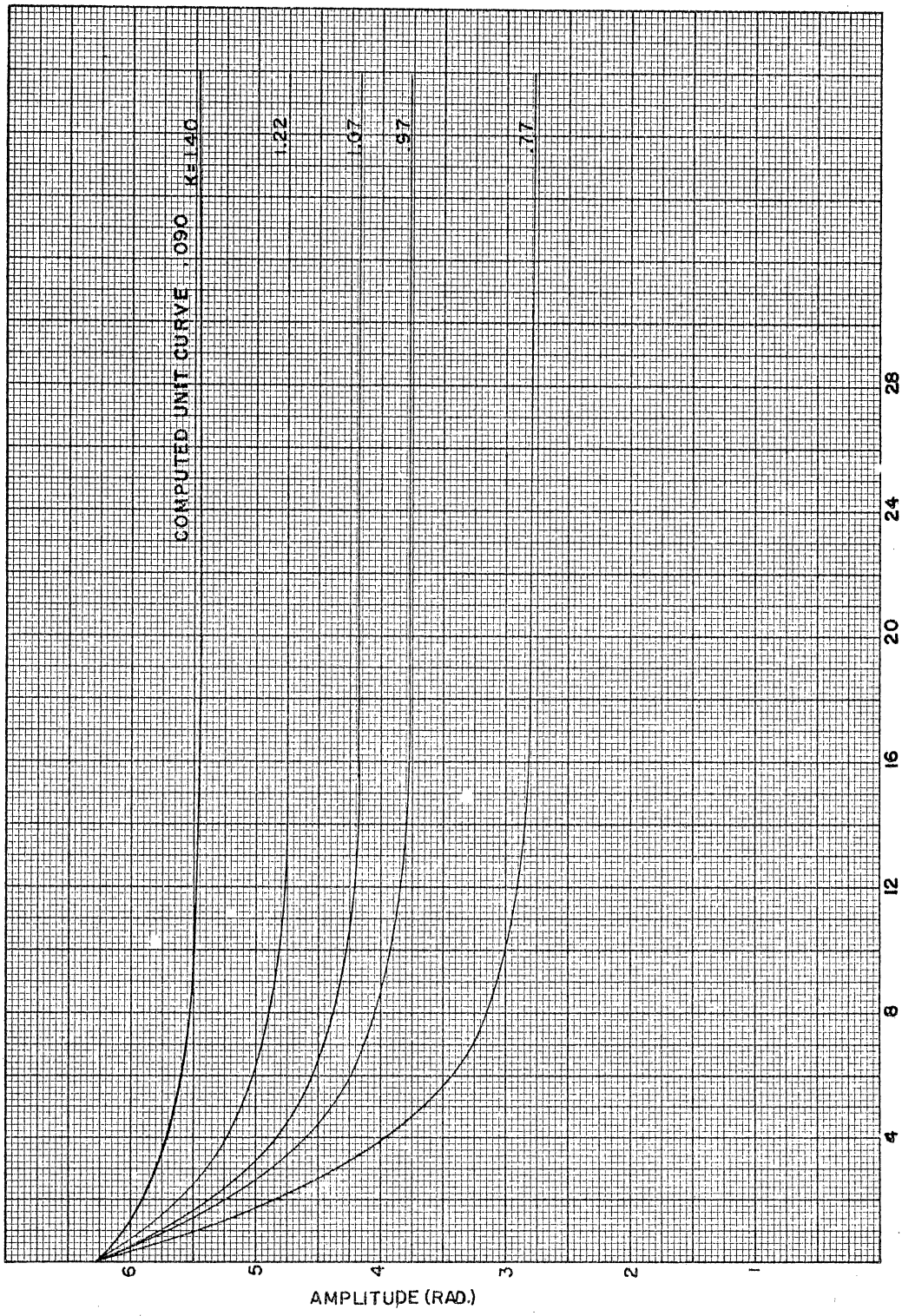

Figure 46. Computed Unit Curve 0.090

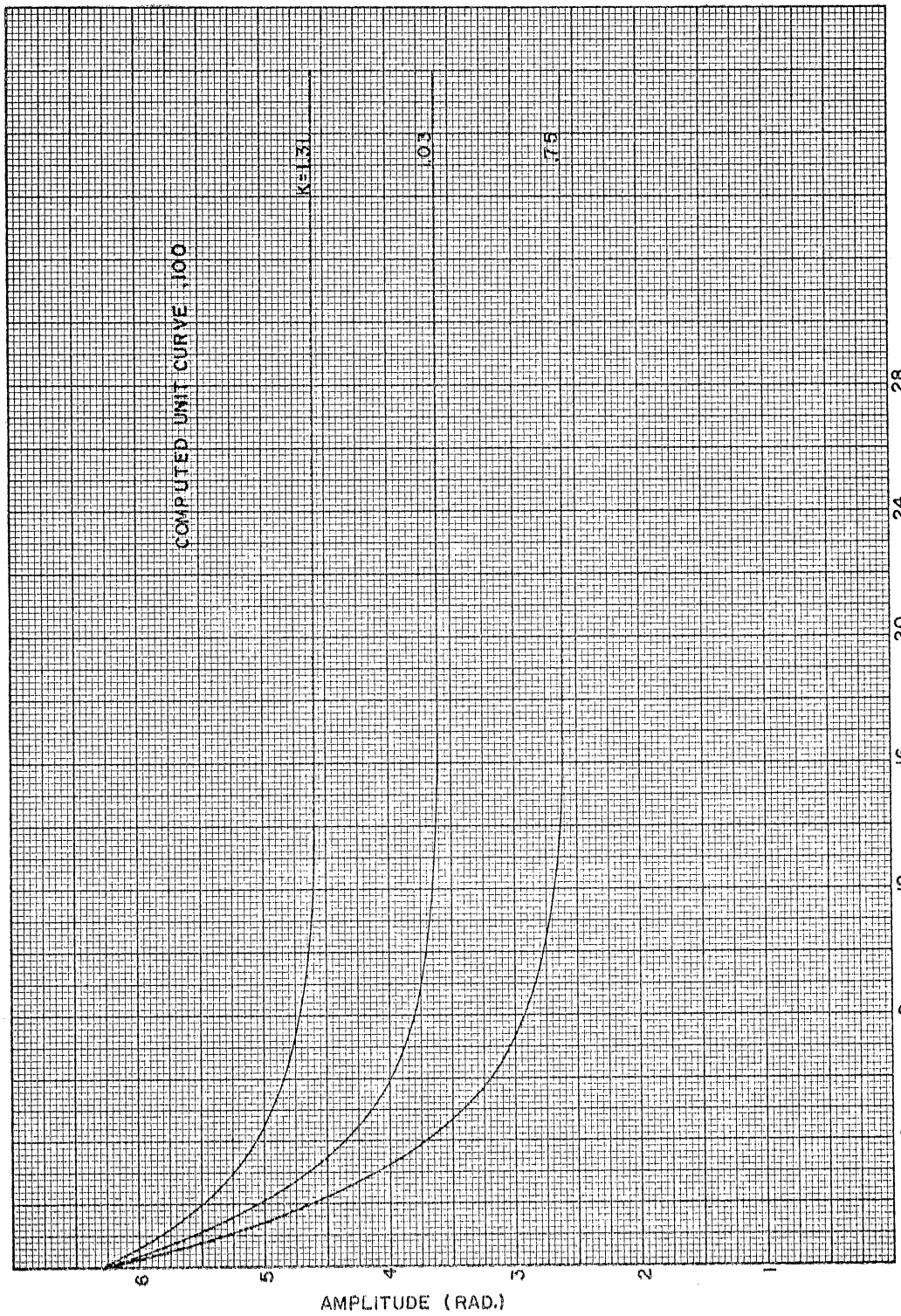

Figure 47. Computed Unit Curve 0.100

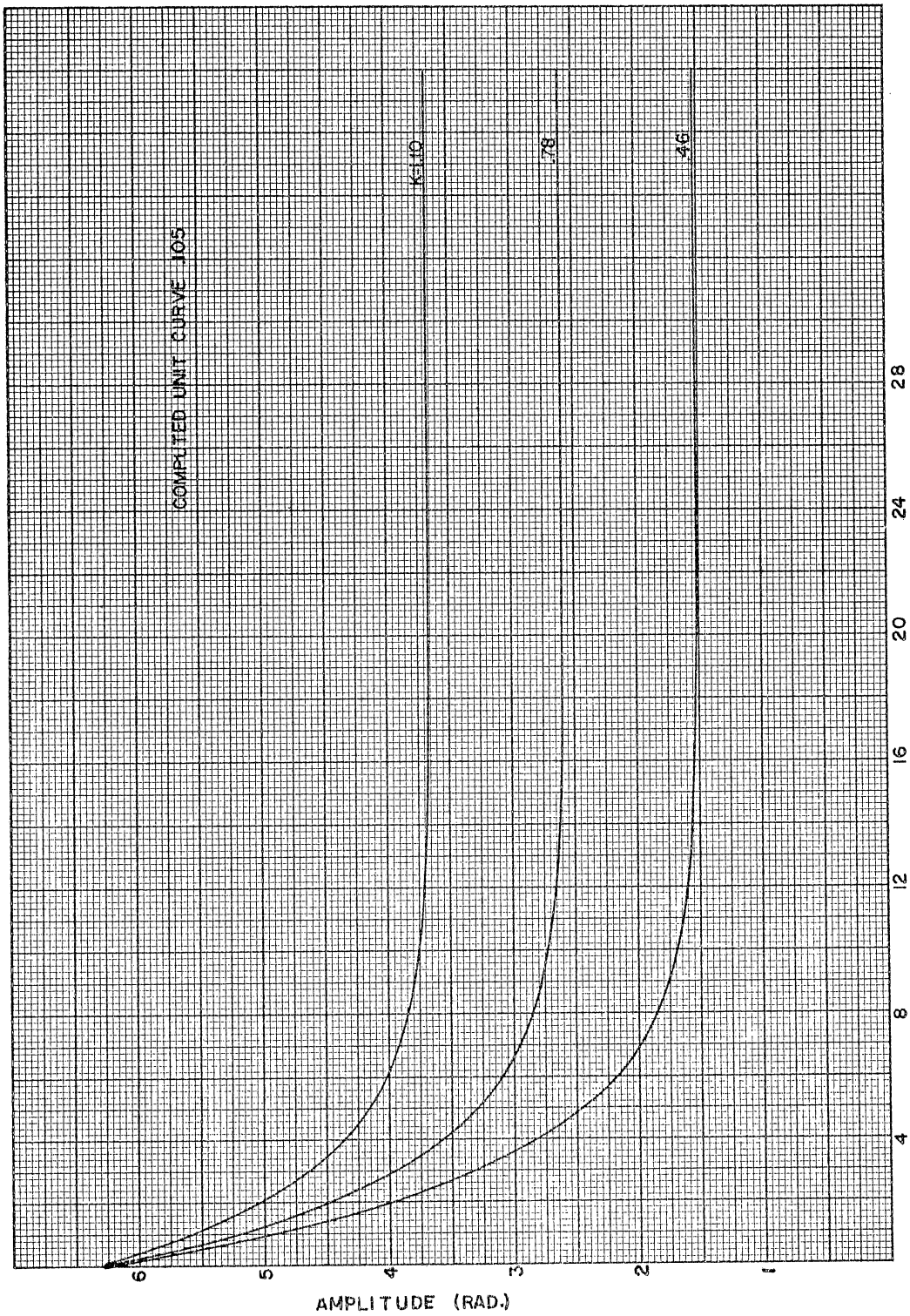

Figure 48. Computed Unit Curve 0.105

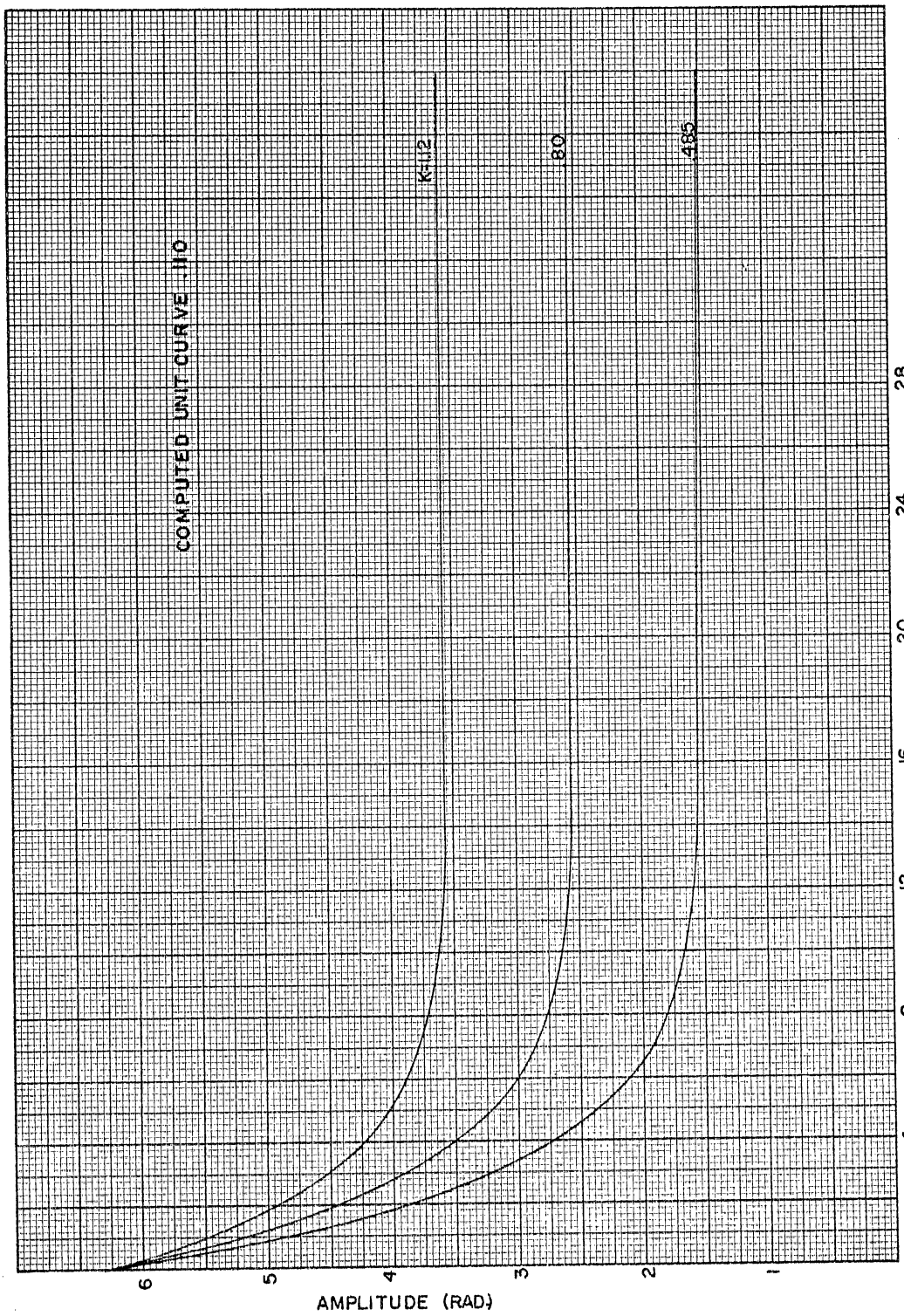

Figure 49. Computed Unit Curve 0.110

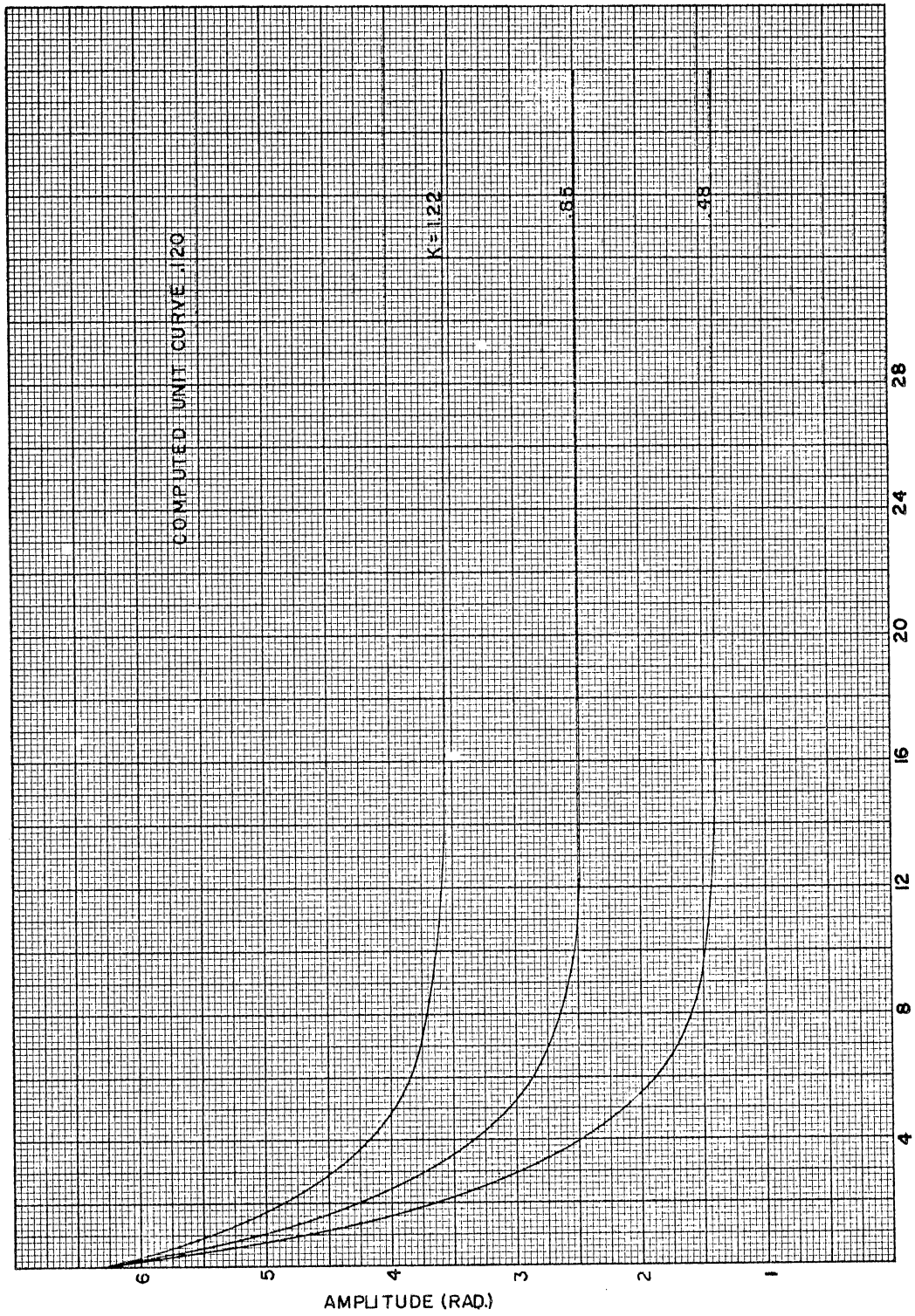

Figure 50. Computed Unit Curve 0.120

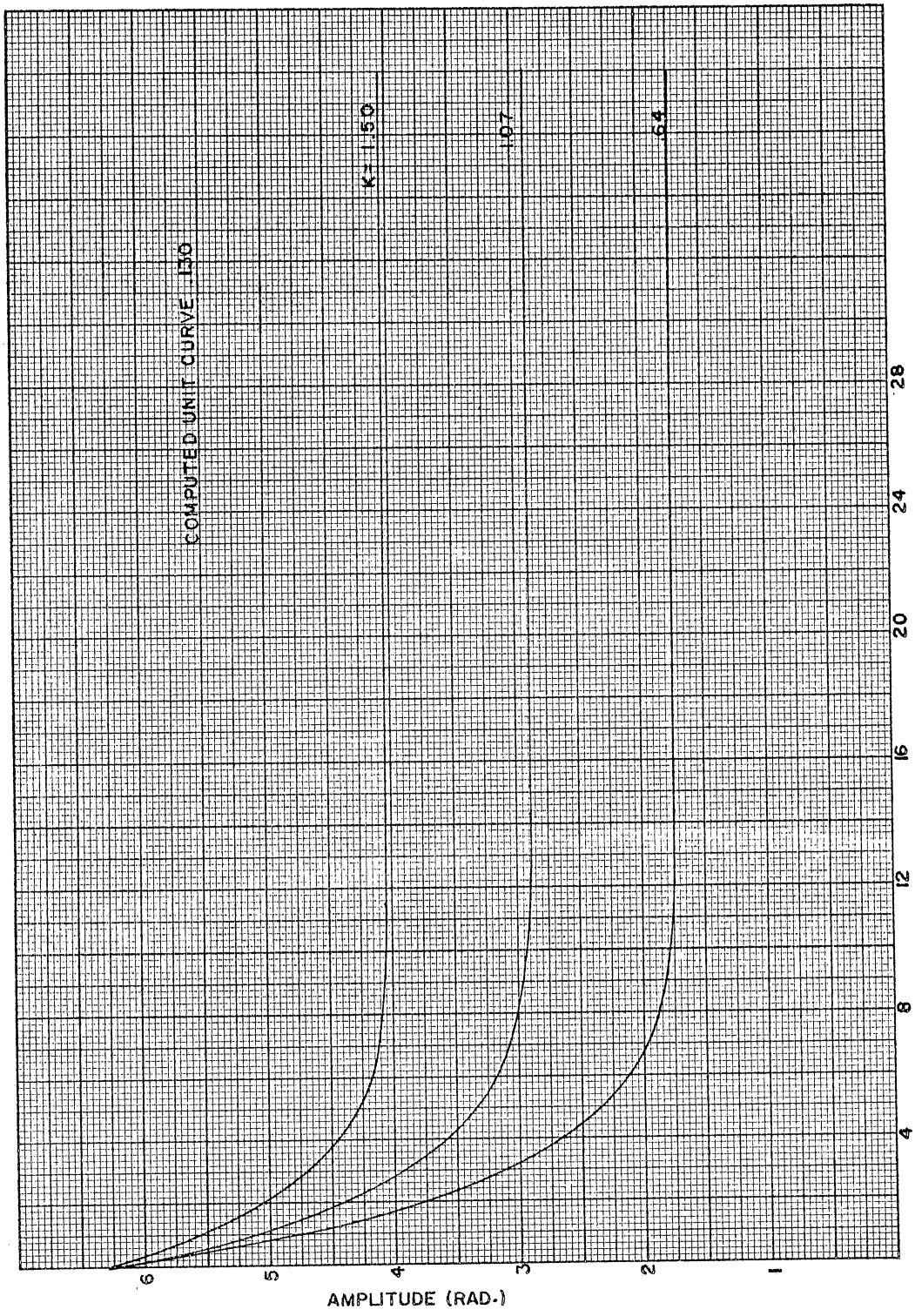

Figure 51. Computed Unit Curve 0.130

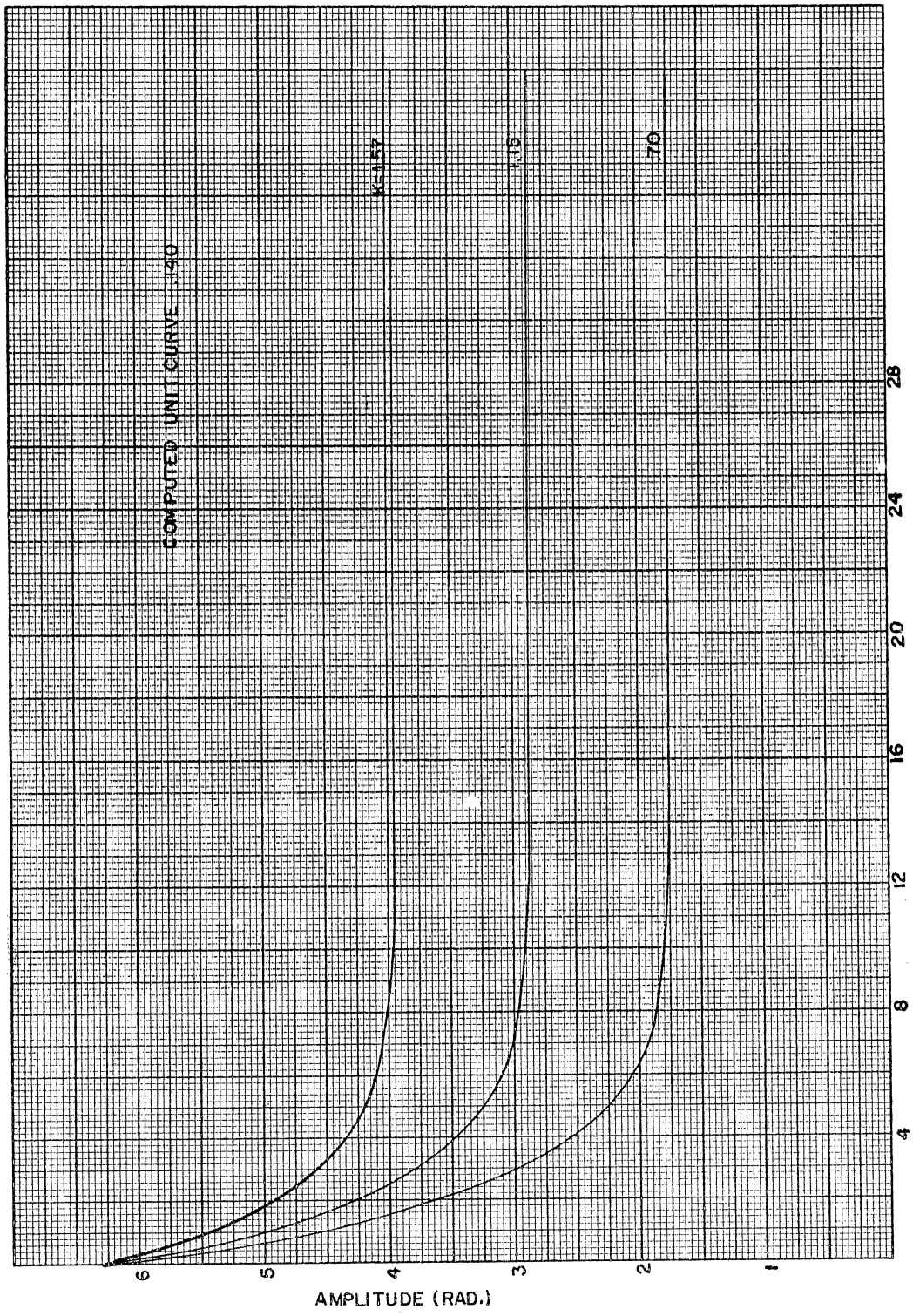

Figure 52. Computed Unit Curve 0.140

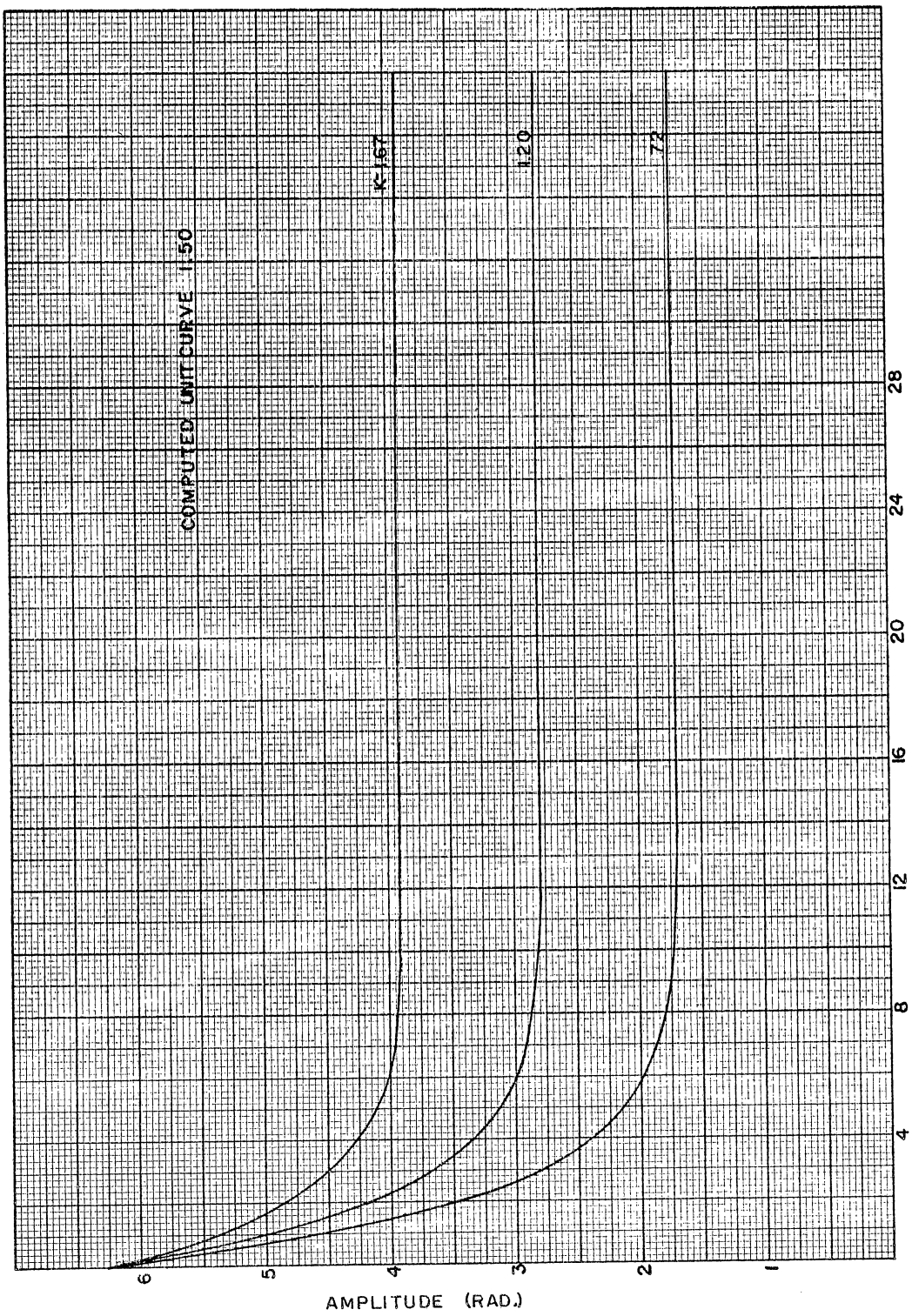

Figure 53. Computed Unit Curve 0.150

APPENDIX D

SYMBOLS

a	$a = k^2 - d^2$, horizontal distance along the surface from the point of the stylus to directly under the torsion wire.
A_n	Solution constants defined in Chapter III.
B_n	Solution constants defined in Chapter III.
BL_n	Solution constants defined in Chapter III.
C	Viscous damping coefficient divided by the polar moment of inertia (I).
d	Vertical distance of the stylus torsion spring above the specimen.
E-H	Defines the ends of the segments in radian measure in Chapter III.
f	Friction function in Giebel's equations.
i	Subscript for ω_{oi} for different hairspring constants.
I	Polar moment of inertia of the balance wheel.
K	Combined function of X_2/ω_o^2, X_3/ω_o^2, and R/ω_o^2.
k	Length from the end of the pallet to the torsion wire.
K_R	K divided by the graph factor (3.65).
L-N	Defines the ends of the segments in radian measure in Chapter III.
M_n	Magnitude of the torque to the balance in that segment n. $M_n = X_n I$.
n	Numerical subscript defining the end of the segments.

P-V Defines the ends of the segments in radian measure in Chapter III.

R Sliding friction function divided by I.

R_n Magnitude of the sliding friction function R over any constant segment n.

R_θ Sliding friction as a function of θ.

R_{X_n}/ω_o^2 This is the results of applying Figures 10 and 11 to X_n/ω_o^2.

t Time.

TT_n Time at the end of segment n.

w Normal force.

Δw Difference between the normal force under operating and nonoperating conditions.

X_θ Forcing function as a function of θ.

X_n Magnitude of forcing function X_θ over any constant segment n.

x Hairspring constant.

$\alpha, \beta, \gamma, \varepsilon, \mu$ Angular measure of the forcing function duration in radians.

ϕ, δ Angular measure of the hairspring constant duration.

ω_i System oscillatory frequency over any segment i.

ω_{on} Undamped natural frequency of the balance wheel at segment n.

θ Angular displacement of the balance wheel.

θ_o Initial displacement of the balance wheel.

$\ddot{\theta}, \dot{\theta}$ Angular acceleration and velocity of the balance wheel.

$\frac{\dot{\theta}}{|\dot{\theta}|}$ The term takes the sign of the velocity.

VITA

William Clair Monday

Candidate for the Degree of

Doctor of Philosophy

Thesis: DETACHED LEVER CLOCK MECHANISM DYNAMICS

Major Field: Mechanical Engineering

Biographical:

Personal Data: Born at Sun City, Kansas, February 25, 1930, the son of William C. and Margaret C. Monday.

Education: Attended grade school and high school at Cherokee, Oklahoma; graduated from Fredonia High School, Fredonia, Kansas, 1948; received Bachelor of Science Degree from the University of Kansas in June, 1952; received Master of Science Degree from the University of Kansas in June, 1956; completed requirements for the Doctor of Philosophy Degree at Oklahoma State University in May, 1965.

Experience: Served two years with the USAF Research and Development Command as project engineer in bombing systems (1/LT) 1952-54 at WPAFB, Ohio; employed by University of Kansas as Instructor in Mechanical Engineering at Lawrence, Kansas, 1954-56; employed by Sandia Corporation as project engineer in timing devices at Albuquerque, New Mexico, 1956-62; employed by Oklahoma State University as engineering research assistant at Stillwater, Oklahoma, 1962-65.

Professional Organizations: Professional Engineer (New Mexico); American Society of Mechanical Engineers; Sigma Tau.